Development of a Two Dimensional, Optically Accessible, Hybrid Rocket Motor

by

Sadie Boyle

A thesis submitted to the Graduate Faculty of
Auburn University
in partial fulfillment of the
requirements for the Degree of
Master of Science

Auburn, Alabama
December 14, 2019

Keywords: Propulsion, Combustion, Hybrid, Rocket

Approved by

David Scarborough, Chair, Assistant Professor of Aerospace Engineering
Brain Thurow, W. Allen and Martha Reed Professor of Aerospace Engineering
Roy Hartfield, Walt & Virginia Woltosz Professor of Aerospace Engineering

Abstract

Traditionally, launch vehicles and in-space vehicles use solid rocket motors (SRM) and liquid rocket engines (LRE) to propel them into and through space. However, there are many drawbacks to both propulsion systems. Hybrid rocket motors (HRM) present a viable alternative and have many advantages over LREs and SRMs as they are safe, simple, comparatively lower cost, have a relatively high specific impulse, and have relight and throttle capabilities. This unique combination of qualities makes HRMs a desirable propulsion choice for launch vehicle upper stages, sounding rockets, boosters, tactical systems, and in-space applications. However, during the development of any new high pressure combustion system, combustion instabilities are likely to occur. HRMs have four unique mechanisms that drive combustion instabilities. The four mechanisms that lead to combustion instabilities in hybrids are (1) oxidizer vaporization, (2) chuffing, (3) pressure coupled regression, and (4) vortex shedding.

This study focuses on the design, development, and testing of a two dimensional, optically accessible, HRM. This thesis outlines the importance of HRMs, the history and previous studies, the design and safety of the HRM, and the initial testing conducted. The initial testing consisted of looking at how the hybrid rocket motor performed using hydroxyl-terminated polybutadiene (HTPB) and high-density polyethylene fuels (HDPE) as well as 0.05 inch, 0.07 inch, and 0.08 inch oxidizer injector diameters. Higher pressures earlier in the burn were seen during the tests that used HTPB as the fuel compared to the tests that used HDPE as the fuel. The burn became more stable with increased oxidizer injector diameters and the burn time decreased with increasing oxidizer injector diameter. This process resulted in a test bed that will allow the Auburn University Combustion Physics Lab to conduct further research. The hope is that in future studies this HRM can be used to investigate vortex shedding as a driving mechanism for combustion instabilities.

Acknowledgments

To my late father, Peter Kazenoff, thank you for demonstrating how to follow your dreams. I miss your practical advice, descriptions of how the world works, and handy-man lessons. I think you would have been the proudest and most excited about this accomplishment.

To my mom, Kelly Boyle, I am eternally grateful for everything you have done for me. I would not be the person I am today and would not have accomplished what I have without your unconditional love and support.

Very special gratitude to Kat Scheibner, Francine Kazenoff, Kieran Vasquez, and my grandparents for your unwavering support, continuous advice, and reminders of the important things in life.

For my siblings Tierra, Joaquin, and Julio, may you follow your dreams to places that are out of this world.

With special mention to all of my friends. Thank you for your listening ears and for providing laughter and light throughout this challenging experience.

Thank you to my adviser, Dr. David Scarborogh, for giving me the opportunity to pursue my masters degree. I truly appreciate your support, advice, and guidance throughout this process.

Thank you to Dr. Brain Thurow and Dr. Roy Hartfield for their willingness to serve on my committee.

I am especially grateful to Auburn University faculty and staff Christian Broadbeck, Prissy Goodson, Rob Kulick, Dr. Eldon Triggs, Dr. Jose Vasconcelos, Ginger Ware, and Andy Weldon.

And finally, thank you to the members of the Auburn University Combustion Physics Lab for your constant help, without all of you this would not have been possible or enjoyable.

Table of Contents

List of Figures

List of Tables

List of Abbreviations

SRM	solid rocket motor
LRE	liquid rocket engine
HRM	hybrid rocket motor
$HTPB$	hydroxyl-terminated polybutadiene
TRL	technology readiness level
CI	combustion instability
$PMMA$	polymethyl methacrylate
$HDPE$	high-density polyethylene
ABS	acrylonitrile butadiene styrene
$\dot{m}_o$	oxidizer mass flow rate
L	chamber length
λ	nozzle efficiency
A_e	nozzle exit area
OF	oxidizer to fuel ratio
A	port cross sectional area
n	regression rate exponent or mass-flux exponent
ρ_f	fuel density
a_o	regression-rate coefficient using just $G_o(a_o = aL^m)$
P	port perimeter
$\dot{m}_{Total}$	total mass flow rate
p_c	chamber pressure
k	ratio of specific heats

R	gas constant
T_c	chamber temperature
$\dot{m}_f$	fuel mass flow rate
V_e	exit velocity
p_e	nozzle exit pressure
$\dot{F}$	thrust vs. time
g	acceleration due to gravity
F	thrust
p_a	ambient pressure
C_f	thrust coefficient
c^*	characteristic velocity
$\dot{r}$	regression rate
m	port length exponent
I_{sp}	specific impulse
t_b	burn time
t_f	fuel thickness
r_f	final port radius
r_i	initial port radius
G	system gain
G_{ox}	mass flux of the oxidizer
A_t	throat area
D_t	throat Diameter
$\dot{m}_{ft}$	fuel mass flow rate through throat
D_p	port diameter
ϵ	nozzle area ratio
$\dot{m}_{sys}$	system mass flow rate
$AUCPL$	Auburn University Combustion Physics Lab
$P\&ID$	piping and instrumentation diagram

$N2$	nitrogen
NTV	nitrogen tank valve
PRV	pressure reducing valve
NV	needle valve
VP	vapor pressure
SRV	safety relief valve
CHK	check valve
SOL	solenoid valve
BV	ball valve
PT	pressure transducer
$N2O$	nitrous oxide
FP	fill port

Chapter 1

Introduction

Traditionally, launch vehicles and in-space vehicles use solid rocket motors (SRMs) and liquid rocket engines (LREs) to propel them into and through space. In recent years, other systems such as electric propulsion have been used for satellites but SRMs and LREs remain the industry standard due to their long-standing flight heritage. SRMs are simple and lightweight but lack the throttle, shutdown, and relight capabilities of their liquid counterparts. LREs provide high specific impulse and have the capability of adjusting the thrust during operation and can be reignited during flight [6, 7]. However, they are expensive, relatively heavy, and complex due to their cryogenic storage and pumping requirements for both the fuel and the oxidizer.

Hybrid rocket motors (HRMs) are a possible alternative to SRMs and LREs [6, 7, 8]. HRMs store one propellant component, typically the fuel, in a solid state and the other propellant component in a liquid state, typically the oxidizer. HRMs have many advantages over SRMs and LREs. Unlike SRMs, HRMs tend to be safer, have a higher specific impulse, and have start, stop, and throttle capabilities. HRMs are simpler and lower cost than LREs, due to their fewer components [9, 10]. This unique combination of qualities make HRMs a desirable propulsion choice for launch vehicle upper stages, sounding rockets, boosters, tactical systems, and in-space applications.

Conventionally, HRMs use polymer fuels such as hydroxyl-terminated polybutadiene (HTPB), which have low fuel regression rates causing HRMs to remain at a low technology readiness level (TRL) [6]. The fuel regression rate is the rate at which fuel is consumed. In HRMs fuel is melted, evaporated, and mixed very slowly. This causes the regression rate of HRMs to be very low, typically around 0.0394 in/s, compared to the regression rate of SRMs, which is closer to 0.394 in/s [11]. However, recently developed liquefying fuels, such as paraffin, offer higher regression rates because of the liquid layer that forms when the fuel burns [6, 12]. The liquid layer allows for faster evaporation and mixing and therefor leads to a higher regression rate. To increase the TRL of HRMs, the performance and reliability of HRMs needs to be improved. Liquefying fuels provide an avenue for improving the performance of HRMs but they do not impact the reliability of HRMs. Combustion instability's (CIs) greatly impact the reliability of HRMs therefor further research on the causes and the mitigation strategies of CIs could lead to improvements of the reliability and an increase in the TRL of HRMs.

CI is characterized by high-amplitude acoustic pressure (greater than 5% of the mean motor chamber pressure [13]) and heat release oscillations. CIs occur at three different frequency ranges; low-frequency (0-200 Hz), medium-frequency (20-100 Hz), and high-frequency (1000-4000 Hz) [13]. Low-frequency combustion instabilities are the most common in hybrids and although they do not typically lead to motor failure, they do inhibit performance and impact reliability. Medium frequency oscillations do occur in HRMs but are less common. High frequency instabilities have not been documented in hybrids [13]. Hybrid motors share characteristics of both solid and liquid propulsion systems and therefor have some similar mechanisms that cause instabilities as well as some unique ones [14]. The four mechanisms that lead to CIs in hybrids are (1) oxidizer vaporization, (2) chuffing, (3) pressure coupled regression, and (4) vortex shedding. Pressure coupled regression has been well studied. But, the other three mechanisms of CIs found in hybrids are not well understood and mitigating strategies have not been developed [13, 15].

This thesis surveys the development of a two dimensional, optically accessible, HRM at Auburn University. The design process began with surveying the history and previous research on HRMs and using that information a MATLAB model and a very simplistic COMSOL acoustics model were created. From there the motor design was created and built. Initial testing looked at two different fuels, HTPB and high-density polyethylene (HDPE) and three different oxidizer injector sizes, 0.05 in, 0.07 in, and 0.08 in. Future experiments on vortex shedding as a mechanism for combustion instabilities are also outlined.

Chapter 2

Review of Hybrid Rocket Motors

2.1 History of Hybrid Rocket Motors

The history of HRMs began in 1933 when the Soviet Union became the first country to fly an HRM. Since then, the popularity of the HRM has ebbed and flowed until they really gained traction in the 1960's [16, 17]. From the 1960s on, HRMs have mostly been used in target drones and high-altitude sounding rockets. Through the years, there have been a number of different studies conducted on HRMs. HRMs have flow on very few spacecraft but recently they have gained attention and consideration for future space missions. This renewed interest is most likely due the development of high regression rate liquefying fuels, which increase the performance capabilities of HRMs [1, 11].

2.2 Combustion Physics of Hybrids

2.2.1 Modeling Hybrid Performance

To model hybrid rocket performance the oxidizer mass flow rate $\dot{m}_o$, the chamber length L, the nozzle exit area A_e, and the nozzle efficiency λ are set as design inputs and the following equations are used to find the performance parameters. An initial guess for chamber pressure p_c must be set to use the following equations. Equation 2.1 is used to calculate the oxidizer to fuel ratio (OF). Where A is the port cross sectional area, ρ_f is the fuel density, a_o is the regression-rate coefficient using just G_o, ($a_o = aL^m$), n is the regression rate exponent, and P is the port perimeter.

$$OF = \frac{\dot{m}_o^{1-n} A^n}{\rho_f a_o L P} \tag{2.1}$$

Equation 2.2 is used to calculate the total mass flow rate through the system ($\dot{m}_{Total}$). Where p_c is the initial guess for chamber pressure, k is the ratio of specific heats, R is the gas constant, and T_c is the combustion temperature.

$$\dot{m}_{Total} = p_c A_e k \sqrt{\frac{(\frac{2}{k+1})^{\frac{k+1}{k-1}}}{\sqrt{kRT_c}}} \tag{2.2}$$

Equation 2.3 is used to calculate the mass flow rate of the fuel $\dot{m}_f$.

$$\dot{m}_f = \dot{m}_o(1 + \frac{1}{OF}) \tag{2.3}$$

Equation 2.4 is used to calculate the nozzle exit velocity (V_e). Where p_e is the nozzle exit pressure.

$$V_e = \sqrt{\frac{2k}{k-1} RT_c [1 - \frac{p_e}{p_c}]^{\frac{k-1}{k}}} \tag{2.4}$$

Equation 2.5 is used to calculate the thrust versus time during the burn ($\dot{F}$) . Where g is the gravitational constant.

$$\dot{F} = \frac{\dot{m}_{Total} V_e}{g} \tag{2.5}$$

Equation 2.6 is used to calculate the instantaneous thrust (F). Where p_a is the ambient pressure.

$$F = \lambda[\dot{m}_f V_e + (p_e - p_a)A_e] \tag{2.6}$$

Equation 2.7 is used to calculate the thrust coefficient (C_f).

$$C_f = \sqrt{\frac{2k^2}{k-1}(\frac{2}{k+1})^{\frac{k+1}{k-1}}[1 - \frac{p_e}{p_c}]^{\frac{k-1}{k}}} \tag{2.7}$$

Equation 2.8 is used to calculate the characteristic velocity (c^*) of the system.

$$c^* = \frac{F}{\dot{m}_{Total} C_f} \tag{2.8}$$

Equation 2.9 is used to calculate the regression rate versus time ($\dot{r}$). Where G is the total propellant mass flux, n is the mass-flux exponent, and m is the port length exponent.

$$\dot{r} = aG^n L^m \tag{2.9}$$

Equation 2.10 is used to calculate the specific impulse (I_{sp}).

$$I_{sp} = \frac{c^* C_f}{g} \tag{2.10}$$

Equation 2.11 is used to calculate the burn time (t_b). Where t_f is the fuel thickness.

$$t_b = \frac{t_f}{\dot{r}} \tag{2.11}$$

Equation 2.12 is used to calculate the chamber pressure (p_c). Where A_t is the nozzle throat area.

$$p_c = \frac{\dot{m}_f c^*}{A_t} \tag{2.12}$$

The chamber pressure from Equation 2.12 is used to iterate the previous equations until the estimated chamber pressure matches the calculated chamber pressure.

2.2.2 Hybrid Stability

Combustion in HREs is complex and coupled. In an HRE the oxidizer is ported into the fuel grain boundary layer. When the right oxidizer to fuel ratio is reached combustion occurs. CI is related to the stability of the motion in the combustion chamber and develops due to the feedback loop between the acoustic response of the motor and the heat release. The frequencies associated with CI range from tens to thousands of hertz [18]. The associated high-amplitude acoustic oscillations frequently results in unpredictable performance and, in some circumstances, outright failure of the motor. Therefore, it is critical to understand the motors acoustic response, the burn rate response, and the coupling mechanisms associated with combustion instabilities. One vital aspect, and an underrepresented area of research, is to understand vortex shedding as a mechanism of driving CIs and to understand the fundamental mechanisms for, which these vortices are shed.

Acoustic and combustion oscillations in rocket thrust chambers are frequently caused by a coupling between the fluid flow, combustion noise, the natural acoustic modes of the system, and the heat release process. Vortices are formed in the shear layer between the high speed and low speed flow regions. During acoustic pressure oscillations the vortex structures can remain stable but if coherent flow structures develop these structures can breakdown into fine-scale turbulence. The fine-scale turbulence can shed, can lead to periodic heat release, and if coupled and in phase with pressure oscillations they can drive combustion instabilities [19]. The frequency of vortex shedding is highly correlated with the Strouhal number, $S_t = f \cdot \frac{L}{V}$, where f is vortex shedding frequency, L is the characteristic length, and V is the mean flow velocity. These vortices, convected by the bulk flow to the nozzle, interact with the exhaust nozzle to cause pressure disturbances, which then propagate back upstream where they induce further vortex shedding. This process ultimately leads to vortex shedding that is coherent with the acoustic oscillations. The amplitude of the pressure oscillations can be quite large when the vortex shedding frequency is closely coupled with one of the natural acoustic modes of the chamber [20].

Vortex shedding, both from protuberances in the flow and from the viscous layer that develops close to the burning propellant, typically convects downstream with the mean flow, where the vorticies impinge upon the nozzle or other hard surfaces. This impingement causes a pressure wave to propagate back upstream, which induces more vortex shedding, and thus a feedback mechanism for development of pressure waves inside the motor is developed. The grain geometry typically plays a large role in the development of these vortices, since potential protuberances as well as the viscous layer are strong functions of the grain geometry. Incomplete mixing near the propellant layer causes unreacted reactants to convect downstream, where vortices shed may enhance the local mixing, causing a local combustible mixture to form. In general, these localized pockets of combustion are highly disordered, and therefore, do not actively contribute to the feedback loop of combustion instability. When coupled with a stable and frequency dependent series of vortices being shed, these previously random combustion events become organized, thereby contributing to the feedback loop of the combustion instability.

Regardless of the mechanism or grain geometry, energy is added to the acoustic field when the burning rate oscillations occur in phase with acoustic pressure oscillations, leading to high-amplitude acoustic pressure oscillations. The amplitude of the oscillation will continue to grow until the net gain is zero. This is frequently expressed using a form of Raleighs criterion, which is given by Equation 2.13. Rayleighs criterion [21], is an expression for the system gain defined as the difference between the system driving and damping.

$$\underbrace{\int_t \int_V p'(x,t) q'(x,t) dV dt}_{\text{Term 1: Driving}} - \underbrace{\int_t \int_{V,S} \psi(x,t)}_{\text{Term 2: Damping}} = G \tag{2.13}$$

G is positive for an unstable system and negative or zero for a stable system. Term 1 represents the driving due to the coupling between the heat release oscillations and the acoustic pressure integrated over the combustion region. Term 2 in Equation 2.13 is integrated over either the surface and/or volume of the system depending on whether the losses are assumed to occur. When the damping and driving are equal, the system is said to be in limit cycle.

Preventing or eliminating the undesirable oscillations requires either increased damping, decreased driving, or some combination of the two. Therefore, understanding and mitigating combustion instabilities requires (1) a thorough understanding of the acoustic response of the system, (2) understanding the origin of any sources of coherent flow induced oscillations and noise generation mechanisms, and (3) the response of the flame to acoustic pressure and velocity oscillations.

2.3 Modeling Studies on Hybrid Rocket Motors

Many previous studies on HRMs have focused on using different types of models to predict performance. In 1971, Netzer [22] presented a summary of HRM internal ballistics based in the heat transfer limited model. This summary focused on applications, major limitations, kinetic effects, controversial aspects, and areas of future investigation. More recently Rocker [23], Majdalani and Vyas [24], Ozawa and Shimada [25], and Venkateswaran and Merkle [26] have created models using different methods to look at the HRM combustion process. Rocker [23] created a transient model of an HRM to study the cause of non-acoustic combustion instabilities. The model simulated four tests from a series of seventeen conducted at NASA Marshall Space Flight Center and the model showed good agreement with the experimental test results. Majdalani and Vyas [24] derived a solution to describe the mean flow motion of the bidirectional coaxial vortex found in HRMs. Chelaru and Mingireanu [27] built a theoretical model to validate experimental results of an HRM focused on increasing scalability and regression rate in HRMs. Ozawa and Shimada [25] used a theoretical model to predict the regression rates of swirl injection HRMs by estimating the heat flux from the boundary layer combustion to the fuel surface. Venkateswaran and Merkle [26] looked at the combustion processes in HRMs through computational fluid dynamics on a two dimensional slab burner HRM. In that study, both the full-length geometry without the aft nozzle section and shorter-length geometries were looked at for parametric characterization. The results found that that fuel surface temperatures were between 900 and 1100 kelvin and the regression rate of the fuel grain were between 0.01 to 0.07 inches per second.

Models on the ignition process have also been created such as the one developed by Tian et al. [28] which is based on a theoretical analysis of HRM ignition. To develop the model, the ignition process was divided into four stages: heating, ignition, flame propagation, and rapid pressure buildup. The results of the model were compared to experimental testing on a 90% hydrogen peroxide and both PMMA and HDPE HRM. The results showed that the ignition process was governed by the temperature and the oxidizer to fuel ratio. It was also concluded that the ignition delay was more sensitive to the oxidizer temperature than to the fuel temperature.

2.4 Experimental Studies on Hybrid Rocket Motors

Through the years, many experimental studies have been conducted on HRMs. Most studies have been done on lab-scale HRMs using nitrous oxide [29, 30], gaseous or liquid oxygen [31, 32, 33, 34], hydrogen peroxide [35] or air as the oxidizer and HTPB [30], polymethyl methacrylate (PMMA) [31, 34], high-density polyethylene (HDPE) [29], acrylonitrile butadiene styrene (ABS) [36, 35] or paraffin wax [32, 33] as the fuel. Numerous HRMs have been built by student groups, senior design teams, and graduate students [29, 30, 37, 38, 36, 32]. These motor designs were mostly used for sounding rockets, laboratory research, or to use on nanosatellite launch vehicles. The motor designed by Platt [37] used the results from a visual basic electronics module, a MathCAD regression rate model, and the equilibrium ratios of the fuel and oxidizer from ProPep to predict the chamber pressure, chamber temperature, ratio of specific heats, and molecular weights. This study was fairly representative of common HRM studies. However, some projects were more unique, such as the work done by Mulato et al. [38] on an HRM, which was designed to launch from a high altitude balloon tethered to a launch platform.

Karabeyoglu et al. [33] and Vidya sagar et al. [32] both designed HRMs that used liquid oxygen and paraffin wax. This combination of fuel and oxidizer delivered a similar total impulse but was found to be 15-18% lighter and had the potential of increasing payload mass by 40% from comparable SRM systems such as the Orion 28. However, during these experiments variations in chamber pressure were experienced, leading to significant changes in mass flow rate, burn rate, and uneven regression over the fuel surface. These results show the need for further studies to ensure the reliability of HRMs.

Both Arena et al. [39] and Summers [40], conducted studies on the effects of swirl injection using HTPB and nitrous oxide. A swirl injector essentially increases the combustion chamber length, which in turn increases the combustion efficiency. Arena et al. [39] redesigned an M-class 98 millimeter motor with a 12 port self-impinging swirl injector. Summers [40] designed and developed a system to better understand the effects of varying the swirl angle on HRMs and found that swirl injection angle had the largest impact on the regression rate.

One of the advantages of HRMs over SRMs are the system relight capabilities, which still requires additional studies. Gracy [34] developed a dual injection gaseous oxygen, propane, and PMMA HRM with the goal of studying the relight reliability of the system. This study was unique and leaves room for further studies on the relight capabilities of HRMs.

Other experiments done by Waxman et al. [41], Whitmore et al. [35], and Lemieux [42] looked at various other performance aspects of HRMs. Waxman et al. [41] developed an experimental test apparatus to study the performance of nitrous oxide injectors and to determine the effects of injector geometry. From that study, it was found that neither rounded nor chamfered edges were more advantageous than the other but both provided improvements over square edged orifices. Whitmore et al. [35] designed and built a laboratory HRM that used 70-85% hydrogen peroxide and additively manufactured ABS with an arc-ignition system. This design was an alternative to catalytically decomposing 90% hydrogen peroxide, which is highly dangerous to work with. Lemieux [42] developed an HRM equipped with an aerospike nozzle to look at how to reduce throat ablation using a regenerative cooling mechanism. The study found that the method was effective in reducing damange to the nozzle and was able to withstand multiple test runs.

In 1992, Greiner and Frederick [31] developed a lab scale HRM to find burn rates for PMMA fuel and replicate the pressure oscillations found in HTPB fuel. The testing showed low-frequency pressure oscillations consistent with the pressure oscillations that occurred when using HTPB. This indicates that pressure oscillations that lead to CIs do not differ with different polymer fuels. In order to make these inferences the lab-scale HRM data must be scaleable to full size HRMs. Swami and Gany [43] determined that to relate lab-scale HRM data to full scale HRMs both must be geometrically similar, use the same fuel and oxidizer, and the mass flow rate of the oxidizer must be scaled to the port diameter.

The two studies that most closely represent the one outlined in this thesis are the studies done by Kuo et al. [44] and Wooldridge et al. [45]. Kuo et al. [44] conducted an experimental study on fuel decomposition and boundary-layer combustion in an HRM through the development of a a high-pressure, 2D slab burner. Fine-wire thermocouples were embedded into the HTPB fuel grain to measure the temperature on the fuel surface and subsurface. This was done by collecting static and dynamic pressure data and by using an x-ray ultrasonic pulse-echo technique to find the instantaneous solid fuel regression rate. Wooldridge et al. [45] investigated hybrid propellant combustion instabilities through experimental studies. The first phase of experiments looked at the delineation of the steady state hybrid propellant regression rate and the pressure coupling in the pressure-sensitive regime. The data showed that the regression rate was dependent on pressure due to the behaviour of the chemical kinetic process in the gas phase flame zone. The experimental results were used to create a theoretical model based on classical turbulent flame theory. The mathematical analysis agreed with the observed steady state regression rate and pressure dependence. The development of a spontaneous instability corresponding to the longitudinal model of the chamber was also observed in the testing.

2.5 Regression Rate Studies on Hybrid Rocket Motors

HRMs have remained at low TRLs due to the low fuel regression rates of traditional polymer HRM fuels. This has led to studies on how to model regression rates of HRMs, regression rate evaluation techniques, and ways to improve regression rates of HRM fuels.

The most common regression rate model for HRMs is Equation 2.14. Where, G is the mass flux of the oxidizer, a is an emperical constant, and n is a burn rate exponent. This equation is an estimation that neglects the fuel grain length by assuming that the regression rate is only dependent on the oxidizer mass flux and usually leads to the underestimation of regression rate but is widely used and accepted [46, 47, 11].

$$\dot{r} = \alpha G_{ox}^{n} \tag{2.14}$$

Greatix [48], Eilers [49], and Lestrade [50] developed models to predict fuel regression rate models for HRMs. Greatix [48] predicted HRMs fuel regression rates using a convective heat feedback modeling approach. When this model was compared to experimental results some discrepancies were found but were determined to be likely due to non-standard flow. Eilers [49] used a longitudinal enthalpy balance between the fuel grain heat of ablation and the convective heat transfer from the flame zone to create a regression rate model that predicts the chamber pressure, specific impulse, and thrust. Lestrade [50] used an integral description of the aerothermal flow coupled to a one equation model of the liquid thin film to develop a 1-D code called the Hydres platform. The model was able to accurately find the regression rate of liquefying fuels in HRMs.

Fuel regression rates have also been a major focus of experimental research with many papers focusing on techniques to evaluate regression rate. DeLuca et al. [51], Boughaba et al. [52], Porrmann et al. [53], Sorge and Carmicino [54], Kumar and Ramakrishna [55], and Shark et al. [56] built HRMs to develop regression rate evaluation techniques. Porrmann et al. [53] and Sorge and Carmicino [54] developed regression rate evaluation techniques that used an ultrasonic measurement system to non-intrusively take measurements. [54] found that pressure and temperature negatively impact the accuracy of the data so further investigation was required to mitigate the impact of those parameters. Kumar and Ramakrishna [55] used the chamber pressure specifying the choked flow condition at the nozzle throat to obtain consumed mass of the fuel and therefore the regression rate. The results of this method proved to determine the regression rate better than the weight loss method. Shark et al. [56] developed an opposed flow burner to screen and characterize solid fuel before use on full scale HRMs. The experiment analyzed the regression rate, flame structure, and flame temperature and showed that the regression rate was sensitive to laminar and turbulent flow regimes.

Low fuel regression rates are a major hindrance to advancing the TRL of HRMs. The low regression rates lead to lower performance and make HRMs a less desirable option. Therefore proponents of HRMs have invested in research to improve regression rates, mainly focusing on three approaches; multi port fuel grains, fuel additives, and liquefying fuels.

Whitmore et al. [57] and Pastrone [58] investigated the regression rates of multi-port fuel grains. Pastrone [58] conducted a study and found that by increasing the number of ports the heat transfer rate to the fuel surface is increased, and therefore the regression rate is increased. Whitmore et al. [57] conducted experiments using additively manufactured fuel grains with embedded helical ports. The fuel grains were tested with gaseous oxygen and were found to have higher fuel regression rates than cylindrical ported grains but the regression rate of the multi port fuel grains diminished throughout the burn. This was due to the reduction of the burning surface once the walls between the ports were consumed.

Advances in HRM development and how to increase performance and regression rate have been investigated by Alkuam and Alobaidi [59], Pastrone [58], Karabeyoglu et al. [60], Doran et al. [61], and Galfetti [62]. Both Alobaidi [59] and Pastrone [58] found that additives to solid fuel grains such as guanidinium azotetrazolate, aluminum alloys, and nano-particles were found to improve regression rates and thrust in HRMs. In recent years liquifying fuels, such as paraffin, have been developed, and based on the work done by Karabeyoglu et al. [60], Doran et al. [61], and Galfetti [62], show that the fuels with additives demonstrate higher regression rates than traditional polymer fuels.

Karabeyoglu et al. [60] developed and tested paraffin based fuels and Galfetti [62] reviewed the literature on hybrid propulsion to compare the average regression rate of HTPB and paraffin fuels. A broader study conducted by Doran et al. [61] looked at the regression rate of HTPB, PMMA, HDPE, sorbitol, and paraffin HRM fuels as well as the effect of multiple injector configurations on axial variation of port diameter, combustion efficiency, and motor stability. All studies concluded that paraffin had a higher regression rate than polymer fuels.

2.6 Optical Studies on Hybrid Rocket Motors

Ramohalli and Yi [63] conducted one of the first optical studies using an infrared camera to study fuel degradation through nitrogen and oxygen mixtures and find the temperature reached by the gases. The 2 inch diameter PMMA fuel grain was not transparent to infrared waves leading to unsatisfactory results. Wright et al. [64] built a co-axially located optical port to view the space in front of the fuel grain where ignition occurred using Visible-imaging fiber optic, UV-Vis fiber optic, and infrared fiber. Fiber optic images were obtained from the experiments.

Chandler et al. [1] developed the apparatus shown in Figure 2.1 to visualize the combustion process of HRMs with high regression rate fuels. The apparatus had three windows on the top and sides. Two high-speed cameras were pointed at the windows with the goal of comparing paraffin to traditional fuels.

Fanton, Paravan, and De Luca [2] performed ballistic characterization on a group of lab-scale HRMs with HTPB fuel. An optical time-resolved technique was used to look at the regression rate of a single cylindrical port fuel grain. The effects of metal additives and radiant heat transfer on regression rate were also investigated. Their experimental set-up is shown in Figure 2.2.

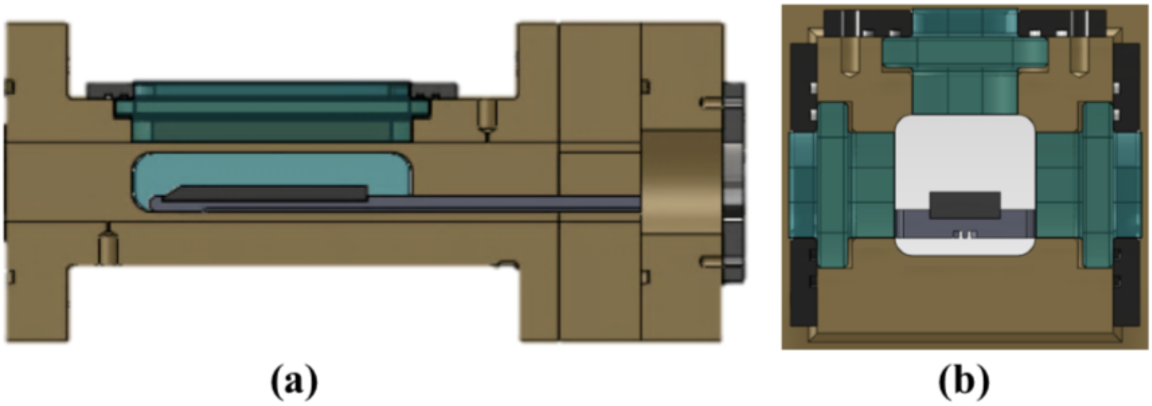

Figure 2.1: CAD drawings of the experimental apparatus from the study conducted by Chandler et al. [1]. (a) is a center line cut through and (b) is a cut through one-third of the way down the combustion chamber.

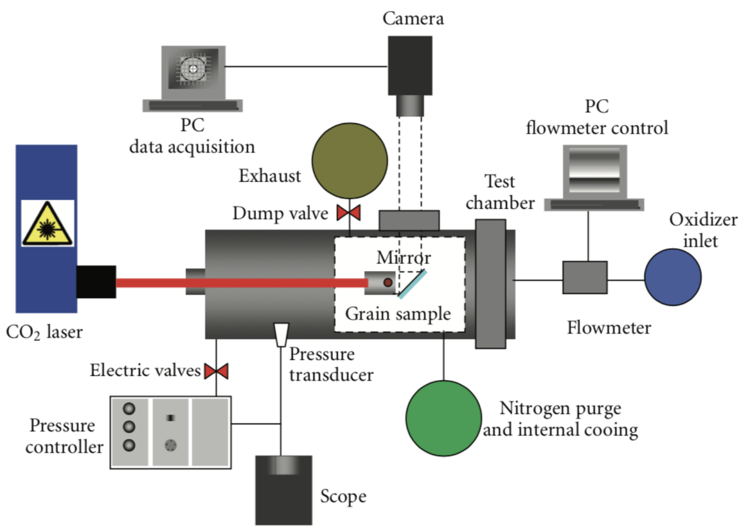

Figure 2.2: Diagram of the experimental set-up of the lab-scale HRMs developed by Fanton, Paravan, and De Luca [2].

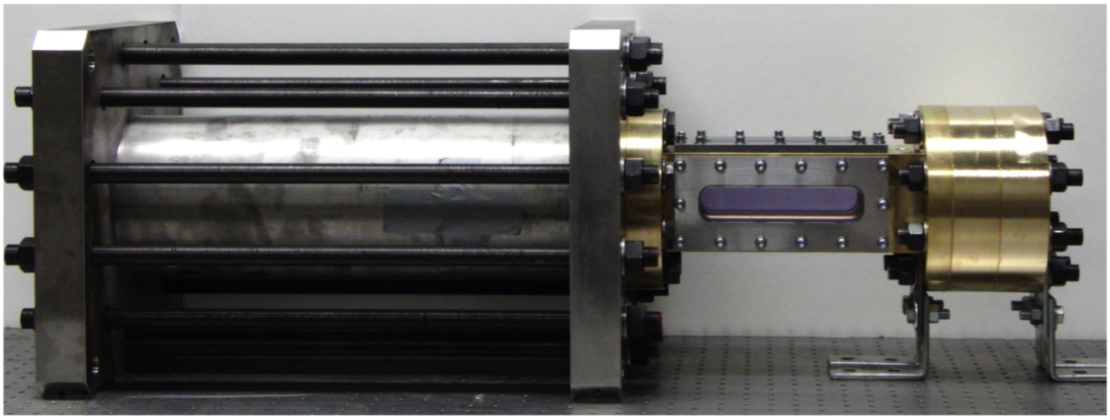

Figure 2.3: Combustion Visualization Facility at Stanford used both experiments by Jens et al. [3, 4]

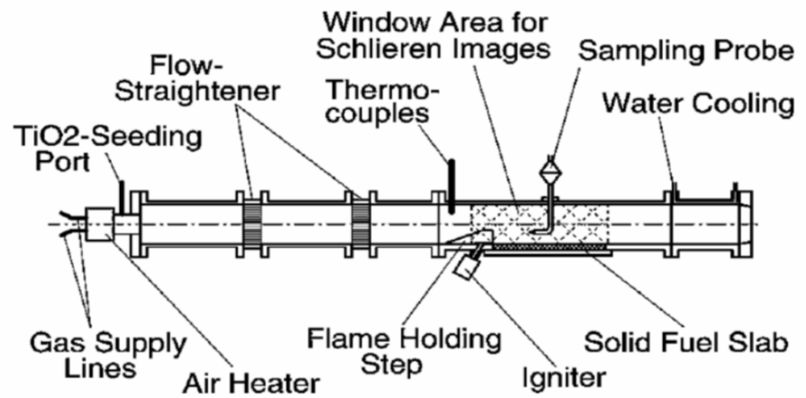

Figure 2.4: Experimental set-up of the combustion chamber for the experiments conducted by Petrarolo and Kobald [5]

Schlieren was a common imaging technique used in recent optical hybrid studies. Jens et al. [3, 4] developed a visualization facility shown in Figure 2.3 to study flow in a turbulent combustion boundary layer with liquefying fuels. In the experiments schlieren and OH* chemiluminescence images were taken to look at the combustion of paraffin and HTPB at a range of pressures. It was found that boundary layer thickness and surface blowing varied greatly with pressure. In a continuing study Jens et al. [4] looked at the development in the turbulent boundary layer of HTPB, HDPE, PMMA, and paraffin fuels using high speed color schlieren videos and determined that boundary layer thickness does not vary significantly over different fuels.

Petrarolo and Kobald [5] performed optical diagnostic evaluation techniques on a 2D slab burner HRM shown in Figure 2.4. The HRM had windows on two sides and used gaseous oxygen and paraffin. High speed videos were taken of tests to look at transient flow dynamics such as the Kelvin-Helmholtz instability, vortex shedding, and the turbulent diffusion flame. Spatial and temporal analysis on the data was carried out using two different techniques. The first was Proper Orthogonal Decomposition and the second was the Independent Component Analysis. These techniques were combined with applying a Power Spectral Density to obtain excited frequencies and wavelengths during combustion.

Based off of the optical experiments conducted by Chandler et al. [1], Jens et al [3, 4], and Petrarolo and Kobald [5] the AUCPL HRM was designed with windows on two sides of the combustion chamber. It was designed with the goal of conducting studies on combustion instabilities using evaluation techniques on high speed camera images.

Chapter 3

Inital Calculations

3.1 MATLAB Calculations

Prior to fabrication, calculations were performed in MATLAB, COMSOL Acoustics, and Excel. The MATLAB model looked at expected performance and sizing of the HRM, the COMSOL Acoustics model calculated the longitudinal and traverse nodes of the HRM, and bolt calculations were done in excel to ensure the safety of the design. The following sections discuss these calculations in more detail.

3.1.1 Initial Hybrid MATLAB Model

Prior to designing the AUCPL HRM a MATLAB model to predict HRM performance was created. The code was based off the concepts presented in Space Propulsion Analysis and Design [65] and Rocket Propulsion Elements [9]. The equations are based off of SRM design principals and were adapted for an HRM. The MATLAB model allows the user to input a desired thrust and to vary ambient pressure, chamber pressure, oxidizer to fuel ratio, inner radius of fuel grain, outer radius of fuel grain, length of the fuel grain, adiabatic flame temperature, gas constant of the oxidizer, density of the fuel grain, ratio of specific heats, the a regression rate coefficient, the n regression rate exponent, and the estimated burn time. The model then calculates the maximum burn time, oxidizer mass flow rate, throat diameter, nozzle exit diameter, and the recommended length of the fuel grain using the user imputed thrust and the equations in Table 3.1. From the inputs in Table 3.2 the outputs in Table 3.3 were calculated. The full code can be found in Appendix A.

Table 3.1: MATLAB Model Equations

	Parameter	Equation
1	Thrust Coefficient	$C_f = \sqrt{\frac{2k^2}{k-1}(\frac{2}{k+1})^{\frac{k+1}{k-1}}[1 - \frac{p_e}{p_c}^{\frac{k-1}{k}}]}$
2	Throat Area	$A_t = \frac{F_t}{C_f p_c}$
3	Throat Diameter	$D_t = \sqrt{\frac{4}{\pi} A_t}$
4	Total Mass Flow Rate	$\dot{m}_{Total} = p_c A_e k \sqrt{\frac{(\frac{2}{k+1})^{\frac{k+1}{k-1}}}{\sqrt{kRT_c}}}$
5	Fuel Mass Flow Rate	$\dot{m}_f = \frac{\dot{m}_T}{OF+1}$
6	Oxidizer Mass Flow Rate	$\dot{m}_o = \dot{m}_T - \dot{m}_f$
7	Nozzle Area Ratio	$\frac{A_t}{A_e} = (\frac{k+1}{2})^{\frac{1}{k-1}}(\frac{p_e}{p_c})^{\frac{1}{k}}\sqrt{\frac{k+1}{k-1}[1 - (\frac{p_e}{p_c})^{\frac{k-1}{k}}]}$
8	Exit Diameter	$D_e = \sqrt{\frac{4}{\pi} A_t}$
9	Exit Area	$A_e = A_t \epsilon$
10	Port Diameter	$D_p = [(at(4n+2))(\frac{4\dot{m}_T}{\pi})^n + 2R^{2n+1}]^{\frac{1}{2n+1}}$
11	Regression Rate vs. Time	$\dot{r}_T = a[\frac{4\dot{m}_T}{(\pi D_p^2)^n}]$
12	Chamber Length	$L = \frac{\dot{m}_f}{\rho_f \dot{r} 2\pi r_i}$
13	Fuel Mass Flow Rate Through Throat	$\dot{m}_{ft} = 2\pi \rho_f \dot{r} L_o \frac{D_p}{2}$
14	Oxygen to Fuel Ratio	$OF = \frac{\dot{m}_o}{\dot{m}_{ft}}$
15	System Mass Flow Rate	$\dot{m}_{sys} = \dot{m}_o + \dot{m}_{ft}$
16	Exit Velocity	$V_e = \sqrt{\frac{2k}{k-1} RT_c [1 - \frac{p_e}{p_c}]^{\frac{k-1}{k}}}$
17	Thrust vs. Time	$\dot{F} = \frac{\dot{m}_T V_e}{g}$
18	Characteristic Velocity	$c^* = \frac{F}{\dot{m}_T C_f}$
19	Specific Impulse	$I_{sp} = \frac{c^* C_f}{g}$
20	Burn Time	$t_b = \frac{(2r_f)^{2n+1} - (2r_i)^{2n+1}}{a(4n+1)(\frac{4\dot{m}_O}{\pi})^n}$

The MATLAB model also outputs graphs of port diameter verse time, mass flow rate verse time, regression rate verse time, thrust verse time, and oxidizer flow rate verse time. Figure 3.1(a) shows the port diameter growing from 1.5 inches to a little over 3.3 inches through the 60 second burn. Since the fuel grain is only 3 inches in diameter this indicates that the fuel will be fully consumed before the 60 seconds. Figure 3.1(b) shows the oxidizer mass flow rate, the fuel mass flow rate, and the total mass flow rate versus time. The graph indicates that the oxidizer flow rate is constant throughout the burn but the fuel mass flow rate and therefore the total mass flow rate starts higher and slowly falls to a constant rate of 0.01 lbs per second. Figure 3.1(c) shows the regression rate of the fuel versus time throughout the 60 second burn.

Table 3.2: Inputs of MATLAB Model

Parameter Name	Parameter Value
Ambient pressure	14.7 psi
Chamber pressure	100 psi
Oxidizer to fuel ratio	8
Thrust	100 lbf
Inner radius of fuel grain	0.75 in
Outer radius of fuel grain	1.5 in
Length of the fuel grain	29 in
Adiabatic flame temperature	5276 R
Gas constant of the oxidizer	35.1 lbf-ft/lbm-R
Density of the fuel grain	0.03425 lb-in^3
Ratio of specific heats	1.144
The a regression rate coefficient	0.1160
The n regression rate exponent	0.9874
The estimated burn time	60 s

Table 3.3: Outputs of MATLAB Model

Parameter Name	Parameter Value
Maximum Burn Time	40.9686 s
Oxidizer Mass Flow Rate	0.635014 lb/s
Throat Diameter	1.04027 in^2
Nozzle Exit Diameter	1.4132 in
Recommended Fuel Grain Length	11.6472 in

The regression rate begins high, between 0.04 and 0.045 inches per second and exponentially decreases to less than 0.01 inches per second during the 60 second burn. Figure 3.1(d) shows the thrust versus time trace of the example MATLAB model run. In the graph the thrust starts at 117 pounds of force and falls to 102 pounds of force by the end of the 60 second burn time. Figure 3.1(e) shows that the oxidizer to fuel ratio increases throughout the burn. It begins at 3 pounds per second and increases to just below 7 pounds per second. This indicates that there is more oxidizer than fuel as the burn progresses.

There are however, some drawbacks of this design code that will be improved with future iterations. The outputs of the model are based off of a desired thrust. Since this was not the main focus of the design, the code will need to be adapted to reflect the equations in the

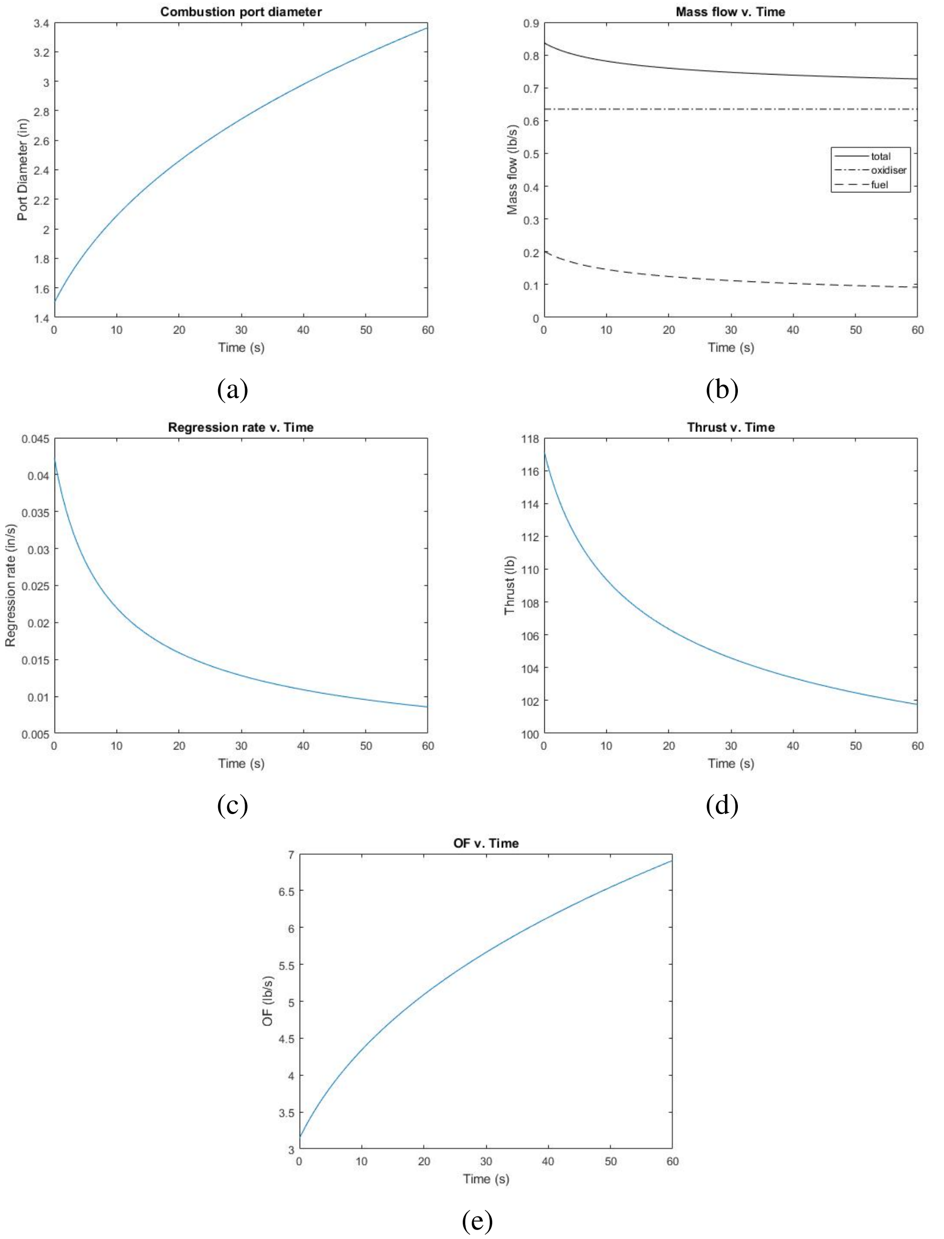

Figure 3.1: (a)Port diameter versus time graph from MATLAB model. (b) Graph of oxidizer mass flow rate, fuel mass flow rate, and total mass flow rate versus time from the MATLAB model. (c) Regression rate of the fuel verse time graph from the MATLAB model. (d) Thrust versus time graph from the MATLAB model. (e) Oxidizer to fuel ratio versus time from the MATLAB model

Modeling Hybrid Performance section of Chapter 2. The code was also not adapted for a non-cylindrical port so although the calculations are based on the same burn surface area they may not be entirely accurate for the two dimensional slab burner design as will be discussed later in the experimental design section. The code is based mostly on SRM equations so it may be advantageous to use current HRM equations or verify the validity of the equations currently in the model for use with HRMs. The tests conducted used both HTPB and HDPE but the model is based solely off of HDPE properties. The fuels are similar in density so this was not determined to be a problem.

3.1.2 Hybrid Nozzle MATLAB Model

A second MATLAB code was created to size the nozzle. The program assumes a two phase nozzle and uses nitrous oxide tables to determine the ideal radius of the injector given the mass flow rate of the nitrous oxide or vice versa for the desired performance parameters. The full code can be found in Appendix B. This code was used to help determine the size of the injector needed for the HRM to perform at the desired parameters.

3.2 COMSOL Acoustic Model

Within COMSOL, the acoustics package solutions for the eigenmodes, mode shapes, and frequencies of various grain geometries, pressures, and lengths can be solved for. To find the first longitudinal node and the first transverse node, the internal geometry of the combustion chamber was modeled. From the analysis, it was found that the distribution of the first longitudinal node occurs at 230.18 Hz and the distribution of the first transverse node occurs at 1689.40 Hz. Figure 3.2(a) shows the distribution of the first longitudinal node and Figure 3.2(b) shows the distribution of the first transverse node from the COMSOL analysis. Due to the high frequency of the transverse node it is likely that the transverse node will never be reached and only the longitudinal node will be observed during the HRMs operation.

The results from the acoustics analysis provides information as to where sensors, such as pressure probes, should be optimally located. Through the modal and frequency analysis in COMSOL, measured experimental values can be compared to calculated simulated pressures.

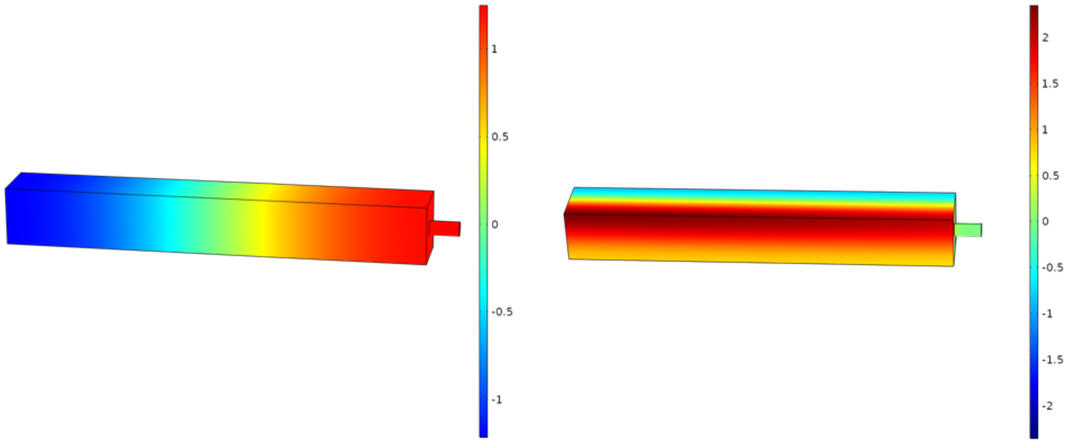

(a) (b)

Figure 3.2: (a) Results from COMSOL analysis show distribution of the first longitudinal node at 230.18 Hz. (b) Results from COMSOL analysis show the distribution of the first transverse node at 1689.40 Hz. The color bar is in terms of hertz for both images

This comparison can then be used to validate heat release and acoustic coupling models and their nonlinear effects. The COMSOL model will continue to be iterated to enhance future experiments.

Chapter 4

Hybrid Motor Design

The HRM is an optically accessible, 2D slab burner designed to use nitrous oxide as the oxidizer and either HTPB or HDPE as the fuel. It was developed to be used as a test bed for future HRM studies. The following sections outline the oxidizer system and the combustion chamber.

4.1 Oxidizer System

The oxidizer system is comprised of a series of tubes and fittings designed to port nitrous oxidize from a fill bottle to the sample cylinders and then into the combustion chamber during testing. The tube diameter was chosen based on a MATLAB code that calculated the pressure drop through the entire piping system. The full MATLAB code can be seen in Appendix C. The full piping and instrumentation diagram (P&ID) of the oxidizer system is shown in Figure 4.2. The P&ID diagram is a detailed view of the piping and process equipment together with the electronic instrumentation. The diagram was used to design the system and then to assemble the system. To fill the sample cylinders with nitrous oxide for testing, the procedures outlined in Table 4.1 are followed.

Nitrous oxide was chosen as the oxidizer for its storability, density, performance, and high vapor pressure [66]. With careful attention to handling and storage, it is safe compared to other oxidizers used in rocket propulsion systems [66]. During normal operation the pressure regulator on the nitrogen is set. The ball valves in the nitrous system are opened sequentially. The nitrous oxide tanks are pressurized by opening a solenoid valve remotely operated by labVIEW. The solenoid valve that allows oxidizer to flow into the combustion chamber is opened and the

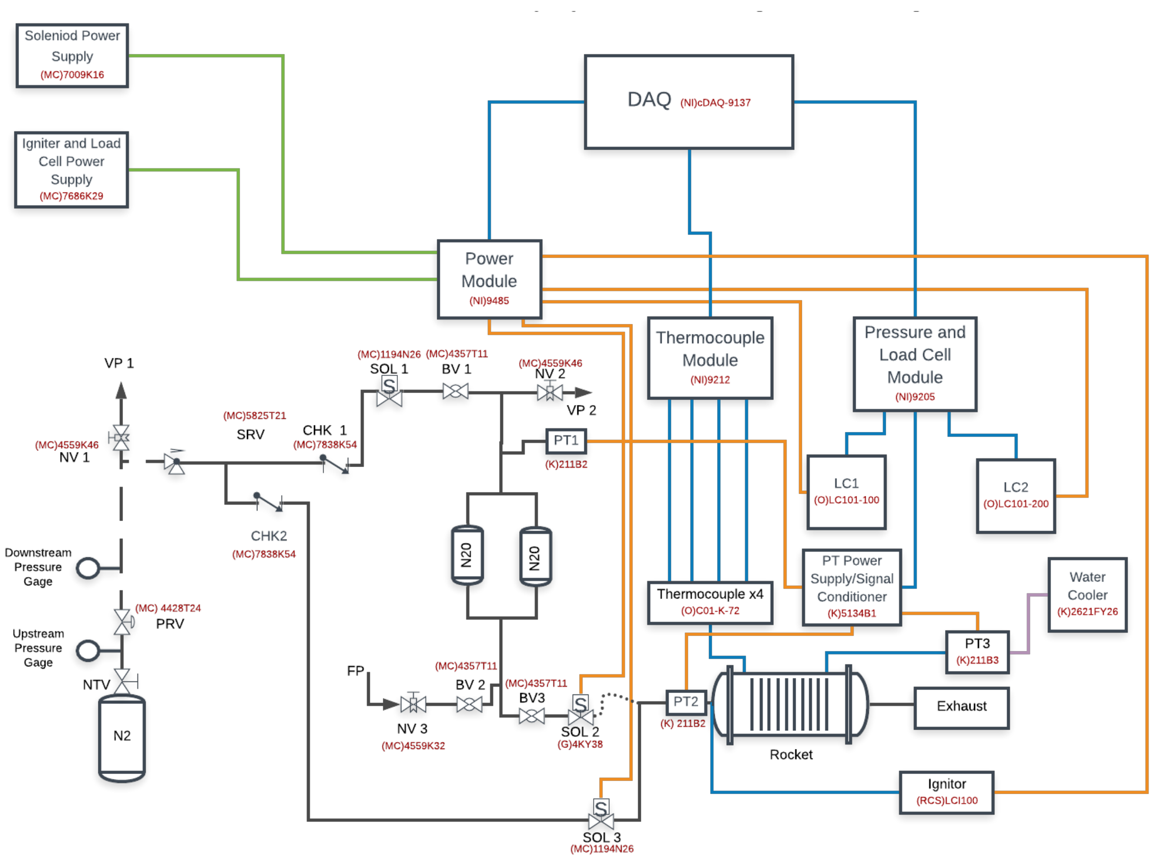

Figure 4.1: Piping and instrumentation diagram for the 2D optically accessible hybrid rocket motor. The diagram gives a detailed view of the piping and process equipment together wth the electronic instrumentation.

igniter is lit to fire the motor. Once the run is completed all valves are closed and the pressure is vented through a needle valve. In the case of an emergency all power is shut off to the system's solenoid valves. If the pressure in the system is ever greater than 1500 psi the safety relief valve will open to depressurize the system. Images of the assembled oxidizer system are show in Figure 4.2.

4.2 Injector

The oxidizer is fed from the sample cylinders to the combustion chamber through a half inch braided hose the oxidizer and is then passed through a yor-lok fitting to a quarter inch tube and then into a eighth inch pipe. Attached to the the pipe is a female-female pipe connector fitting that connects the pipe to the injector. The top view and side view of the internal oxidizer system is shown in Figure 4.3 and Figure 4.4 respectively. The injector system was designed

(a) (b)

Figure 4.2: (a) Front of the oxidizer piping and instrumentation system. (b) Back of the oxidizer piping and instrumentation system.

Table 4.1: Sample Cylinder Fill Procedure

1. Attach fill line to 10 lb N2O bottle.
2. Ensure all hand operated valves are closed.
3. Attach other end of fill line to BV 2.
4. Open BV 2.
5. Open valve on 10 lb N2O bottle.
6. Slowly open NV 2 until nitrogen begins to vent.
7. Monitor weight from LC 1.
8. When liquid N2O is ejected from NV 2, or desired weight is reached, close NV 2.
9. Close BV 2.
10. Repeat steps 1-9 until full.
11. Detach fill line from BV 2.
12. Proceed to normal operation procedure.

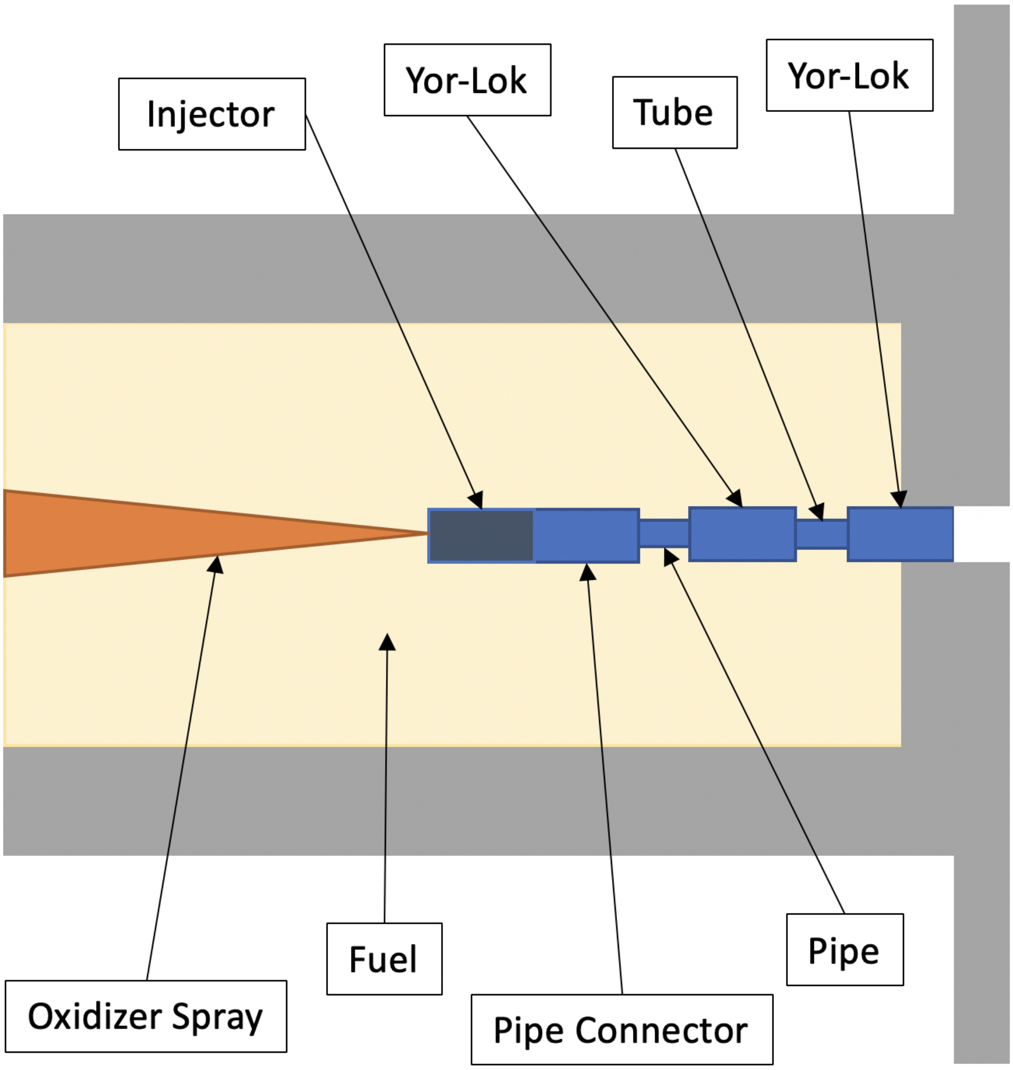

Figure 4.3: Top view of internal injector geometry

with a quick-disconnect spray nozzle to allow the researchers to easily change the nozzle size and spray angle. For all of the experiments conducted in this study the nozzle spray angle was 15 degrees. The drawing of the nozzle can be found in Appendix E.

4.3 Combustion Chamber

The structure of the engine is primarily made of steel. On the forward end of the motor there are three ports. The first port is for a pressure transducer to obtain static pressure data in the combustion chamber during operation. The second port is for the igniter. The motor is ignited

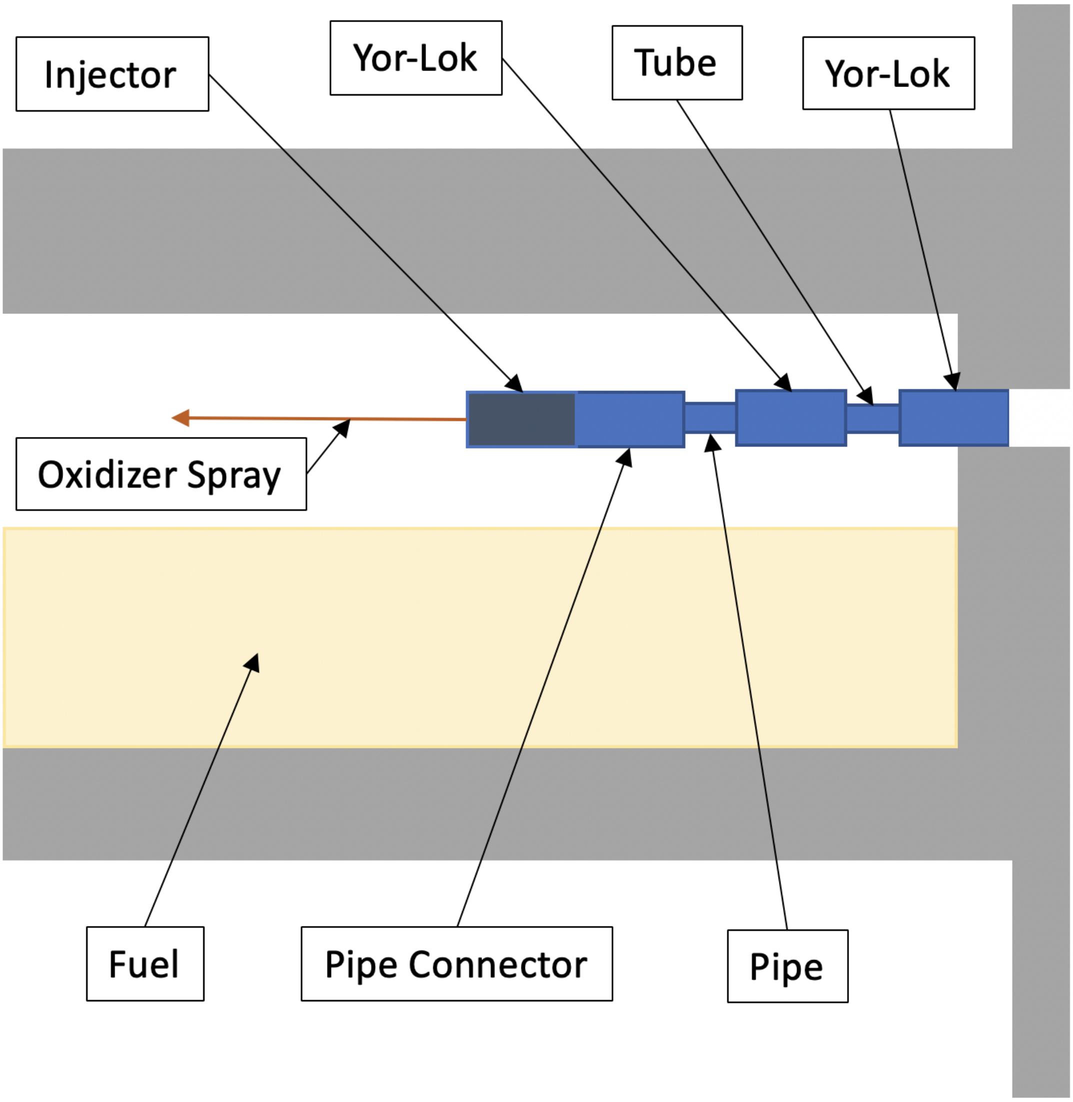

Figure 4.4: Side view of internal injector geometry

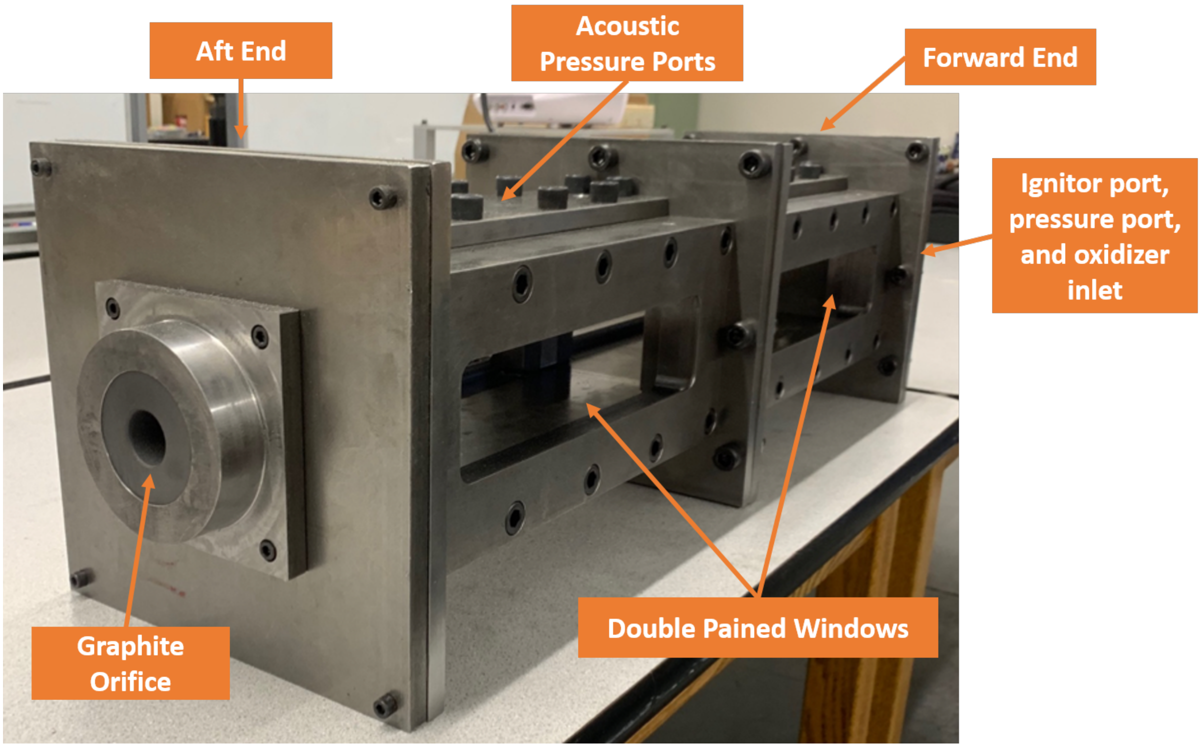

Figure 4.5: Fully Assembled 2D Optically Accessible Hybrid Rocket Motor

by a small solid propellant fuel grain that is lit by an electronic match. The last port is a half inch national pipe thread (NPT) hole used to port oxidizer into the combustion chamber.

The combustion chamber is 4 inches wide, 4 inches high, and 28 inches in length. It is designed in 2 segments, 14 inches each. Each segment has a double pained window on each side. The idea was to build a modular design that could be added to or subtracted from if a future experiment needed a longer or shorter combustion chamber. The internal geometry was based off the creating the same burn surface area as a HRM with a single spherical port. The internal window is quartz and the external window is Lexan. There is an open volume between the two windows to allow for water cooling during motor operation. The top of the combustion chamber is designed with water cooling channels to be used during operation and has 10 acoustic pressure ports evenly spaced to allow for acoustic mapping. The aft end of the motor is equipped with a circular graphite orifice. The diameter of the exit orifice is interchangeable to allow for different operating pressures. The expected operating pressure and burn time is under 100 psi and 40 seconds respectively. Figure 4.5 shows the fully assembled HRM and the drawings for the HRM can be seen in Appendix E.

4.4 Safety

Careful attention was paid to the safety of the system. With a hot fire combustion system there are concerns of over-pressurization and fire that could lead to injury of the personnel and destruction of equipment. To mitigate any potential safety problems the AUCPL worked with Integrated Engineering Services to build a safety mitigation strategy. The strategy included extensive calculations on safety parameters, scrutinizing of the components, development of a emergency shut down procedure, decisions on the proper personal protection equipment that personnel should use, and the development of the safety relief system.

The calculations included determining bolt loads, pressure, and pressure drop through the oxidizer system. The maximum pressure rating for every component was verified and the compatibility of component material with the expected temperature and the oxidizer was checked. In the case of any emergency the emergency procedure outlined in Table 4.2 would be executed. During operation it was decided that the HRM would be placed outside and all personnel would located inside of control building. All personnel will wear safety glasses, hearing protection, and close toe shoes. The AUCPL member who fills the oxidizer tanks will wear a full face mask during the fill procedure and stand behind a blast shield placed between them and the oxidizer system. In the case of over pressurization the aft end of the combustion chamber is designed to non-destructively break open to stabilize the pressure. The aft end of the HRM is secured with four aluminum bolts that can withstand 1200 pounds force each. At an operating pressure of greater than 300 pounds per square inch the force on each bolt will be greater than 1200 pounds of force and the bolts will break. The expected operating pressure of the HRM is below 100 pounds per square inch so an operating pressure of greater than 300 pounds per square inch is unexpected. The safety relief system was hydrostatically tested and the case successfully broke open at 300 pounds per square inch during each of the 5 tests. Images from one of the hydrostatic tests is shown in Figure 4.6.

During one of the initial tests a piece of the igniter came lose and momentarily clogged the exit orifice. This caused a pressure build up and when the piece of igniter was ejected from the exit orifice it flew nearly 200 feet into a patch of dry brush. This started a brush fire which can

Table 4.2: Emergency Shutdown Procedures

1. Kill power to all SOLs.
2. Ensure pressure on PT1 is less than 1500 psi.
3. Close BV 1, BV 2, and BV 3.
4. Close NTV.
5. Release pressure in main assembly by opening NV 2.
6. Release line pressure by opening NV 1.

(a) (b) (c)

Figure 4.6: Sequence of high speed images from one of the hyrdrostatic tests of the safety relief system.

(a) (b)

Figure 4.7: (a) During brush fire caused by ejected piece of igniter. (b) Post fire caused by ejected piece of igniter.

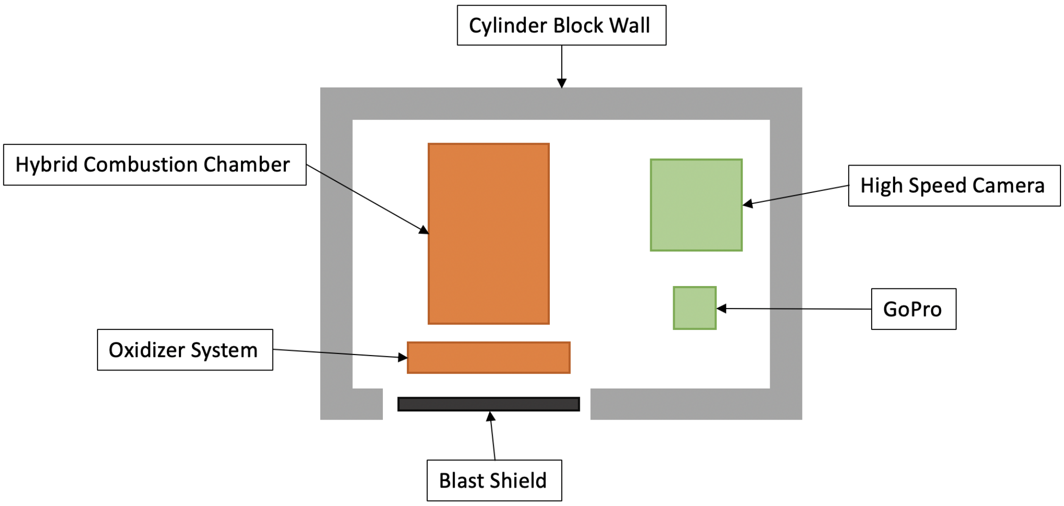

Figure 4.8: Schematic of the Auburn Combustion Physics Lab hot fire test cell for the hybrid rocket motor.

be seen in Figure 4.7. After the fire, the placement of the HRM during testing was reconsidered. It was decided that a cylinder block wall should be built with a opening that would allow for the HRM to be moved into and out of the structure. The opening would be covered by a blast shield during operation. The revised test set-up can be seen in Figure 4.8. After the extensive safety review of the design, test plans, and facilities it was concluded that the commissioning process for the HRM could commence.

Chapter 5

Commissioning

Once the HRM was designed and built, a series of hot fire tests were conducted to test and observe the performance of the HRM over a range of operating conditions. The tests used three different oxidizer injector sizes and two different fuel types. The test matrix is shown in Table 5.1. Six tests were conducted using HDPE and HTPB fuels and 0.05 inch, 0.07 inch, 0.08 inch orifice diameter oxidizer injectors. The three diameters of oxidizer injectors were chosen to give a range of oxidizer flow rate. The three injectors are designed to pass 1.1 gallons per minute, 2.2 gallons per minute, and 3.3 gallons per minute at an operating pressure of 300 pounds per square inch. The HRM is not expected to operate at that high of a pressure so the flow rate is expected to be less than the listed flow rates. Burn time, oxidizer mass flow rate, maximum recorded pressure, and the time at the maximum recorded pressure was collected for each of the six tests.

Table 5.1: Test Matrix

Fuel	Oxidizer Diameter Size (in)	Burn Time (s)	Oxidizer Mass Flow Rate (lb/s)	Maximum Recorded Pressure (psi)	Time at Maximum Recorded Pressure (s)
HTPB	0.05 0.07 0.08				
HDPE	0.05 0.07 0.08				

To set up the hot fire tests the motor was placed in the cinder-block test cell in the arrangement shown in Figure4.8. The test specific fuel grain was placed in the combustion chamber

Table 5.2: Hybrid Rocket Motor Normal Operating Procedure

1. Check sample cylinders for N2O. If empty, go to fill procedure.
2. Set nitrogen pressure on pressure regulator.
3. Ensure all hand-operated valves are closed.
4. Open BV 1.
5. Open BV 3.
6. Pressurize N2O tanks by opening SOL 1.
7. Fire by opening SOL 2 and SOL 3.
8. After run, close SOL 1, SOL 2, and SOL 3.
9. Close BV 1 and BV 3.
10. Vent pressure in main assembly by opening NV 2.
11. Vent pressure in lines by opening NV 1.
12. Close all valves and proceed to fill procedure.

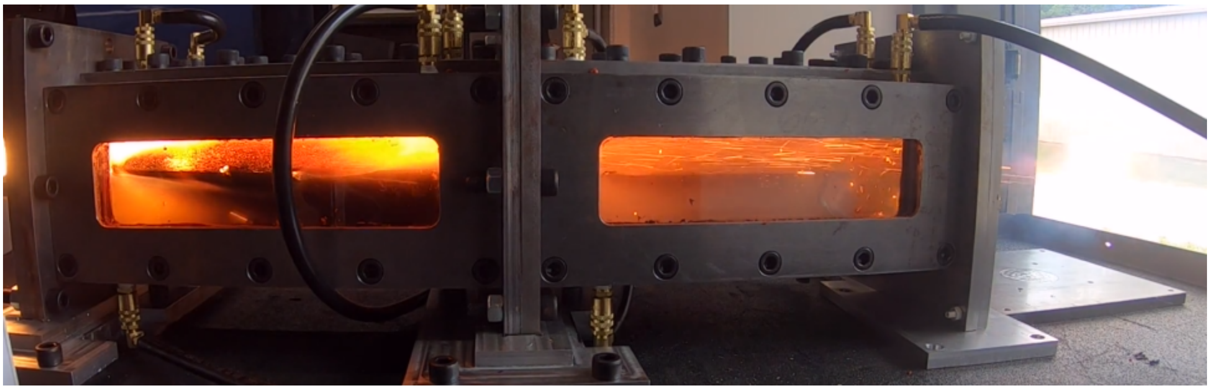

Figure 5.1: First test fire of HRM using air and HTPB

and the test specific oxidizer injector was installed in the forward end of the HRM. All sizes of injectors had a flat spray at an angle of 15 degrees. Water lines were attached to the water cooling system on the HRM, all of the electronics in the nitrous oxide system were connected and powered, and the sample cylinders were filled using the fill procedure outlined in Table 4.1. During testing pressure data was collected using a static pressure transducer, a Photron Fastcam SA-X2 high speed video camera, and a GoPro camera. For each test, pressure and oxidizer weight data was collected at a sample rate of 25000 samples per seconds. The ignition system was wired and armed. To conduct each test, the normal operating procedure outlined in Table 5.2 was followed. The system was controlled using a labVIEW program.

After initial test fires, the motor showed nominal performance. The igniters successfully fired, the fuel grain ignited, and the HRM extinguished when the oxidizer flow was turned off.

Multiple tests were conducted using the same fuel grains showing that relight is possible. The first test fire of the motor used air as the oxidizer and HTPB as the fuel and an image from the test is shown in Figure 5.1.

Chapter 6

Results and Discussion

The following sections show the results and analysis of the six hot fire tests laid out in Table 5.1. The testing focused on two different fuels, HTPB and HDPE, and three different oxidizer orifice diameters, 0.05 inch, 0.07 inch, and 0.08 inch. All hot fire tests were successful in the sense that combustion occurred and performance was nominal. The data from each tests showed a significant amount of noise and each test resulted in over 1,000,000 data points. The noise was most likely due to the high sensitivity of the load cell to vibrations. The oxidizer system was connected to the combustion chamber through a flexible hose. The combustion chamber was sitting on a wheeled cart and the oxidizer system also had wheels. During testing there is a high likelihood that vibrations were transmitted to the oxidizer system through the flexible hose and the vibrations were exacerbated by the fact that the oxidizer system was on wheels, which caused the readings on the load cell to fluctuate and noise to present in the data. To better understand the trend in the data and to reduce the number of data points to a manageable size, the pressure and weight were averaged over the 2500 data points per each 0.1 second. On the graphs below, the averaged data is labeled and shown in red and the raw data is labeled and shown in blue. Each test will be addressed in detail in the following sections. The code used to process the data can be found in Appendix D.

6.1 0.05 Inch Oxidizer Injector With HTPB Fuel

The first test used a 0.05 inch diameter oxidizer injector with HTPB fuel. Figure 5.1 shows the pressure verses time graph and the oxidizer weight verses time graph for the test. From the

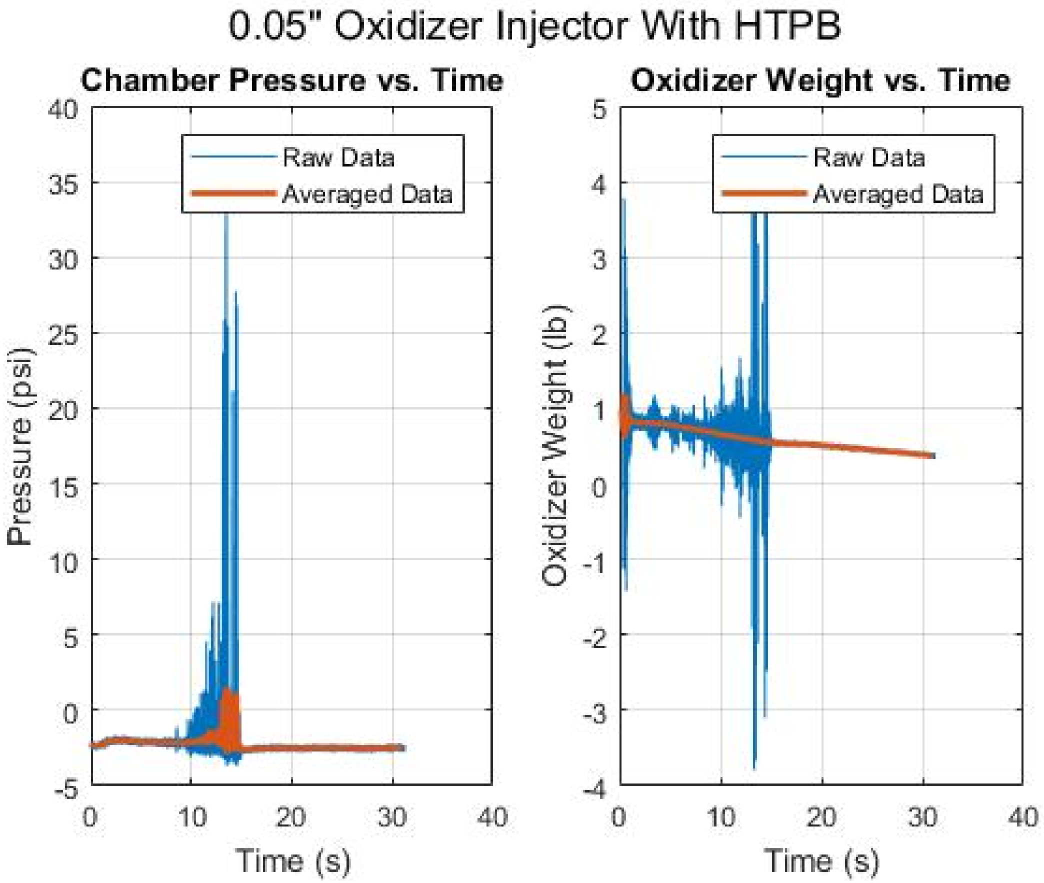

Figure 6.1: Pressure vs. time graph and oxidizer weight vs. time graph of hybrid rocket motor test using 0.05 inch diameter oxidizer injector and HTPB

pressure versus time graph it can be seen that the pressure was fairly consistent until about 12 seconds into the test when it begins to fluctuate and continues to fluctuate until about 15 seconds into the test. During this time pressure spikes occurred with, the maximum pressure of 35.509 pounds per square inch being recorded at 13.466 seconds. Until the pressure fluctuations the combustion looked steady. The solid propellant ignition system lit and when the solenoid valve was opened to allow for the nitrous oxide to flow into the combustion chamber the chamber pressure increased slightly. At around 12 seconds a repeated popping noise was observed. This was thought to be due to the low flow rate of the oxidizer and will be discussed in more depth in later sections.

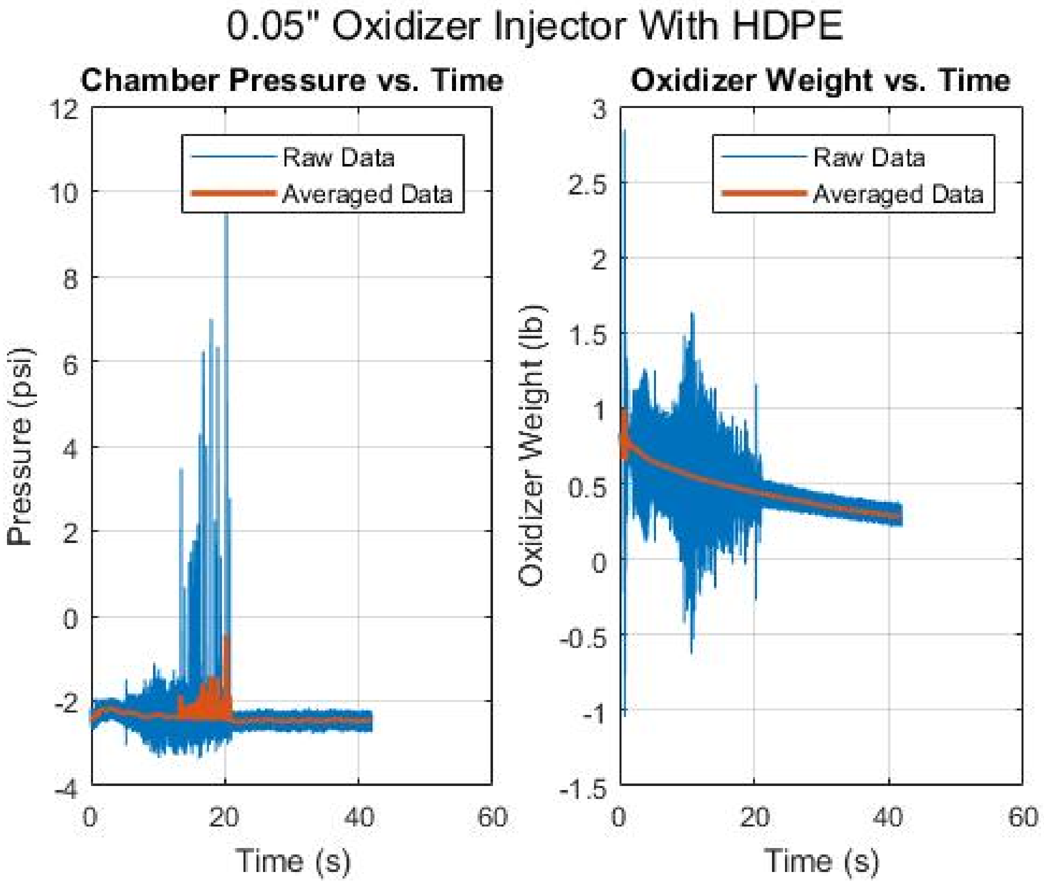

Figure 6.2: Pressure vs. time graph and oxidizer weight vs. time graph of hybrid rocket motor test using 0.05 inch diameter oxidizer injector and HDPE

6.2 0.05 Inch Oxidizer Injector With HDPE Fuel

The second test used the same 0.05 inch diameter oxidizer injector and HDPE as the fuel. Figure 6.2 shows the pressure versus time graph and the oxidizer weight versus time graph. Like the previous test, the pressure at the beginning was fairly constant with a slight increase when the nitrous oxide was first injected into the combustion chamber. Subsequently, at about 5 seconds into the test more noise was recorded in the raw data with pressure spikes being seen in both the raw and averaged data from about 15 to 20 seconds into the test. This aligns with the maximum pressure shown on the graph. The maximum pressure occurs at 10.710 seconds and is 20.262 pounds per square inch. An image of the test fire is shown in Figure 6.3.

At about the 15 second mark the same popping noise that occurred in the previous test was observed. In this case, as in the last test, this was thought to be attributed to the low oxidizer

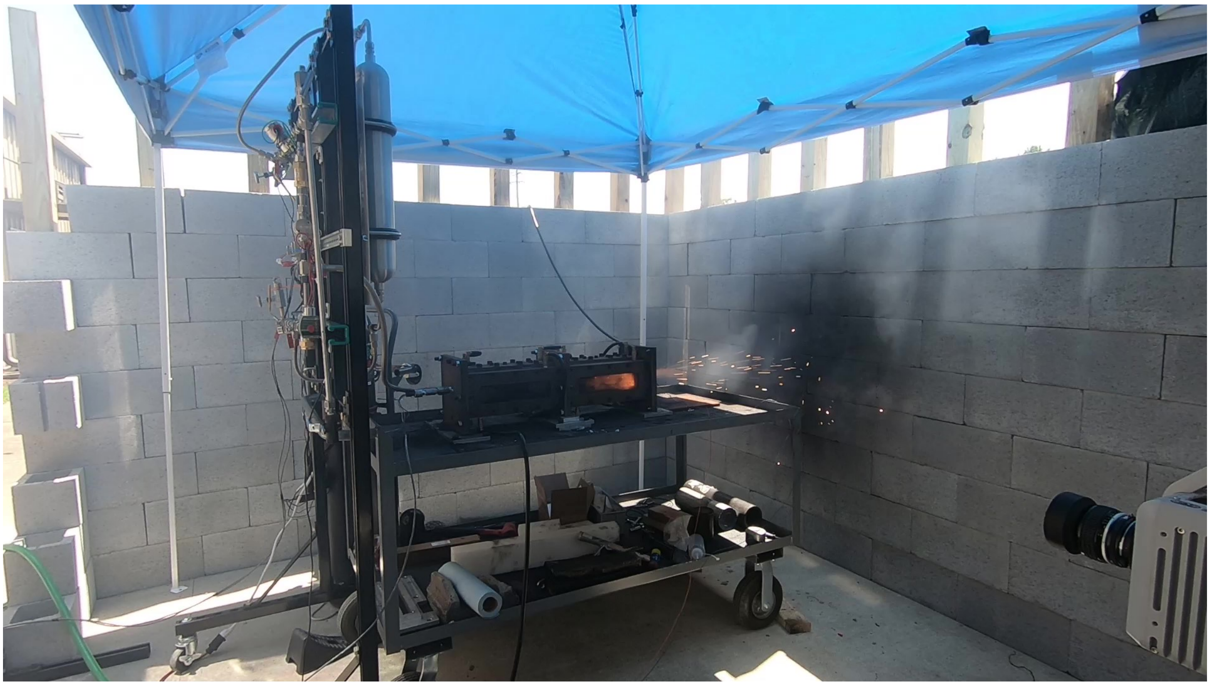

Figure 6.3: Hybrid rocket motor test fire using 0.05 inch diameter oxidizer injector and HDPE

flow rate. The series of images shown in Figure 6.4 and Figure 6.5 show the combustion chamber when the popping noise was occurring. These images overlap the maximum pressure of the test. It can be seen that the combustion chamber goes dark in the first image then fires in the second then goes dark again in the third. The images in Figure 6.4 are taken from GoPro footage and the images in Figure 6.5 are taken from high speed video footage.

6.3 0.07 Inch Oxidizer Injector With HTPB Fuel

The third test used the 0.07 inch diameter oxidizer injector with HTPB fuel. Figure 6.6 shows the pressure versus time graph and the oxidizer weight versus time graph. The pressure versus time graph for this test resembles much more closely a typical pressure curve on a SRM test. The pressure begins low and builds in about the first three seconds after oxidizer is injected into the combustion chamber. The pressure then peaks at about 4 seconds and then drops and levels off. At 5.633 seconds the pressure spikes to 82.020 psi, which is the highest pressure spike of all of the 6 tests. After the pressure spike the pressure levels off again.

(a)

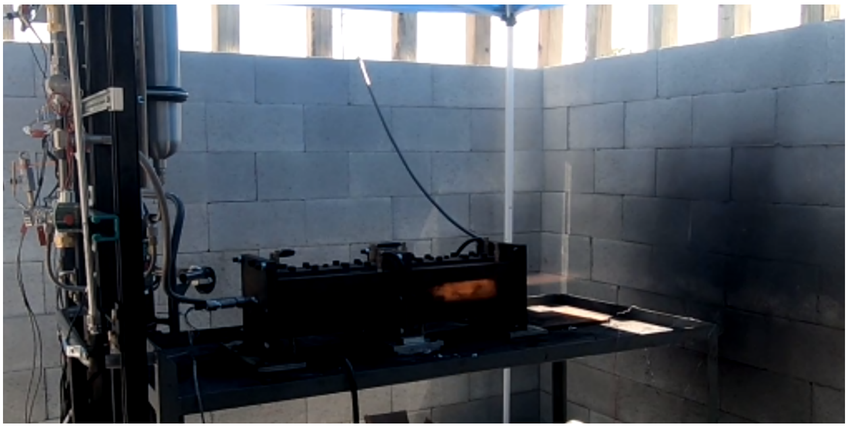

(b)

(c)

Figure 6.4: This series of images shows the combustion chamber of the hybrid rocket motor during the test using a 0.05 inch diameter oxidizer injector and HDPE fuel. The images overlap with the maximum pressure of the test and show the combustion chamber when a popping noise is happening. It can be seen that the combustion chamber goes dark in the first image then fires in the second then goes dark again in the third. The images are taken from GoPro footage.

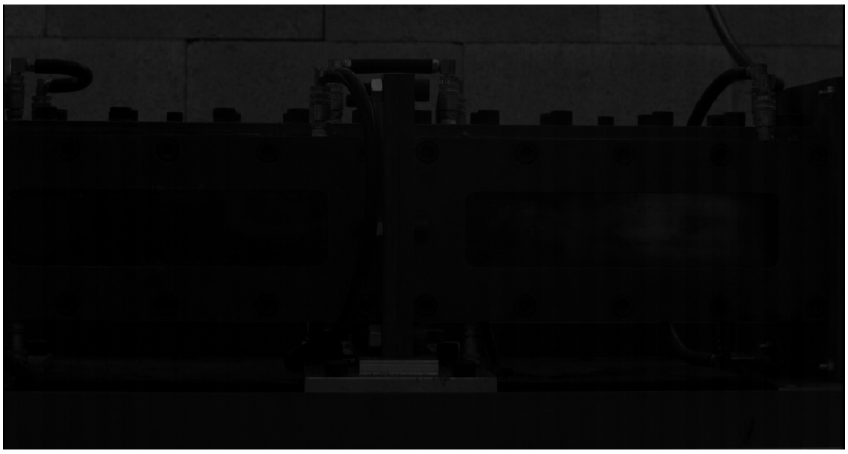

(a)

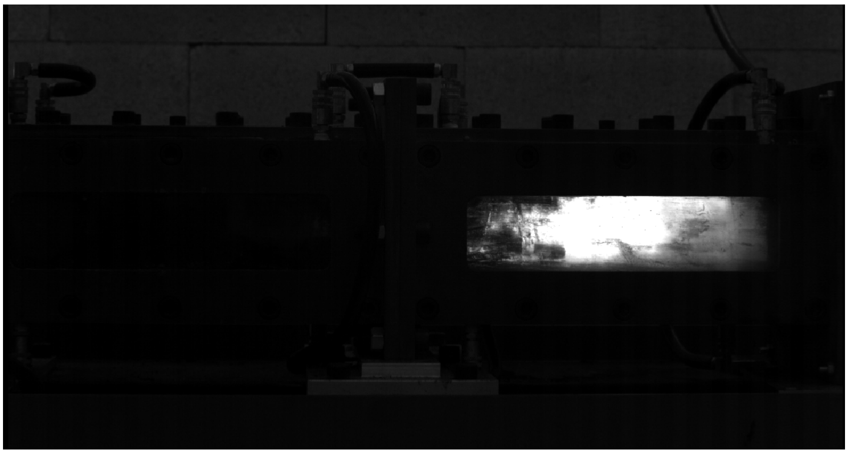

(b)

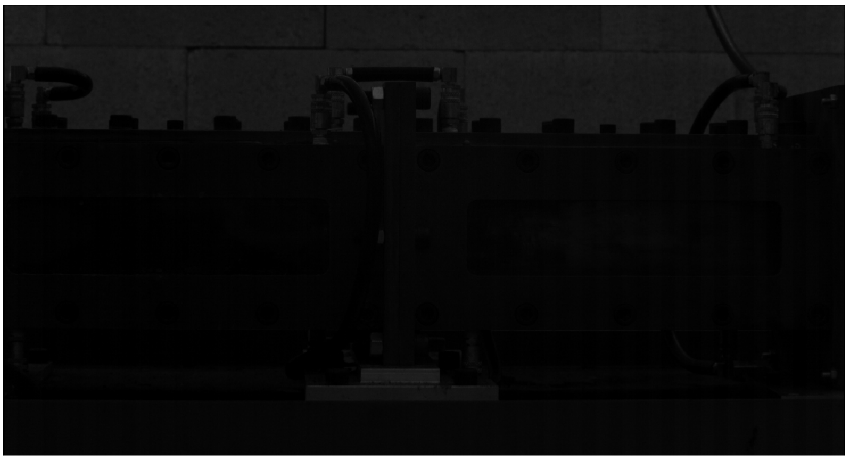

(c)

Figure 6.5: This series of images shows the combustion chamber of the hybrid rocket motor during the test using a 0.05 inch diameter oxidizer injector and HDPE fuel. The images overlap with the maximum pressure of the test and show the combustion chamber when a popping noise is happening. It can be seen that the combustion chamber goes dark in the first image then fires in the second then goes dark again in the third. The images are taken from high speed video footage.

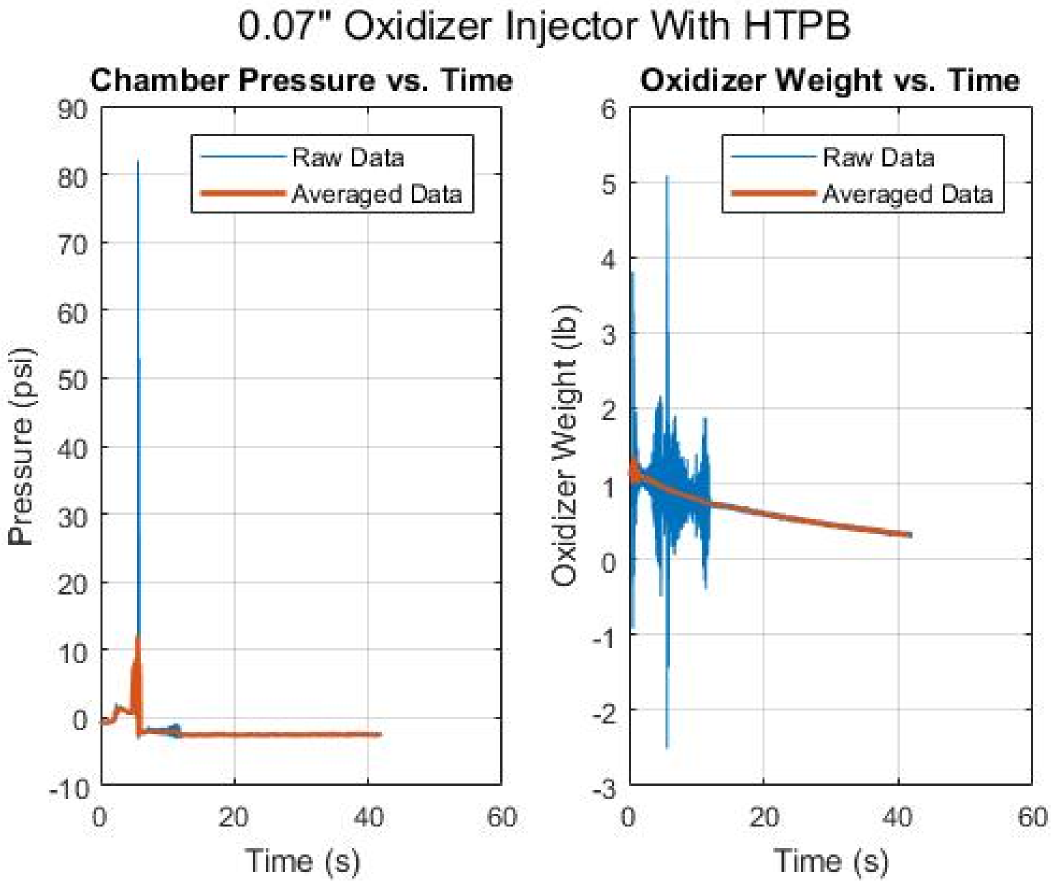

Figure 6.6: Pressure vs. time graph and oxidizer weight vs. time graph of hybrid rocket motor test using 0.07 inch diameter oxidizer injector and HTPB.

The pressure spike was due to the nozzle being clogged. Most likely the clog was caused by a small piece of the solid fuel grain from the igniter or a small chunk of fuel. This phenomenon is called chuffing and is one of the four mechanisms that cause combustion instabilities in HRMs. It is difficult to study because it can be hard to reproduced in a controlled manner. Figure 6.7 shows a series of pictures taken from GoPro footage. Figure 6.8 shows series of pictures from high speed video footage. Both figures show the combustion chamber before, during, and after the chuffing occurs. Unlike the previous two tests the popping noise did not occur in this test. This was likely because the oxidizer flow rate was higher, thus causing more stable combustion.

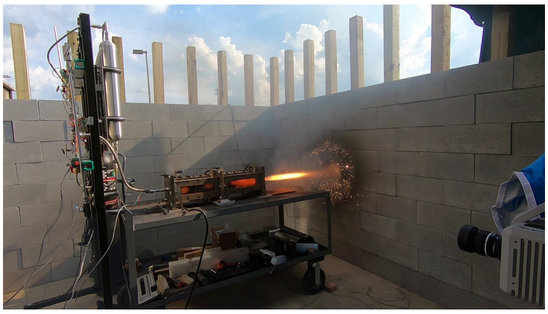

(a)

(b)

(c)

(d)

(e)

(f)

Figure 6.7: This series of images shows the combustion chamber of the hybrid rocket motor during the test using a 0.07 inch diameter oxidizer injector and HTPB fuel. The images overlap with the maximum pressure of the test and show the combustion chamber before, during, and after the chuffing event occurs. The images are taken from GoPro footage.

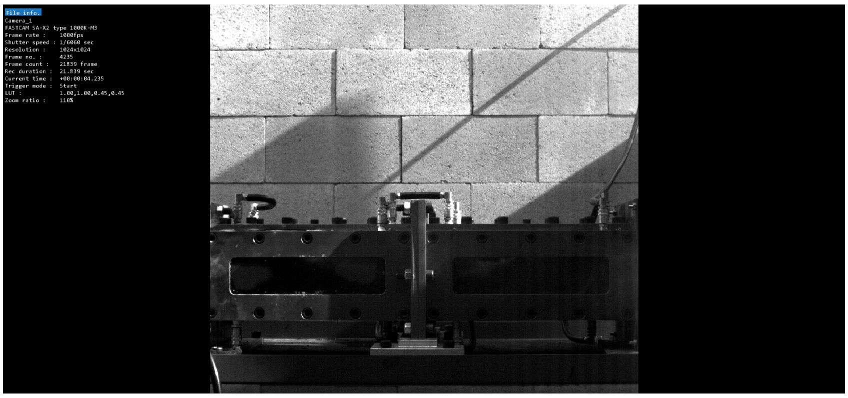

(a)

(b)

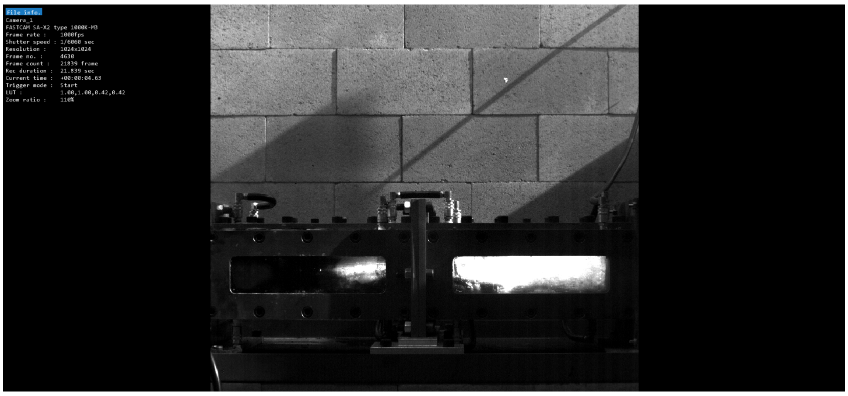

(c)

Figure 6.8: This series of images shows the combustion chamber of the hybrid rocket motor during the test using a 0.07 inch diameter oxidizer injector and HTPB fuel. The images overlap with the maximum pressure of the test and show the combustion chamber during and after the chuffing event occurs. It can be seen that the combustion chamber is dark and then over the next two images returns to nominal operation. The images are taken from high speed video footage.

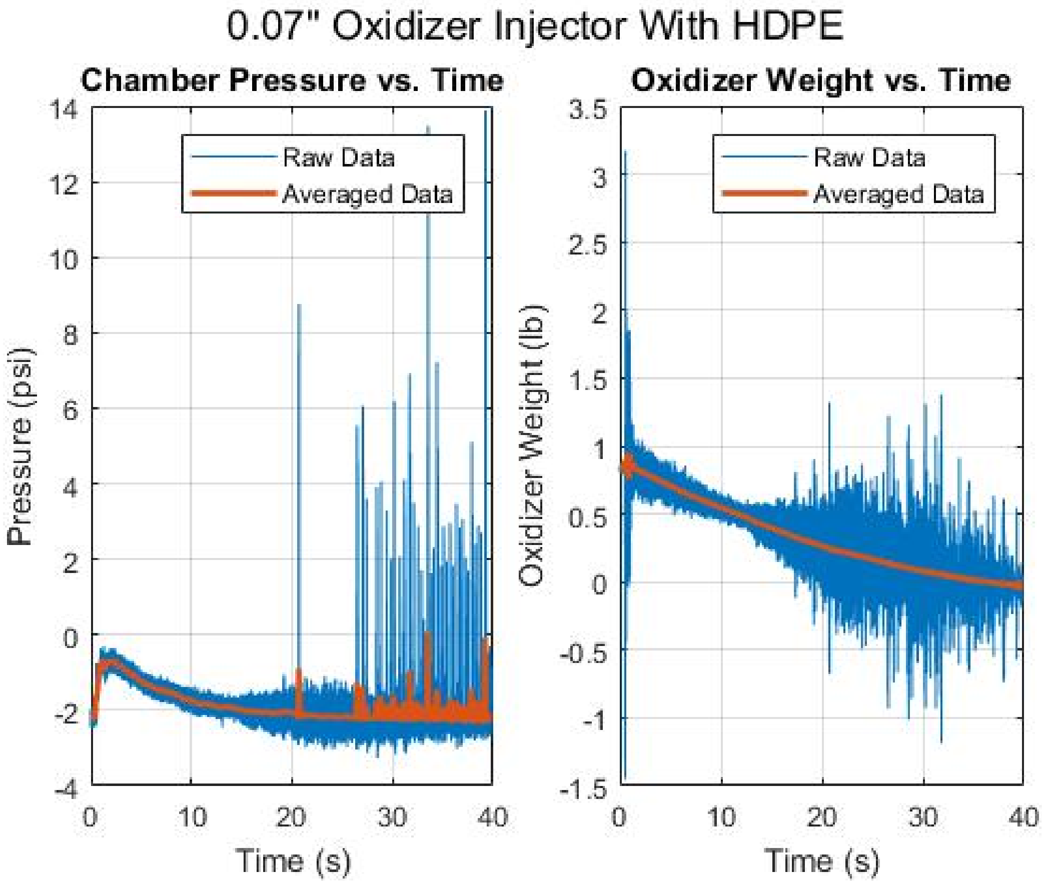

Figure 6.9: Pressure vs. time graph and oxidizer weight vs. time graph of hybrid rocket motor test using 0.07 inch diameter oxidizer injector and HDPE.

6.4 0.07 Inch Oxidizer Injector With HDPE Fuel

The fourth test used the 0.07 inch diameter oxidizer injector with HDPE fuel. Figure 6.9 shows the pressure versus time graph and the oxidizer weight versus time graph. The pressure trace for this test shows a fairly regressive pressure curve. Through most of the burn the flame was very steady with little acoustic noise. This nominal burning can be seen in Figure 6.10. Beginning at about 20 seconds the popping noise observed in the first two tests was also observed in this test. The popping was consistent through the remaining portion of the test and was likely due to there not being the right oxidizer to fuel mixture. The continuous build up and burn of the oxidizer caused pressure spikes with the largest spike occurring at 39.260 seconds and was measured at 13.894 pounds per square inch.

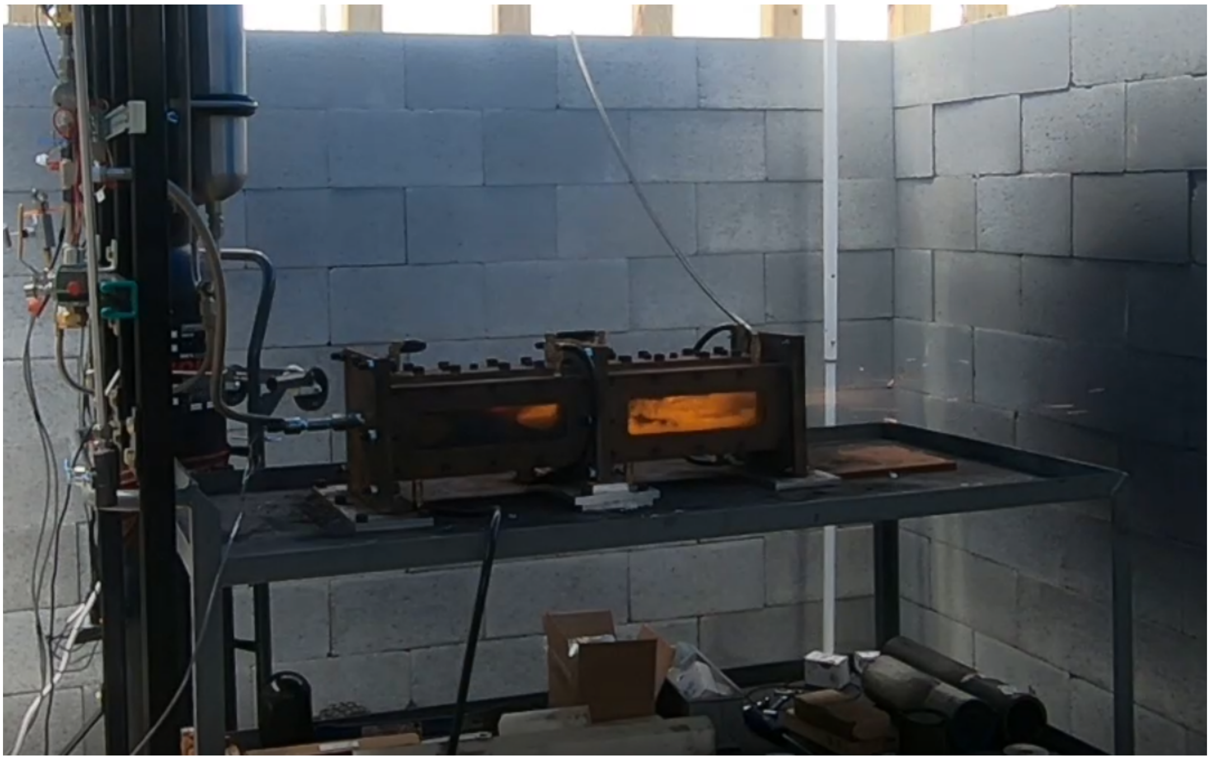

Figure 6.10: Hybrid rocket motor test fire using 0.07 inch diameter oxidizer injector and HDPE. Shows steady flame throughout the first 20 seconds of the test firing.

6.5 0.08 Inch Oxidizer Injector With HTPB Fuel

The fifth test used the 0.08 inch diameter oxidizer injector with HTPB fuel. Figure 6.11 shows the pressure versus time graph and the oxidizer weight versus time graph. The pressure trace for this test saw some of the highest operating pressures of the six tests with the maximum pressure of 28.428 pounds per square inch being reached at 1.439 seconds into the test. The pressure curve was regressive and had little noise compared to the other tests. The oxidizer weight versus time graph shows a lot of noise in the data.

This test had one of the fastest burn times, one of the largest flames, and seemed to burn more steadily than the tests that used the smaller injector diameters. This was likely due to the higher oxidizer flow rate from the larger injector diameter.

6.6 0.08 Inch Oxidizer Injector With HDPE Fuel

The sixth test used the 0.08 inch diameter oxidizer injector with HDPE fuel. Figure 6.12 shows the pressure versus time graph and the oxidizer weight versus time graph. The pressure during

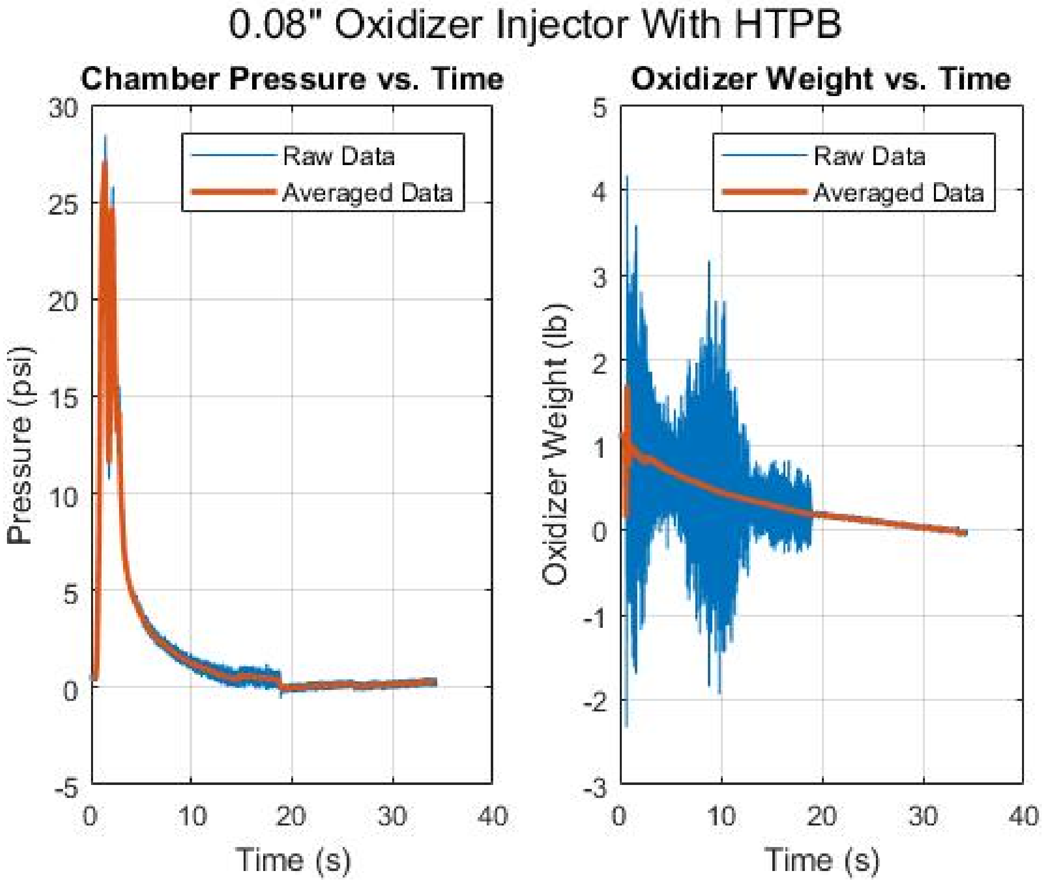

Figure 6.11: Pressure vs. time graph and oxidizer weight vs. time graph of hybrid rocket motor test using 0.08 inch diameter oxidizer injector and HTPB.

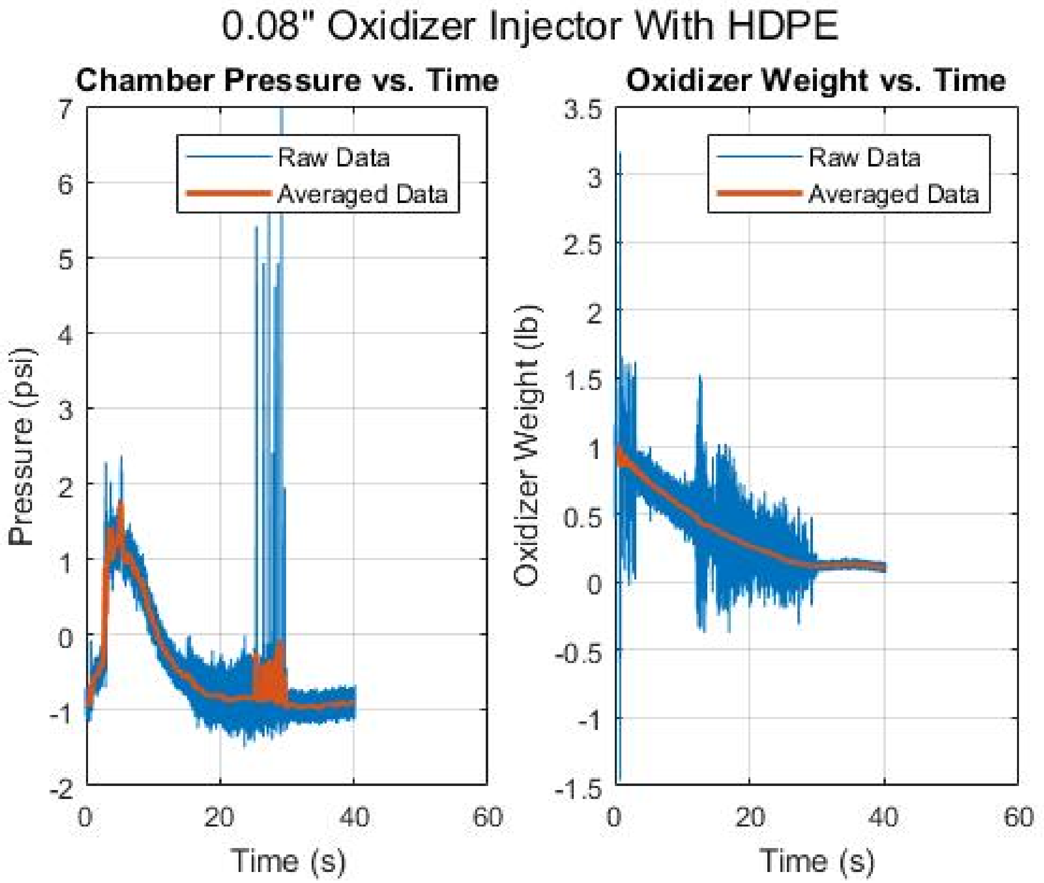

Figure 6.12: Pressure vs. time graph and oxidizer weight vs. time graph of hybrid rocket motor test using 0.08 inch diameter oxidizer injector and HDPE.

this test built over the first five seconds after the oxidizer was injected into the combustion chamber. The pressure then began to decline indicating a regressive pressure trace. At about 17 seconds, more noise began to show in the data, which is indicated on both the pressure versus time graph and the oxidizer weight versus time graph. This was likely due to an insufficient supply of oxidizer to the combustion process, which likely caused the combustion to extinguish and reignite leading to pressure spikes. The highest pressure spike shown occurred at 29.190 seconds and was 6.975 pounds per square inch.

Overall, this test had a very steady burn with a consistent flame, which can be seen in Figure 6.13. This was likely do to the higher oxidizer flow rate from the largest injector diameter tested.

Figure 6.13: Hybrid rocket motor test fire using 0.08 inch diameter oxidizer injector and HDPE. Shows steady flame throughout the first 20 seconds of the test firing.

6.7 Discussion and Comparison

The following section will discuss the popping noise observed during some of the tests, the differences between the observed performance and the MATLAB model predictions, and the differences seen over the six tests using the two different fuels and three different diameters of oxidizer injectors.

The popping noise observed in some of the tests was thought to be due to the diminished flow rate of the oxidizer over the burn caused by the tanks not being back pressuirzed by nitrogen. When there was not enough nitrous oxide combustion would stop and once enough nitrous oxide built up, combustion occurred causing the repetitive popping noise. Another thoery is that the popping noise was the nitrous oxide decomposing. If this theory is true, then the popping could lead to the pipes exploding. Back pressurizing the tanks with nitrogen and imediately after conducting a test running a nitrogen purge will help keep the flow of nitrous oxide consistent and not allow for the decomposition of nitrogen to occur in the pipping system.

The MATLAB models outputs shown in Table 3.3 do not exactly match the data obtained from the hot fire testing. On top of imaging, only burn time, oxidizer mass flow rate, and pressure was collected during the testing. Table 6.1 shows the burn time and oxidizer mass flow rate from the six hot fire tests. The burn time of each of the six hot fire tests fell between 31 and 42 seconds, which is comparable to the MATLAB predicted maximum burn time of about 41 seconds. The oxidizer mass flow rate predicted by the MATLAB code was 0.635 pounds per second. This is significantly higher then the oxidizer flow rates observed during the hot fire tests. For the six experimental tests the oxidizer flow rate was between 0.0124 and 0.0334 pounds per second. However, the MATLAB model was build around a desired thrust imputed by the user whereas the experimental tests the oxidizer flow rate was set by the injector size making the two parameter incomparible.

Table 6.1: Test Results

Fuel	Oxidizer Diameter Size (in)	Burn Time (s)	Oxidizer Flow Rate (lb/s)
HTPB	0.05	31.0	0.0180
	0.07	41.7	0.0198
	0.08	34.2	0.0334
HDPE	0.05	31.0	0.0124
	0.07	39.7	0.0226
	0.08	40.0	0.0219

Table 6.2 shows the maximum pressure observed during each of the six hot fire tests and the time at, which the pressure was recorded. The test fires using HTPB fuel showed higher pressure spikes at earlier points in the burn compared to the tests using HDPE. The reason for this difference is not understood and should be further investigated to see if these results are repeated and if so to better explain the reasoning for them.

Table 6.2: Pressure Spikes

Fuel	Oxidizer Diameter Size (in)	Time (s)	Maximum Pressure (psi)
HTPB	0.05	13.466	35.509
	0.07	5.633	82.020
	0.08	1.439	28.428
HDPE	0.05	20.262	10.710
	0.07	39.260	13.894
	0.08	29.190	6.975

The three oxidizer injector sizes did show differences. The 0.05 inch diameter injectors had very short steady burn times and resulted repeated ignition and extinguishing of the flame make a loud popping noise. The 0.07 inch diameter injector shared similarities to both the 0.05 inch diameter injector and the 0.08 inch diameter injector. The burn was steady at the beginning like the 0.08 diameter injector but ended in the same popping noises as the 0.05 inch diameter injector. The 0.08 inch diameter injector resulted in the most steady and energetic burn. This indicates that higher oxidizer flow rate leads to better combustion, which is expected.

Chapter 7

Conclusions and Future Work

HRMs are a compelling alternative to LREs and SRMs due to their relative low cost, safety, simplicity, high I_{sp}, relight, and throttle capabilities. Traditional HRM polymer fuels have low regression rates, meaning the rate at which the fuel is melted, evaporated, and mixed is slow. This had led to to mediocre performance deterring investment to further the technology. However, in recent years high regression rate liquefying fuels, such as paraffin, have been developed making HRMs a viable propulsion option as long as the TRL increases.

In order to increase the TRL of HRMs, the performance and reliability needs to be well understood. To contribute to this effort the AUCPL developed a two dimensional, optically accessible, HRM. The HRM was designed for versatility and can be used with different fuels, oxidizer injector sizes, and the combustion chamber length can be changed. The AUCPL's HRM has been proven to operate at a range of condition repeatably, which opens the opportunity for new research areas.

The first area of future work is for the AUCPL's HRM is to repeat testing described in the commissioning section in order to observe if the same results occur. Both the MATLAB and COMSOL models require further improvements. The MATLAB model should reflect the process outlined in section 2.2.1 of this thesis. This change will allow the performance to be calculated based on the inputted oxidizer flow rate instead of an inputted thrust. This change will allow the model to more accurately reflect the experiment. In future testing it will be imperative to instrument the HRM with a load cell and dynamic pressure transducers to have the data from the test better reflect the outputs from the MATLAB model. This work will allow for more accurate predictions of HRM performance.

Future work should be focused on identifiying the cause of the popping phenomenon observed in some of the testing. This can be done by attaching a flow meter and a pressure gauge to the outlet of the oxidizer system upstream of the combustion chamber. Then the sample cylinders should be filled and empited in both cold flow and hot fire tests. The flow rates and pressures should be recorded to identify if pressure or flow rate change significantly as the sample cylinders are empitied. The nitrogen system should also be incorporated so that the sample cylinders can be back puessurized during testing and a nitrogen purge of the system can be conducted imediately after each test.

The results from these experiments showed that the size of the oxidizer injector plays a large role in the stability of the combustion. Because of this, a proposed area of future work would be to find the optimal flow rate of oxidizer into the combustion chamber. This work can be done by testing a larger range of oxidizer orifice diameters and observe the results.

In the intial testing, the tests using HTPB saw higher maximum pressures much earlier in the burn compared to the tests using HDPE. The reason for this is not well understood. A repeatability study should be conducted to see if the results are similar. This testing should be fully instrumented with a load cell and dynamic pressure transducers so that more parameters can be observed to see if they change with the different fuels. HDPE and HTPB are both polymers and they are both commonly used in HRM designs so understanding the difference in performance could have large implications on laboratory HRM testing.

Since regression rate is such an important factor in advancing the TRL of HRMs, further research to better understand high regression rate liqufying fuels is needed. The AUCPL HRM provides an excellent test bed to conduct a study that compares liquefying fuels, such as paraffin, to polymer fuels, such as HDPE and HTPB. Liquefying fuels have a higher regression rates and therefore better performance than polymer fuels. The study should focus on the stability of the burn for each fuel since this has not been well studied for paraffin in the past.

In the development of most high pressure combustion systems CIs often occur and for HRMs it is no different. HRMs have four unique mechanisms that drive CI; oxidizer vaporization, chuffing, pressure coupled regression, and vortex shedding. Of the four mechanisms that cause CIs in HRMs, vortex shedding is the least understood and the easiest to replicate in a laboratory environment. Delving into the stability of HRM combustion is a logical path for the AUCPL's HRM. In order to look into vortex shedding further, conditions that cause vortex shedding will need to be identified. High speed imaging analysis techniques such as the ones presented by Petrarolo and Kobald [5] and plenoptic imaging could be used to better understand the consequences of vortex formation. These techniques enable viewing of the formation and effect of the vortices and could even allow for unrolling the vortices during data analysis. Applying data reduction techniques across the entire suite of data could also help to provide quantitative information about the acoustic instabilities developing in the data.

This project has the potential to impact the rocket propulsion field by providing unique optical research on HRMs. The two dimensional, optically accessible HRM is a fairly novel idea, with only a few other groups attempting the design. This allows for the AUCPL to find a niche to contribute to the HRM community in a meaningful way.

References

[1] A. Chandler, E. Jens, B. J. Cantwell, and G. S. Hubbard, "Visualization of the liquid layer combustion of paraffin fuel for hybrid rocket applications," *48th AIAA/ASME/SAE/ASEE Joint Propulsion Conference & Exhibit AIAA 2012-3961*, p. 11, 2012.

[2] L. Fanton, C. Paravan, and L. T. De Luca, "Testing and modeling fuel regression rate in a miniature hybrid burner," *International Journal of Aerospace Engineering*, vol. 2012, 2012.

[3] E. Jens, V. Miller, F. Mechentel, B. Cantwell, and G. Hubbard, "Visualisation of combustion in a turbulent boundary layer over a melting fuel," *Proceedings of the 19th Australasian Fluid Mechanics Conference, AFMC 2014*, pp. 8–11, 2014.

[4] E. T. Jens, P. Narsai, B. Cantwell, and G. S. Hubbard, "Schlieren imaging of the combustion of classical and high regression rate hybrid rocket fuels," *50th AIAA/ASME/SAE/ASEE Joint Propulsion Conference*, pp. 1–8, 2014.

[5] A. Petrarolo and M. Kobald, "Evaluation techniques for optical analysis of hybrid rocket propulsion," *Journal of Fluid Science and Technology*, vol. 11, no. 4, pp. JFST0028–JFST0028, 2016.

[6] A. Mazzetti, L. Merotto, and G. Pinarello, "Paraffin-based hybrid rocket engines applications: A review and a market perspective," *Acta Astronautica*, vol. 126, pp. 286–297, 2016-09.

[7] N. Davydenko, R. Gollender, A. Gubertov, V. Mironov, and N. Volkov, "Hybrid rocket engines: The benefits and prospects," *Aerospace Science and Technology*, vol. 11, no. 1, pp. 55–60, 2007-01.

[8] A. Okninski, "On use of hybrid rocket propulsion for suborbital vehicles," *Acta Astronautica*, vol. 145, pp. 1–10, 2018-04.

[9] G. P. Sutton and O. Biblarz, *Rocket Propulsion Elements*. John Wiley & Sons, Inc., 7 ed., 2001.

[10] A. Fraters and A. Cervone, "Experimental characterization of combustion instabilities in high-mass-flux hybrid rocket engines," *Journal of Propulsion and Power*, vol. 32, no. 4, pp. 958–966, 2016.

[11] B. Cantwell, A. Karabeyoglu, and D. Altman, "RECENT ADVANCES IN HYBRID PROPULSION," *International Journal of Energetic Materials and Chemical Propulsion*, vol. 9, no. 4, pp. 305–326, 2010.

[12] F. Piscitelli, G. Saccone, A. Gianvito, G. Cosentino, and L. Mazzola, "Characterization and manufacturing of a paraffin wax as fuel for hybrid rockets," *Propulsion and Power Research*, vol. 7, no. 3, pp. 218–230, 2018-09.

[13] B. Greiner and J. Frederick, R., "Hybrid rocket instability," in *29th Joint Propulsion Conference and Exhibit*, Joint Propulsion Conferences, American Institute of Aeronautics and Astronautics, 1993-06-28.

[14] R. Jenkins and J. Cook, "A preliminary analysis of low frequency pressure oscillations in hybrid rocket motors," in *31st Joint Propulsion Conference and Exhibit*, Joint Propulsion Conferences, American Institute of Aeronautics and Astronautics, 1995-07-10.

[15] F. Barato, N. Bellomo, and D. Pavarin, "Integrated approach for hybrid rocket technology development," *Acta Astronautica*, vol. 128, pp. 257–261, 2016-11.

[16] B. Cantwell, *Aircraft and Rocket Propulsion*. Sanford University, 2019.

[17] D. Altman, "Overview and history of hybrid rocket propulsion," *Progress in Astronautics and Aeronautics*, vol. 207, pp. 1–36, 2007.

[18] F. E. C. Culick, "Combustion instabilities in solid propellant rocket motors," *Internal Aerodynamics in Solid Rocket Propulsion*, 2002.

[19] K. Schadow and E. Gutmark, "Combustion instability related to vortex shedding in dump combustors and their passive control," *Progress in Energy and Combustion Science*, vol. 18, no. 2, pp. 117–132, 1992-01.

[20] R. Chanaud, "Aerodynamic whistles," *Scientific American*, vol. 222, no. 1, pp. 40–47, 1970.

[21] J. W. S. B. Rayleigh, *The theory of sound*. Macmillan, 1896.

[22] D. W. Netzer, "Hybrid rocket internal ballistics," *Calhoun: The Naval Postgraduate School Institutional Archive*, p. 65, 1972.

[23] M. Rocker, "Simulation of non-acoustic combustion instability in a hybrid rocket motor," *NASA Technical Reports Server*, pp. 1–17, 1999.

[24] J. Majdalani and A. Vyas, "Rotational axisymmetric mean flow for the vortex injection hybrid rocket engine," in *40th AIAA/ASME/SAE/ASEE Joint Propulsion Conference and Exhibit*, American Institute of Aeronautics and Astronautics, 2004-07-11.

[25] K. Ozawa and T. Shimada, "Theoretical prediction of regression rates in swirl-injection hybrid rocket engines," *Progress in Propulsion Physics*, vol. 8, pp. 283–306, 2016.

[26] S. Venkateswaran and C. L. Merkle, "Combustion processes in hybrid rocket engines," *NASA Technical Reports*, pp. 1313–1336, 1996.

[27] T. V. Chelaru and F. Mingireanu, "Hybrid rocket engine, theoretical model and experiment," *Acta Astronautica*, vol. 68, no. 11, pp. 1891–1902, 2011.

[28] H. Tian, X. Li, and G. Cai, "Ignition theory investigation and experimental research on hybrid rocket motor," *Aerospace Science and Technology*, vol. 42, pp. 334–341, 2015.

[29] M. Lieberbaum, W. Jefferson, M. Rottenberg, and D. Scarborough, *Hazard Ops Presentation*. 2003.

[30] O. Krauss, "Design and test of a lab-scale n2o/HTPB hybrid rocket," *Impulse*, pp. 1–11, 2003.

[31] B. Greiner and R. Frederick, Jr., "Results of labscale hybrid rocket motor investigation," in *28th Joint Propulsion Conference and Exhibit*, American Institute of Aeronautics and Astronautics, 1992-07-06.

[32] G. Vidya, U. Grover, and S. A. Hasim, "Design, modelling, fabrication and testing of hybrid rocket engine and evaluation of burning rate for different solid fuels," *International Journal of Advances in Scientific Research and Engineering*, vol. 3, no. 2, pp. 2–712, 2016.

[33] A. Karabeyoglu, J. Stevens, D. Geyzel, B. Cantwell, and D. Micheletti, "High performance hybrid upper stage motor," in *47th AIAA/ASME/SAE/ASEE Joint Propulsion Conference & Exhibit*, American Institute of Aeronautics and Astronautics, 2011-07-31.

[34] J. Gracy, "Restart capabilities of hybrid rocket motor utilizing gaseous propane and oxygen injection system," *University of Arkansas, Fayetteville*, 2008.

[35] S. A. Whitmore and D. P. Merkley, "Arc-ignition of a 70%-85% hydrogen peroxide/ABS hybrid rocket system," *53rd AIAA/SAE/ASEE Joint Propulsion Conference*, pp. 1–26, 2017.

[36] C. R. Potter, "Design of economical upper stage hybrid rocket engine," *University of Tenneesee, Knoxville*, 2013.

[37] K. Platt, "Design and fabrication of a full-featured labscale hybrid rocket engine," *University of Central Florida*, 2006.

[38] R. Mulato, J. Baillargeon, J. DAmato, K. Etienne, R. Kuhns, G. Lucas, D. J. Kozak, and D. D. Patru, "System optimization of a hybrid rocket," *Multi-Disciplinary Engineering Design Conference*, p. 8, 2007.

[39] Z. Arena, A. Athougies, A. Rodulfo, A. Athougies, and D. Deturris, “Hybrid rocket motor,” *California Polytechnic State University, San Luis Obispo*, 2010.

[40] M. H. Summers, J. D. Dennis, and J. K. Villarreal, “Small-scale hybrid rocket test stand & characterization of swirl injectors,” in *49th AIAA/ASME/SAE/ASEE Joint Propulsion Conference*, American Institute of Aeronautics and Astronautics, 2013-07-14.

[41] B. S. Waxman, J. E. Zimmerman, B. J. Cantwell, and N. Ames, “Mass flow rate and isolation characteristics of injectors for use with self-pressurizing oxidizers in hybrid rockets,” *49th AIAA/ASME/SAE/ASEE Joint PropulsionConference AIAA 2013-3636*, pp. 1–32, 2013.

[42] P. Lemieux, “Nitrous oxide cooling in hybrid rocket nozzles,” *Progress in Aerospace Sciences*, vol. 46, no. 2, pp. 106–115, 2010.

[43] R. D. Swami and A. Gany, “Analysis and testing of similarity and scale effects in hybrid rocket motors,” *Acta Astronautica*, vol. 52, no. 8, pp. 619–628, 2003.

[44] K. Johnson, J. Chiaverini, K. Kuo, C. Harting, and T. Pennsylvania, “Fundamental phenomena on fuel decomposition and boundary-layer combustion processes with application to hybrid rocket motors,” *AIAA*, 1995.

[45] R. J. Ier, G. A. Marxman, and C. E. Wooldridge, “Investigation of combustion instability in hybrid rockets final report,” *Experimental and model studies of combustion instability in hybrid rocket propellants in pressure sensitive regime*, pp. 1–66, 1969.

[46] G. A. Marxman, C. E. Wooldridge, and R. J. Muzzy, “Fundamentals of hybrid boundary-layer combustion,” in *Heterogeneous Combustion* (H. G. Wolfhard, I. Glassman, and L. Green, eds.), vol. 15 of *Progress in Astronautics and Rocketry*, pp. 485 – 522, Elsevier, 1964.

[47] G. Marxman and M. Gilbept, “TURBULENT BOUNDARY LAYER COMBUSTION IN THE HYBRID ROCKET,” *International Symposium on Combustion*, vol. 9, pp. 371–383, 1963.

[48] D. R. Greatrix, "Regression rate estimation for standard-flow hybrid rocket engines," *Aerospace Science and Technology*, vol. 13, no. 7, pp. 358–363, 2009.

[49] S. D. Eilers, "Correlation of hybrid rocket propellant regression measurements with enthalpy-balance model predictions," *Journal of Spacecraft and Rockets*, p. 14, 2008.

[50] J. Y. Lestrade, J. Anthoine, and G. Lavergne, "Modeling of liquefying fuel regression rates in hybrid propulsion," *5th European Conference for Aerospace Sciences (EUCASS)*, pp. 1–9, 2013.

[51] L. T. DeLuca, L. Galfetti, G. Colombo, F. Maggi, A. Bandera, M. Boiocchi, G. Gariani, L. Merotto, C. Paravan, and A. Reina, "Time-resolved burning of solid fuels for hybrid rocket propulsion," *Progress in Propulsion Physics*, vol. 2, pp. 405–426, 2011.

[52] K. Boughaba, P. Hendrick, N. Lebrun, M. Lefebvre, and C. Van De Velde, "Regression rate study in a small hybrid rocket engine using n 2 o / paraffin propellant," *9th National Congress on Theoritical and Applied Mechanics*, pp. 9–10, 2012.

[53] D. Porrmann, J. Wilken, O. Bozic, and D. Lancelle, "First results of regression rate measurements on ultrasonic basis in the AHRES hybrid rocket motor," *Space Propulsion 2014*, pp. 1–7, 2014.

[54] A. R. Sorge and C. Carmicino, "Non-intrusive regression rate measurements in a hybrid rocket," *5th European Conference for Aeronautics and Space Sciences*, pp. 23–26, 2002.

[55] R. Kumar and P. A. Ramakrishna, "Measurement of regression rate in hybrid rocket using combustion chamber pressure," *Acta Astronautica*, vol. 103, pp. 226–234, 2014.

[56] S. C. Shark, C. R. Zaseck, T. L. Pourpoint, and S. F. Son, "Solid-fuel regression rates and flame characteristics in an opposed flow burner," *Journal of Propulsion and Power*, vol. 30, no. 6, pp. 1675–1682, 2014.

[57] S. A. Whitmore, S. D. Walker, D. P. Merkley, and M. Sobbi, "High regression rate hybrid rocket fuel grains with helical port structures," *Journal of Propulsion and Power*, vol. 31, no. 6, pp. 1727–1738, 2015.

[58] D. Pastrone, “Approaches to low fuel regression rate in hybrid rocket engines,” *International Journal of Aerospace Engineering*, vol. 2012, 2012.

[59] E. A. Alkuam and W. M. Alobaidi, “Experimental and theoretical research review of hybrid rocket motor techniques and applications,” *Advances in Aerospace Science and Technology*, vol. 01, no. 3, pp. 71–82, 2016.

[60] M. Karabeyoglu, B. Cantwell, and D. Altman, “Development and testing of paraffin-based hybrid rocket fuels,” *37th Joint Propulsion Conference and Exhibit*, 2001.

[61] E. Doran, J. Dyer, K. Lohner, Z. Dunn, B. Cantwell, and G. Zilliac, “Nitrous oxide hybrid rocket motor fuel regression rate characterization,” *43rd AIAA/ASME/SAE/ASEE Joint Propulsion Conference & Exhibit*, 2007.

[62] L. Galfetti and M. Khattab, “Innovative solid fuels for hybrid rocket propulsion,” *3rd European Conference for Aerospace Sciences*, pp. 1–34, 2011.

[63] K. Ramohalli and J. Yi, “Hybrids revisited,” in *26th Joint Propulsion Conference*, American Institute of Aeronautics and Astronautics, 1990-07-16.

[64] A. B. Wright, J. E. Elsasser, M. K. Hudson, and A. M. Wright, “Optical studies of combustion chamber flame in a hybrid rocket motor,” *Design*, no. 21, pp. 21–30, 2005.

[65] R. Humble, G. Henry, and W. Larson, *Space Propulsion Analysis and Design*. Learning Solutions, 1st ed., 2007.

[66] Z. Thicksten, F. Macklin, and J. Campbell, “Handling considerations of nitrous oxide in hybrid rocket motor testing,” *AIAA*, 2008.

Appendices

Appendix A

MATLAB Hybrid Model Code

```
% Updated May 17, 2019
%
% This script will calculate design parameters for known design constraints
% for a single port slab hybrid rocket engine. User can vary the following:
%
% pe = ambient pressure
% pc = chamber pressure
% OF = oxidiser/fuel ratio
% Ft = thrust force
% Ri = inner radius of fuel grain
% Rf = outer radius of fuel grain
% L = fuel grain length
% Tc = adiabatic flame temperature
% R = gas constant of oxidiser
% roe_fuel = density of fuel grain
% g = acceleration due to gravity
% gamma = ratio of specific heats
% a = regression rate coefficient
% n = regression rate exponent
% t = vector of times, start at 0

%clear command window
clear
clc
close all

% Global parameters
pe = 14.7; % psia
Tc = 5276; % R
R = 35.1; % (lbf*ft)/(lbm*R)
roe_fuel = 0.035; % lb/in^3
```

```
g = 32.2; % ft/s^2
gamma = 1.144;
a = .1160;
n = .9874;
t = linspace(0,60,100); % s

%system parameters
% Engine Variables
pc = 100; % psia
L = 29; % in
OF = 8;
Ft = 100; % lb
Ri = 0.75; % in
Rf = 1.5; % in


% Calculations
% Thrust coefficient
Cf =sqrt(((2.*(gamma.^2))./(gamma-1)).*((2./(gamma+1)).^((gamma+1)...
    ./(gamma-1))).*(1-((pe./pc).^((gamma-1)./gamma))));

% Required throat area and diameter
At = Ft./(Cf.*pc);
Dt = sqrt((4.*At)./pi);

% Mass flow of the system
mdotsys = (At.*pc.*gamma.*((sqrt((2./(gamma+1)).^((gamma+1)./(gamma-1)))))...
    ./(sqrt(Tc.*gamma.*R)))).*sqrt(32.2);

% Mass flow rates of fuel and oxidiser
mdotfuel = mdotsys./(OF+1);
mdotox = (mdotsys - mdotfuel);

% Nozzle expansion ratio
Ep = ((((gamma+1)./2).^(1./(gamma-1))).*((pe./pc).^(1./gamma))...
    .*sqrt(((gamma+1)./(gamma-1)).*(1-(pe./pc).^((gamma-1)./gamma))))).^-1;

% Nozzle exit area and diameter
Ae = At.*Ep;
De = sqrt((4.*Ae)./pi);

% Combustion port burn diameter as a function of time
```

```
Db_t = ((a.*t.*((4.*n)+2).*(((4.*mdotox)./pi).^n))+((2.*Ri)
    .^(2.*n+1))).^(1./(2.*n+1));

% Regression rate as a function of time
rdot_t = a.*(((4.*mdotox)./(pi.*(Db_t.^2))).^n);

% Optimal length of fuel grain
Lo = (mdotfuel./(roe_fuel.*rdot_t(1).*2.*pi.*Ri));

% Mass flow of fuel as a function of time
mdotfuel_t = roe_fuel.*rdot_t.*L.*2.*pi.*(Db_t./2);

% OF ratio as a function of time
OF_t = mdotox./mdotfuel_t;

% Mass flow of the system as a function of time
mdotsys_t = mdotox + mdotfuel_t;

%% -------------Calculating Area of injector-------------
press = 20:10:1000;
cd = 0.65;
filename = ('N2Otable.xlsx');
P1 = 900;
P2 = 100;

% Read in spreadsheet data
h_liq = xlsread(filename,'Sheet1','X4:X102');
h_vap = xlsread(filename,'Sheet1','G4:G102');
s_liq = xlsread(filename,'Sheet1','Y4:Y102');
s_vap = xlsread(filename,'Sheet1','H4:H102');
rho_liq = xlsread(filename,'Sheet1','U4:U102');
rho_vap = xlsread(filename,'Sheet1','D4:D102');

% Interpolate for P1
P1_1 = find(press <= P1,1,'last');
P1_2 = P1_1 + 1;
s1 = s_liq(P1_1) + (P1-press(P1_1))*(s_liq(P1_2)-s_liq(P1_1))
    /(press(P1_1)-press(P1_2));
rho1 = rho_liq(P1_1) + (P1-press(P1_1))*(rho_liq(P1_2)-rho_liq
    (P1_1))/(press(P1_1)-press(P1_2));
h1 = h_liq(P1_1) + (P1-press(P1_1))*(h_liq(P1_2)-h_liq(P1_1))
    /(press(P1_1)-press(P1_2));

% Find new quality
P2_1 = find(press <= P2,1,'last');
P2_2 = P2_1 + 1;
s2 = s1;
```

```
s2_liq = s_liq(P2_1) + (s2-s_liq(P2_1))*((P2-press(P2_1))/(
    press(P2_2)-press(P2_1)));
s2_vap = s_vap(P2_1) + (s2-s_vap(P2_1))*((P2-press(P2_1))/(
    press(P2_2)-press(P2_1)));
qual2 = (s2-s2_liq)/(s2_vap-s2_liq);

% Interpolate using quality
h2_liq = h_liq(P2_1) + (h_liq(P2_2)-h_liq(P2_1))*((P2-press(
    P2_1))/(press(P2_2)-press(P2_1)));
h2_vap = h_vap(P2_1) + (h_vap(P2_2)-h_vap(P2_1))*((P2-press(
    P2_1))/(press(P2_2)-press(P2_1)));
h2 = h2_liq + qual2*(h2_vap-h2_liq);

rho2_liq = rho_liq(P2_1) + (rho_liq(P2_2)-rho_liq(P2_1))*((P2-
    press(P2_1))/(press(P2_2)-press(P2_1)));
rho2_vap = rho_vap(P2_1) + (rho_vap(P2_2)-rho_vap(P2_1))*((P2-
    press(P2_1))/(press(P2_2)-press(P2_1)));
rho2 = rho2_liq + qual2*(rho2_vap-rho2_liq);

% Compute area
% Equation found in AIAA paper done by Stanford
Ainject = mdotfuel_t/(cd*rho2*sqrt(2*(h1-h2)*1000)); % m^2
rinject = sqrt(Ainject/pi)*39.36996; %inches

%% -------------------------------------------------------
% Exit velocity
Ve = sqrt(((2.*gamma)./(gamma-1)).*(R).*Tc.*(1-(pe./pc).^((
    gamma-1)./gamma))).*sqrt(32.2);

% Thrust as a function of time
Ft_t = (1./32.2).*mdotsys_t.*Ve;

% Characteristic velocity as a function of time
cstar_t = Ft_t./(mdotsys_t.*Cf);

% Isp as a function of time
Isp_t = (cstar_t.*Cf)./g;

% Time to burnout
Tb = (((2.*Rf).^(2.*n+1))-(2.*Ri).^(2.*n+1))./(a.*(4.*n + 2)
    .*((4.*mdotox)./pi).^n);

% Constant oxidiser flow as a function of time
mdotox_t = 1:100;
for i = 1:100
    mdotox_t(i) = mdotox;
end % for
```

```
% Print data
fprintf('Max burn time: %g s\n',Tb);
fprintf('Oxidiser mass flow: %g lb/s\n',mdotox);
fprintf('Throat diameter: %g in^2\n',Dt);
fprintf('Nozzle exit diameter: %g in\n',De);
fprintf('Equation reccomended length: %g in\n',Lo);


% Generate plots
figure(1)
plot(t,Db_t)
title 'Combustion port diameter'
xlabel 'Time (s)'
ylabel 'Port Diameter (in)'

figure(2)
plot(t,mdotsys_t,'-k',t,mdotox_t,'-.k',t,mdotfuel_t,'--k')
title 'Mass flow v. Time'
legend('total','oxidiser','fuel','location','Best')
xlabel 'Time (s)'
ylabel 'Mass flow (lb/s)'

figure(3)
plot(t,rdot_t)
title 'Regression rate v. Time'
xlabel 'Time (s)'
ylabel 'Regression rate (in/s)'

figure(4)
plot(t,Ft_t)
title 'Thrust v. Time'
xlabel 'Time (s)'
ylabel 'Thrust (lb)'

figure(5)
plot(t,OF_t)
title 'OF v. Time'
xlabel 'Time (s)'
ylabel 'OF'
```

Appendix B

MATLAB Injector Sizing Code

```
clc
clear
close all
% This program uses N2O tables to determine either radius of the injector
% given a mass flow of N2O, or it will give an mass flow of N2O given an
% area of the injector (might change this to radius). Further improvements
% will be to determine thurst given the mass flow.


%Constants
qual1 = 0;
press = 20:10:1000;
cd = 0.65;
filename = ('N2Otable.xlsx');

%% Get input variables
P1 = input('Pressure in the line (psia) = ');
P2 = input('\nChamber Pressure (psia) = ');
mdot = input('\nmdot (kg/s) = ');
Diameter = input('\nDiameter of injector (in) = ');

%% Read in spreadsheet data
h_liq = xlsread(filename,'Sheet1','X4:X102');
h_vap = xlsread(filename,'Sheet1','G4:G102');
s_liq = xlsread(filename,'Sheet1','Y4:Y102');
s_vap = xlsread(filename,'Sheet1','H4:H102');
rho_liq = xlsread(filename,'Sheet1','U4:U102');
rho_vap = xlsread(filename,'Sheet1','D4:D102');

%% Interpolate for P1
```

```
P1_1 = find(press <= P1,1,'last');
P1_2 = P1_1 + 1;
s1 = s_liq(P1_1) + (P1-press(P1_1))*(s_liq(P1_2)-s_liq(P1_1))/(press(P1_1)-press(P1_2));
rho1 = rho_liq(P1_1) + (P1-press(P1_1))*(rho_liq(P1_2)-rho_liq(P1_1))/(press(P1_1)-press(P1_2));
h1 = h_liq(P1_1) + (P1-press(P1_1))*(h_liq(P1_2)-h_liq(P1_1))/(press(P1_1)-press(P1_2));

%% Find new quality
P2_1 = find(press <= P2,1,'last');
P2_2 = P2_1 + 1;
s2 = s1;
s2_liq = s_liq(P2_1) + (s2-s_liq(P2_1))*((P2-press(P2_1))/(press(P2_2)-press(P2_1)));
s2_vap = s_vap(P2_1) + (s2-s_vap(P2_1))*((P2-press(P2_1))/(press(P2_2)-press(P2_1)));
qual2 = (s2-s2_liq)/(s2_vap-s2_liq);

%% Interpolate using quality
h2_liq = h_liq(P2_1) + (h_liq(P2_2)-h_liq(P2_1))*((P2-press(P2_1))/(press(P2_2)-press(P2_1)));
h2_vap = h_vap(P2_1) + (h_vap(P2_2)-h_vap(P2_1))*((P2-press(P2_1))/(press(P2_2)-press(P2_1)));
h2 = h2_liq + qual2*(h2_vap-h2_liq);

rho2_liq = rho_liq(P2_1) + (rho_liq(P2_2)-rho_liq(P2_1))*((P2-press(P2_1))/(press(P2_2)-press(P2_1)));
rho2_vap = rho_vap(P2_1) + (rho_vap(P2_2)-rho_vap(P2_1))*((P2-press(P2_1))/(press(P2_2)-press(P2_1)));
rho2 = rho2_liq + qual2*(rho2_vap-rho2_liq);

%% Compute area
% Equation found in AIAA paper done by Stanford 2013
A = mdot/(cd*rho2*sqrt(2*(h1-h2)*1000));          % m^2
r = sqrt(A/pi)*39.36996;                          % inches

%% Compute mdot using the Area input
inch_to_meter = .0254;
Ainput = (Diameter.^2/4) * pi * inch_to_meter^2;          % m^2
mdot_1 = Ainput*(cd*rho2*sqrt(2*(h1-h2)*1000));           % kg/s

%% Print relevant data

fprintf('\nRadius of Injector from mdot input = %.6f inches',r)
```

```
fprintf('\nMass flow from the Area input = %.4f kg/m^3\n',
    mdot_1)
```

Appendix C

MATLAB Pressure Drop Code

```
%AUCPLab Hybrid
%calculations of pressure drop through tubing
clear
clc
close all
format long

L = 63/12; %ft
D = .43/12; %ft
rho_ox = 48.21/32.2; %slugs/ft^3 %http://edge.rit.edu/edge/P07106/public/Nox.pdf
mdot_ox = 0.635014/32.2; %slugs/s
vf = mdot_ox/rho_ox*7.48*60;
E = 0.000007; %steel
mu = 213e-6/(32.2); %slugs/ft*s %http://webserver.dmt.upm.es/~isidoro/dat1/eLIQ.pdf

A = (pi/4)*D^2; %ft^2
V = mdot_ox/(rho_ox*A);
Re = (rho_ox*V*D)/mu;
f = 0.022; %from fluid mechanics textbook white pg. 366 %if laminar: 64/Re;

dP = (f*(L/D)*(rho_ox/2)*V^2)/(12^2); %psi

hL = f*((L/D)+(3.30));
fprintf('Pressure drop: %0.3f psi\n',dP)

(vf/1/4)^2*1.23;
```

Appendix D

MATLAB Data Processing Code

```
%Hybrid Data Processing

%clear command window
clear
clc
close all

%Universals
n = 2500; %samples per .1 seconds
sheet = 1;

%read in excel files
%% 3.3 GPM 0.08" Oriface HTPB Test 1
filename = '3.3GPM_HTPB_1.xlsx';

xlRange = 'A24:A859022';
time = xlsread(filename,sheet,xlRange);

xlRange = 'B24:B859022';
F = xlsread(filename,sheet,xlRange);
 windowSize = 25;

xlRange = 'C24:C859022';
P = xlsread(filename,sheet,xlRange);

num = round(length(time)/n)-1;
start = 1;
fin = n;
sampletime = zeros(num,1);
sampleF = zeros(num,1);
sampleP = zeros(num,1);

for k = 1:num
```

```
    sampletime(k,1) = time(start);
    sampleF(k,1) = sum(F(start:fin),1)/n;
    sampleP(k,1) = sum(P(start:fin),1)/n;
    start = start + n;
    fin = fin + n;
end

%find max P
[maxP,I] = max(P);
timeMP = time(I);
fprintf('0.08" HTPB\n')
fprintf('The max pressure is %0.3f psi and occurs at %.3f seconds\n',maxP,timeMP)

%find oxidizer flow rate
ofr = ((sampleF(1) - sampleF(end))/sampletime(end));%*7.19; % gal/min
fprintf('The oxidizer flow rate is %0.4f lb/s\n',ofr)
fprintf('The burn time was %0.04f s\n',sampletime(end))

%Plots
figure(1)

subplot(1,2,1)
plot(time,P)
hold on
plot(sampletime,sampleP,'LineWidth',2)
grid on
title('Chamber Pressure vs. Time')
xlabel('Time (s)')
ylabel('Pressure (psi)')
legend('Raw Data','Averaged Data')

subplot(1,2,2)
plot(time,F)
hold on
plot(sampletime,sampleF,'LineWidth',2)
grid on
%plot(time,ffilter)
title('Oxidizer Weight vs. Time')
xlabel('Time (s)')
ylabel('Oxidizer Weight (lb)')
legend('Raw Data','Averaged Data')

suptitle('0.08" Oxidizer Injector With HTPB')

%% 3.3 GPM 0.08" Oriface HDPE Test 1
```

```
filename = '3.3GPM_HDPE_1.xlsx';

xlRange = 'A44025:A1048576';
time = xlsread(filename,sheet,xlRange);

xlRange = 'B44025:B1048576';
F = xlsread(filename,sheet,xlRange);

xlRange = 'C44025:C1048576';
P = xlsread(filename,sheet,xlRange);

num = round(length(time)/n)-1;
start = 1;
fin = n;
sampletime = zeros(num,1);
sampleF = zeros(num,1);
sampleP = zeros(num,1);

for k = 1:num
    sampletime(k,1) = time(start);
    sampleF(k,1) = sum(F(start:fin),1)/n;
    sampleP(k,1) = sum(P(start:fin),1)/n;
    start = start + n;
    fin = fin + n;
end

newtime = zeros(length(time),1);
newsampletime = zeros(length(sampletime),1);

for n = 1:length(time)
    if n == 1
        newtime(n) = 0;
    else
        newtime(n) = newtime(n-1)+0.00004;
    end
end

for n = 1:length(sampletime)
    if n == 1
        newsampletime(n) = 0;
    else
        newsampletime(n) = newsampletime(n-1)+.1;
    end
end

%find max P
[maxP,I] = max(P);
```

```
timeMP = newtime(I);
fprintf('0.08" HDPE\n')
fprintf('The max pressure is %0.3f psi and occurs at %.3f
    seconds\n',maxP,timeMP)

%find oxidizer flow rate
ofr = ((sampleF(1) - sampleF(end))/newsampletime(end));%*7.19;
    %gal/min
fprintf('The oxidizer flow rate is %0.4f lb/s\n',ofr)
fprintf('The burn time was %0.04f s\n',newsampletime(end))

%Plots
figure(2)

subplot(1,2,1)
plot(newtime,P)
hold on
plot(newsampletime,sampleP,'LineWidth',2)
grid on
title('Chamber Pressure vs. Time')
xlabel('Time (s)')
ylabel('Pressure (psi)')
legend('Raw Data','Averaged Data')

subplot(1,2,2)
plot(newtime,F)
hold on
plot(newsampletime,sampleF,'LineWidth',2)
grid on
%plot(time,ffilter)
title('Oxidizer Weight vs. Time')
xlabel('Time (s)')
ylabel('Oxidizer Weight (lb)')
legend('Raw Data','Averaged Data')

suptitle('0.08" Oxidizer Injector With HDPE')

%% 2.2 GPM 0.07" Oriface HTPB Test 2
n = 2500;
sheet = 1;
filename = '2.2GPM_HTPB_2.xlsx';

xlRange = 'A24:A1048576';
time = xlsread(filename,sheet,xlRange);

xlRange = 'B24:B1048576';
F = xlsread(filename,sheet,xlRange);
```

```
xlRange = 'C24:C1048576';
P = xlsread(filename,sheet,xlRange);

num = round(length(time)/n)-1;
start = 1;
fin = n;
sampletime = zeros(num,1);
sampleF = zeros(num,1);
sampleP = zeros(num,1);

for k = 1:num
    sampletime(k,1) = time(start);
    sampleF(k,1) = sum(F(start:fin),1)/n;
    sampleP(k,1) = sum(P(start:fin),1)/n;
    start = start + n;
    fin = fin + n;
end

%find max P
[maxP,I] = max(P);
timeMP = time(I);
fprintf('0.07" HTPB\n')
fprintf('The max pressure is %0.3f psi and occurs at %.3f
    seconds\n',maxP,timeMP)

%find oxidizer flow rate
ofr = ((sampleF(1) - sampleF(end))/sampletime(end));%*7.19; %
    gal/min
fprintf('The oxidizer flow rate is %0.4f lb/s\n',ofr)
fprintf('The burn time was %0.04f s\n', sampletime(end))

%Plots
% figure(7)
% subplot(1,2,1)
% plot(sampletime,sampleP)
% subplot(1,2,2)
% plot(sampletime,sampleF)

figure(3)

subplot(1,2,1)
plot(time,P)
hold on
plot(sampletime,sampleP,'LineWidth',2)
grid on
title('Chamber Pressure vs. Time')
```

```
xlabel('Time (s)')
ylabel('Pressure (psi)')
legend('Raw Data','Averaged Data')

subplot(1,2,2)
plot(time,F)
hold on
plot(sampletime,sampleF,'LineWidth',2)
grid on
%plot(time,ffilter)
title('Oxidizer Weight vs. Time')
xlabel('Time (s)')
ylabel('Oxidizer Weight (lb)')
legend('Raw Data','Averaged Data')

suptitle('0.07" Oxidizer Injector With HTPB')

%% 2.2 GPM 0.07" Oriface HDPE Test 1
n = 2500;
sheet = 1;
filename = '2.2GPM_HDPE_1.xlsx';

xlRange = 'A52024:A1048576';
time = xlsread(filename,sheet,xlRange);

xlRange = 'B52024:B1048576';
F = xlsread(filename,sheet,xlRange);

xlRange = 'C52024:C1048576';
P = xlsread(filename,sheet,xlRange);

num = round(length(time)/n)-1;
start = 1;
fin = n;
sampletime = zeros(num,1);
sampleF = zeros(num,1);
sampleP = zeros(num,1);

for k = 1:num
    sampletime(k,1) = time(start);
    sampleF(k,1) = sum(F(start:fin),1)/n;
    sampleP(k,1) = sum(P(start:fin),1)/n;
    start = start + n;
    fin = fin + n;
end

newtime = zeros(length(time),1);
```

```
newsampletime = zeros(length(sampletime),1);

for n = 1:length(time)
    if n == 1
        newtime(n) = 0;
    else
        newtime(n) = newtime(n-1)+0.00004;
    end
end

for n = 1:length(sampletime)
    if n == 1
        newsampletime(n) = 0;
    else
        newsampletime(n) = newsampletime(n-1)+.1;
    end
end


%find max P
[maxP,I] = max(P);
timeMP = newtime(I);
fprintf('0.07" HDPE\n')
fprintf('The max pressure is %0.3f psi and occurs at %.3f seconds\n',maxP,timeMP)

%find oxidizer flow rate
ofr = ((sampleF(1) - sampleF(end))/newsampletime(end));%*7.19;%gal/min
fprintf('The oxidizer flow rate is %0.4f lb/s\n',ofr)
fprintf('The burn time was %0.04f s\n', newsampletime(end))

%Plots
figure(4)

subplot(1,2,1)
plot(newtime,P)
hold on
plot(newsampletime,sampleP,'LineWidth',2)
grid on
title('Chamber Pressure vs. Time')
xlabel('Time (s)')
ylabel('Pressure (psi)')
legend('Raw Data','Averaged Data')

subplot(1,2,2)
plot(newtime,F)
```

```
hold on
plot(newsampletime,sampleF,'LineWidth',2)
grid on
%plot(time,ffilter)
title('Oxidizer Weight vs. Time')
xlabel('Time (s)')
ylabel('Oxidizer Weight (lb)')
legend('Raw Data','Averaged Data')

suptitle('0.07" Oxidizer Injector With HDPE')

%% 1.1 GPM 0.05" Oriface HTPB Test 1
n = 2500;
sheet = 1;
filename = '1.1GPM_HTPB_1.xlsx';

xlRange = 'A268024:A1048576';
time = xlsread(filename,sheet,xlRange);

xlRange = 'B268024:B1048576';
F = xlsread(filename,sheet,xlRange);

xlRange = 'C268024:C1048576';
P = xlsread(filename,sheet,xlRange);

num = round(length(time)/n)-1;
start = 1;
fin = n;
sampletime = zeros(num,1);
sampleF = zeros(num,1);
sampleP = zeros(num,1);

for k = 1:num
    sampletime(k,1) = time(start);
    sampleF(k,1) = sum(F(start:fin),1)/n;
    sampleP(k,1) = sum(P(start:fin),1)/n;
    start = start + n;
    fin = fin + n;
end

newtime = zeros(length(time),1);
newsampletime = zeros(length(sampletime),1);

for n = 1:length(time)
    if n == 1
        newtime(n) = 0;
    else
```

```
            newtime(n) = newtime(n-1)+0.00004;
        end
end

for n = 1:length(sampletime)
        if n == 1
            newsampletime(n) = 0;
        else
            newsampletime(n) = newsampletime(n-1)+.1;
        end
end

%find max P
[maxP,I] = max(P);
timeMP = newtime(I);
fprintf('0.05" HTPB\n')
fprintf('The max pressure is %0.3f psi and occurs at %.3f
    seconds\n',maxP,timeMP)

%find oxidizer flow rate
ofr = ((sampleF(1) - sampleF(end))/newsampletime(end));%*7.19;
    %gal/min
fprintf('The oxidizer flow rate is %0.4f lb/s\n',ofr)
fprintf('The burn time was %0.04f s\n', newsampletime(end))

%Plots
figure(5)

subplot(1,2,1)
plot(newtime,P)
hold on
plot(newsampletime,sampleP,'LineWidth',2)
grid on
title('Chamber Pressure vs. Time')
xlabel('Time (s)')
ylabel('Pressure (psi)')
legend('Raw Data','Averaged Data')

subplot(1,2,2)
plot(newtime,F)
hold on
plot(newsampletime,sampleF,'LineWidth',2)
grid on
%plot(time,ffilter)
title('Oxidizer Weight vs. Time')
xlabel('Time (s)')
ylabel('Oxidizer Weight (lb)')
```

```matlab
legend('Raw Data','Averaged Data')

suptitle('0.05" Oxidizer Injector With HTPB')

%% 1.1 GPM 0.05" Oriface HDPE Test 2
n = 2500;
sheet = 1;
filename = '1.1GPM_HDPE_2.xlsx';

xlRange = 'A24:A1048576';
time = xlsread(filename,sheet,xlRange);

xlRange = 'B24:B1048576';
F = xlsread(filename,sheet,xlRange);

xlRange = 'C24:C1048576';
P = xlsread(filename,sheet,xlRange);

num = round(length(time)/n)-1;
start = 1;
fin = n;
sampletime = zeros(num,1);
sampleF = zeros(num,1);
sampleP = zeros(num,1);

for k = 1:num
    sampletime(k,1) = time(start);
    sampleF(k,1) = sum(F(start:fin),1)/n;
    sampleP(k,1) = sum(P(start:fin),1)/n;
    start = start + n;
    fin = fin + n;
end

%find max P
[maxP,I] = max(P);
timeMP = time(I);
fprintf('0.05" HDPE\n')
fprintf('The max pressure is %0.3f psi and occurs at %.3f
    seconds\n',maxP,timeMP)

%find oxidizer flow rate
ofr = ((sampleF(1) - sampleF(end))/sampletime(end));%*7.19; %
    gal/min
fprintf('The oxidizer flow rate is %0.4f lb/s\n',ofr)
fprintf('The burn time was %0.04f s\n', newsampletime(end))

%Plots
```

```
figure(6)

subplot(1,2,1)
plot(time,P)
hold on
plot(sampletime,sampleP,'LineWidth',2)
grid on
title('Chamber Pressure vs. Time')
xlabel('Time (s)')
ylabel('Pressure (psi)')
legend('Raw Data','Averaged Data')

subplot(1,2,2)
plot(time,F)
hold on
plot(sampletime,sampleF,'LineWidth',2)
grid on
%plot(time,ffilter)
title('Oxidizer Weight vs. Time')
xlabel('Time (s)')
ylabel('Oxidizer Weight (lb)')
legend('Raw Data','Averaged Data')

suptitle('0.05" Oxidizer Injector With HDPE')
```

Appendix E

Drawings

ITEM NO.	PART NUMBER	DESCRIPTION	QTY.
1	BASE01	Base Plate	2
2	TOP01	Base top plate with cooling channels	2
3	TOP02	Top plate covers TOP01	2
4	WindowHolder01	Window Holder	4
5	ENDPLATE01	Generic End Plate	3
6	AFTENDPLATE01	Aft End Inner Plate	1
7	ORIFACE01	Oriface	1
8	ORIFACECAP01	Oriface Cap	1
9	AFTENDPLATE02	Aft End Outter Plate	1
10	FWDENDPLATE01	Forward End Plate	1
12	TABLESTOP01	Table stop	2
13	WINDOWPLATE01	Window Holder	4
14	WINDOW01	Lexan Window	4
15	WINDOW02	Quartz Window	4
16	LIFT01		3

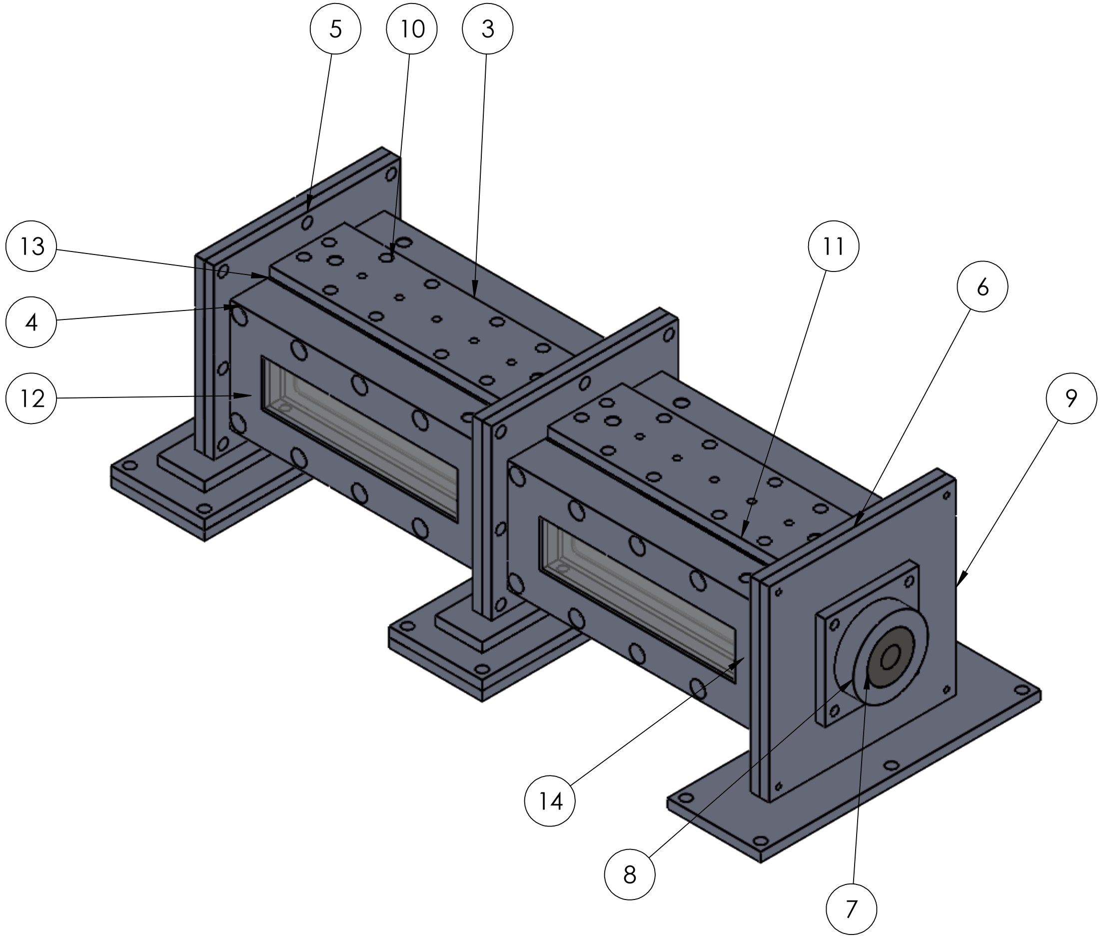

Top View (Item No. 2 and No. 14 Hidden)

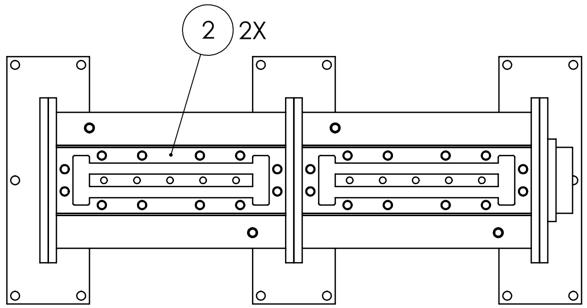

Bottom View (Item No. 14 Hidden)

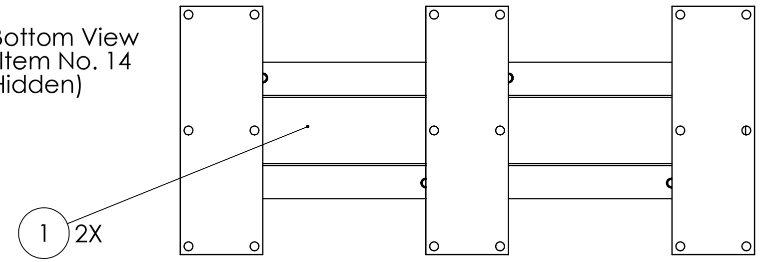

NEXT ASSY	USED ON	
APPLICATION		DO NOT SCALE DRAWING

UNLESS OTHERWISE SPECIFIED:
DIMENSIONS ARE IN INCHES
TOLERANCES:
TWO PLACE DECIMAL ±0.005
THREE PLACE DECIMAL ±0.001
INTERPRET GEOMETRIC TOLERANCING PER:
MATERIAL Carbon Steel
FINISH

	NAME	DATE
DRAWN	SB	11/28/2018
CHECKED		
ENG APPR.		
MFG APPR.		
Q.A.		
COMMENTS:		

TITLE: Two Section Hybrid Assembly

SIZE B | DWG. NO. Hybrid | REV A

SCALE: 1:6 | WEIGHT: | SHEET 1 OF 16

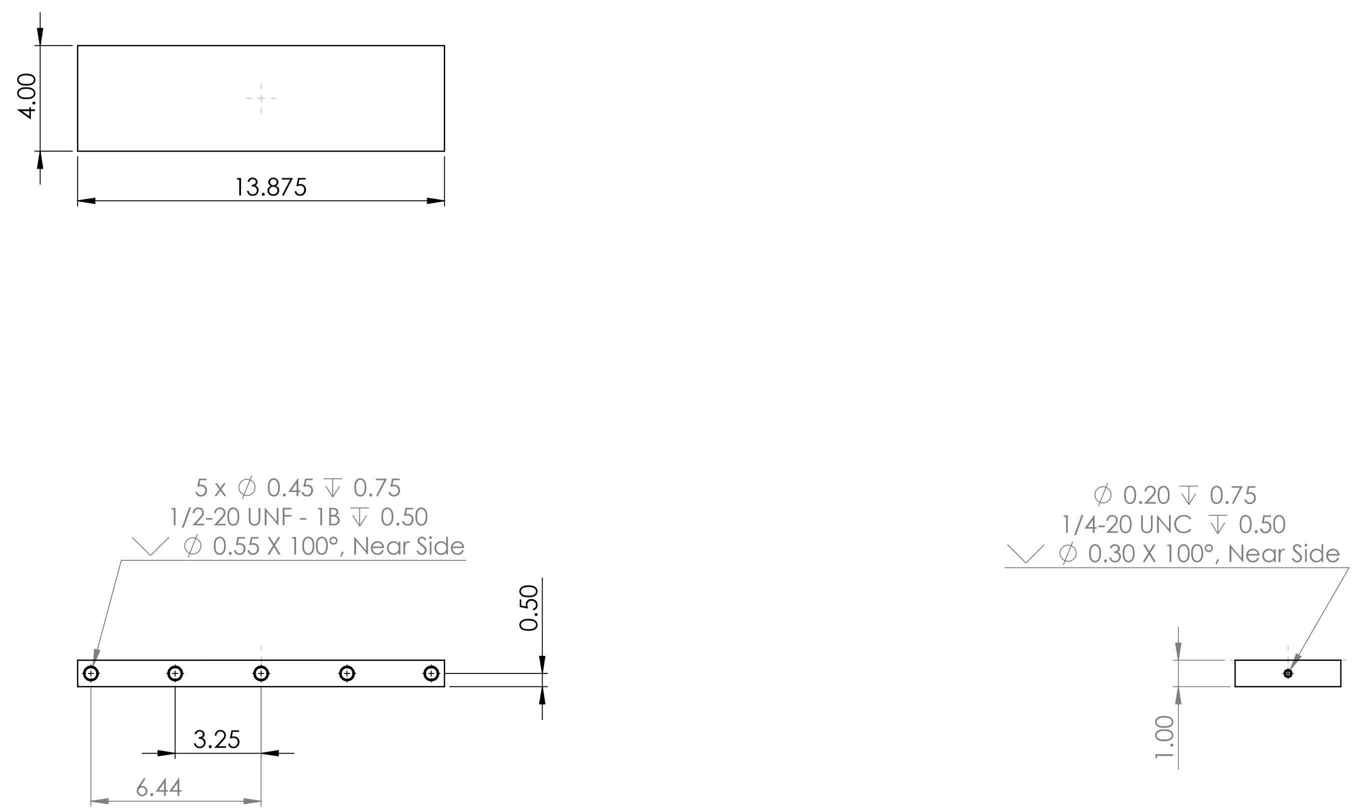

BASE01

Cut and chamfer all edges

NEXT ASSY	USED ON	
APPLICATION		DO NOT SCALE DRAWING

UNLESS OTHERWISE SPECIFIED:

DIMENSIONS ARE IN INCHES
TOLERANCES:
TWO PLACE DECIMAL ±0.005
THREE PLACE DECIMAL ±0.001

INTERPRET GEOMETRIC TOLERANCING PER:

MATERIAL: Carbon Steel

FINISH

	NAME	DATE
DRAWN	SB	11/28/2018
CHECKED		
ENG APPR.		
MFG APPR.		
Q.A.		

COMMENTS:

TITLE: Two Section Hybrid Assembly

SIZE	DWG. NO.	REV
B	Hybrid	A

SCALE: 1:5 WEIGHT: SHEET 2 OF 16

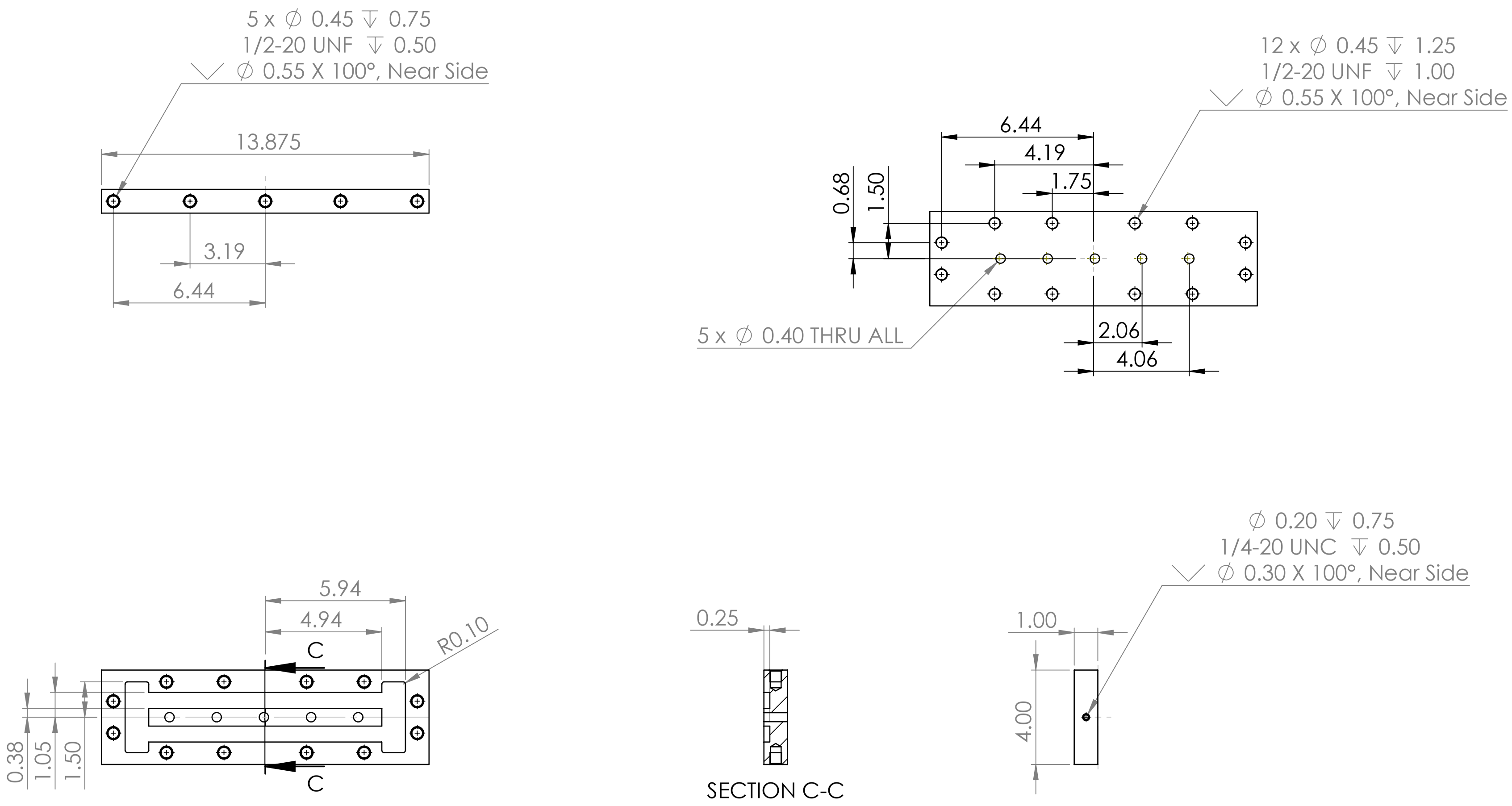

TOP01

Cut and chamfer all edges

NEXT ASSY	USED ON
APPLICATION	

UNLESS OTHERWISE SPECIFIED:

DIMENSIONS ARE IN INCHES
TOLERANCES:
TWO PLACE DECIMAL ±0.005
THREE PLACE DECIMAL ±0.001

INTERPRET GEOMETRIC TOLERANCING PER:

MATERIAL: Carbon Steel

FINISH

DO NOT SCALE DRAWING

	NAME	DATE
DRAWN	SB	11/28/2018
CHECKED		
ENG APPR.		
MFG APPR.		
Q.A.		
COMMENTS:		

TITLE: Two Section Hybrid Assembly

SIZE	DWG. NO.	REV
B	Hybrid	A

SCALE: 1:5 WEIGHT: SHEET 3 OF 16

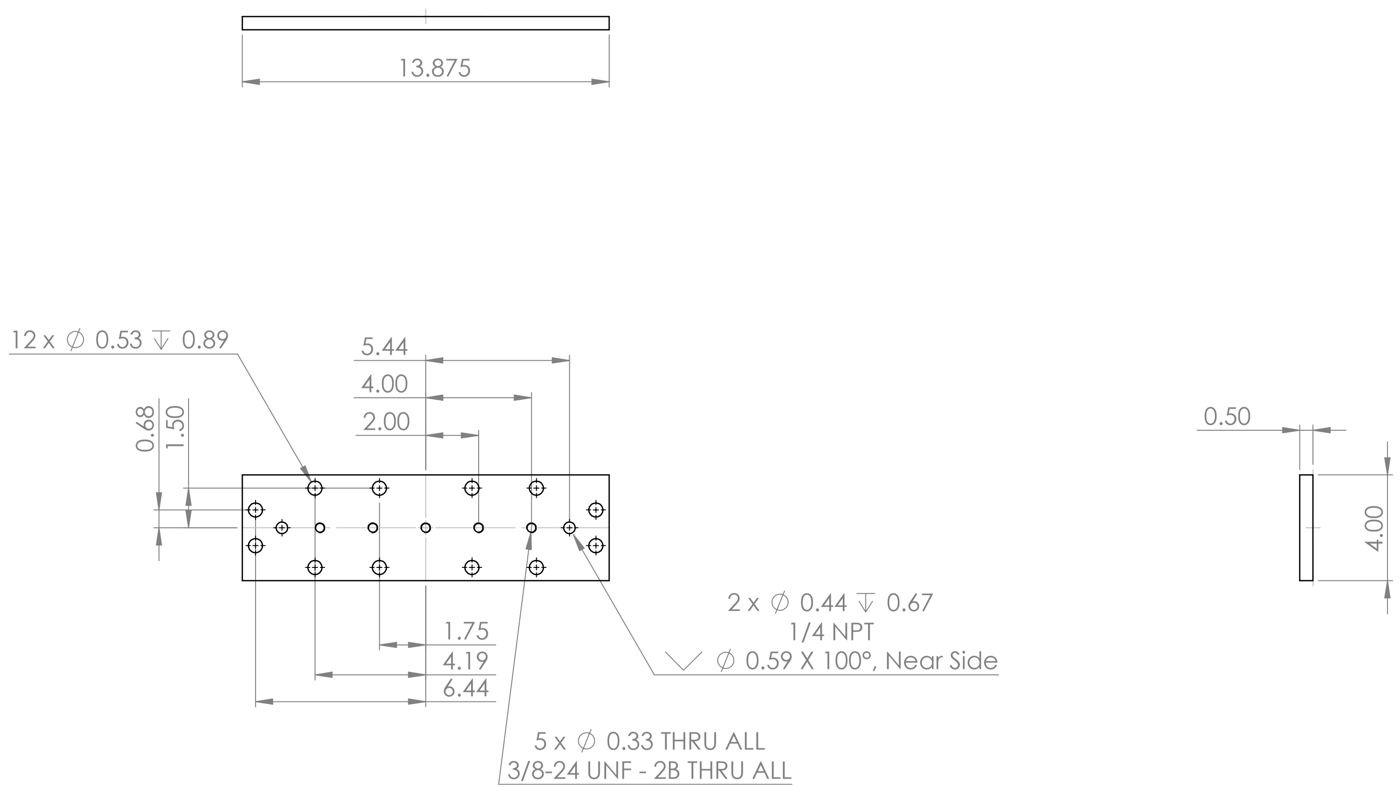

TOP02

Cut and chamfer all edges

NEXT ASSY	USED ON
APPLICATION	

UNLESS OTHERWISE SPECIFIED:
DIMENSIONS ARE IN INCHES
TOLERANCES:
TWO PLACE DECIMAL ±0.005
THREE PLACE DECIMAL ±0.001

INTERPRET GEOMETRIC TOLERANCING PER:

MATERIAL: Carbon Steel

FINISH

DO NOT SCALE DRAWING

	NAME	DATE
DRAWN	SB	11/28/2018
CHECKED		
ENG APPR.		
MFG APPR.		
Q.A.		

COMMENTS:

TITLE: Two Section Hybrid Assembly

SIZE: B | DWG. NO.: Hybrid | REV: A

SCALE: 1:5 | WEIGHT: | SHEET 4 OF 16

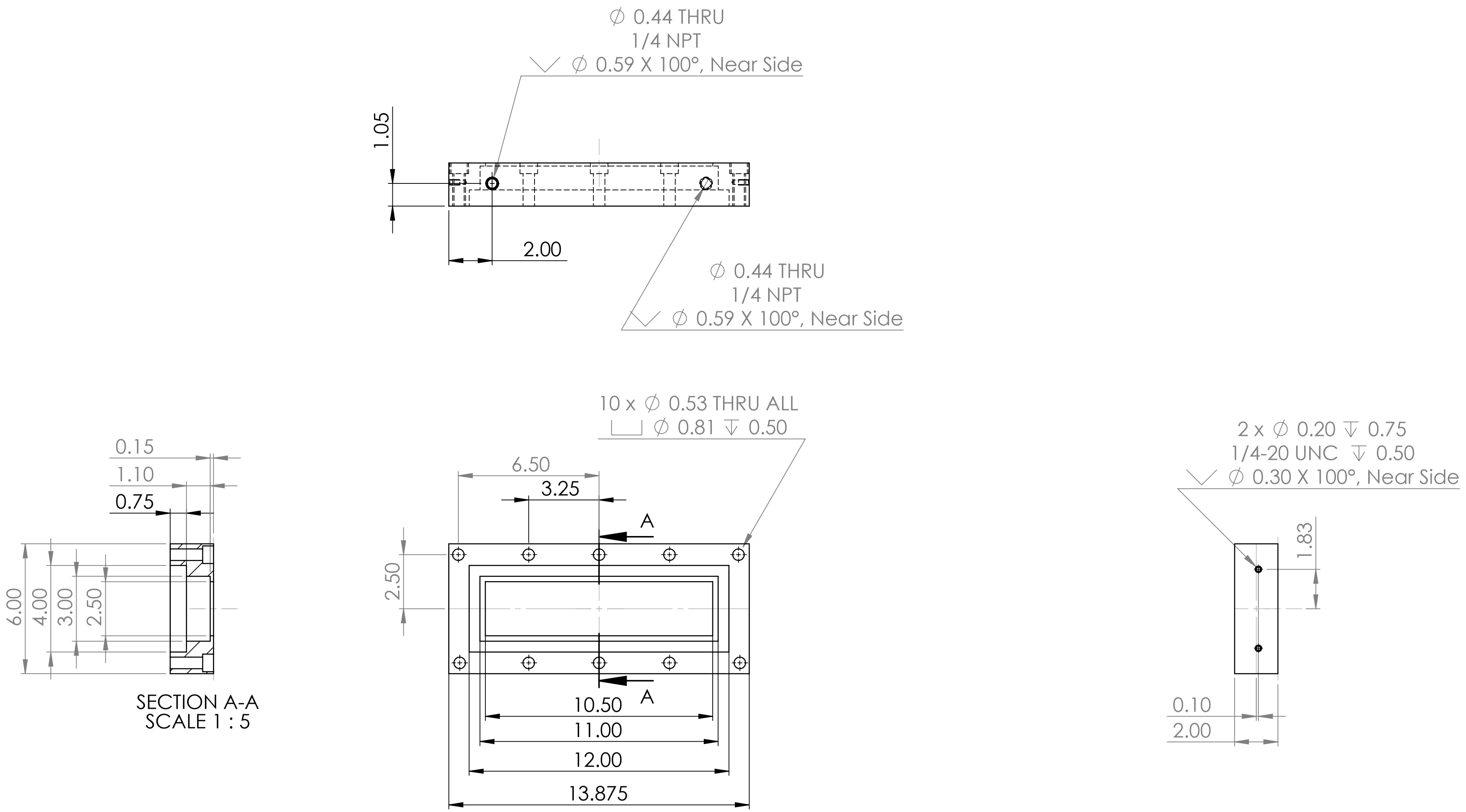

WINDOWHOLDER01
Cut and chamfer all edges

PROPRIETARY AND CONFIDENTIAL
THE INFORMATION CONTAINED IN THIS DRAWING IS THE SOLE PROPERTY OF <INSERT COMPANY NAME HERE>. ANY REPRODUCTION IN PART OR AS A WHOLE WITHOUT THE WRITTEN PERMISSION OF <INSERT COMPANY NAME HERE> IS PROHIBITED.

				NAME	DATE
		UNLESS OTHERWISE SPECIFIED: DIMENSIONS ARE IN INCHES TOLERANCES: TWO PLACE DECIMAL ±0.005 THREE PLACE DECIMAL ±0.001	DRAWN	SB	11/28/2018
			CHECKED		
			ENG APPR.		
			MFG APPR.		
		INTERPRET GEOMETRIC TOLERANCING PER:	Q.A.		
		MATERIAL Carbon Steel	COMMENTS:		
NEXT ASSY	USED ON	FINISH			
APPLICATION		DO NOT SCALE DRAWING			

TITLE:
Two Section Hybrid Assembly

SIZE	DWG. NO.	REV
B	Hybrid	A
SCALE: 1:5	WEIGHT:	SHEET 5 OF 16

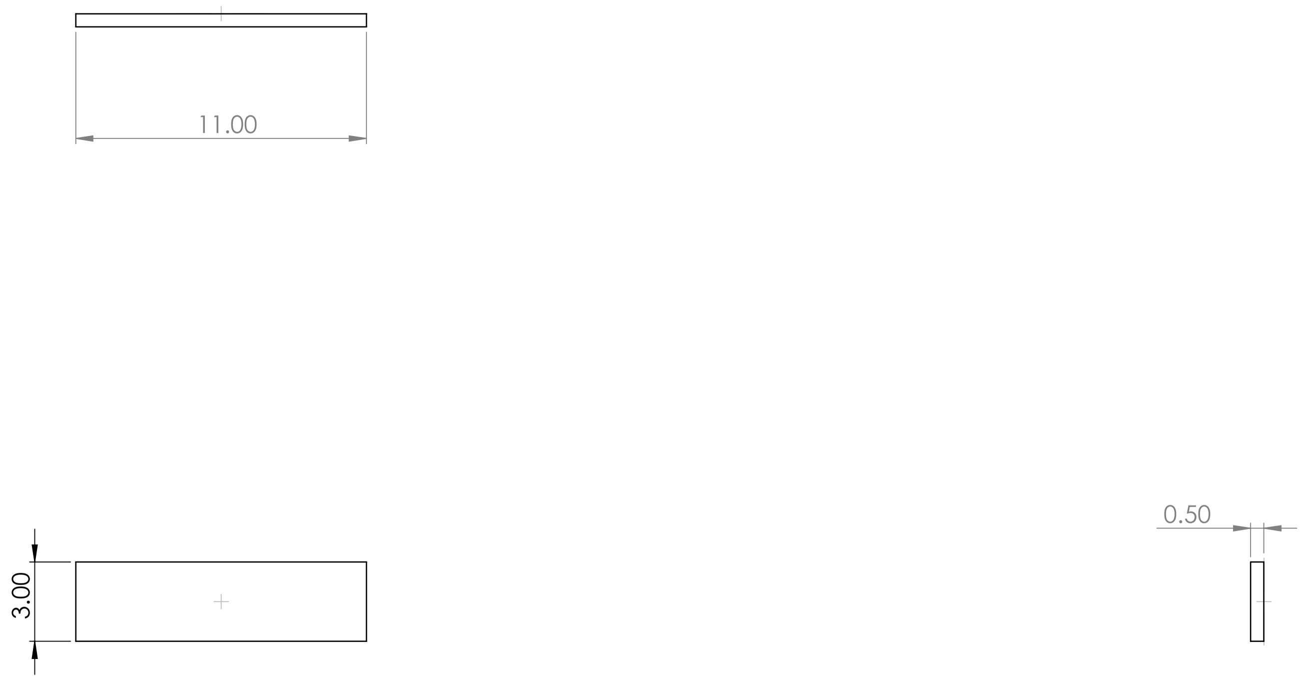

WINDOW01

UNLESS OTHERWISE SPECIFIED:		NAME	DATE		
DIMENSIONS ARE IN INCHES TOLERANCES: TWO PLACE DECIMAL ±0.005 THREE PLACE DECIMAL ±0.001	DRAWN	SB	11/28/2018	TITLE: Two Section Hybrid Assembly	
	CHECKED				
	ENG APPR.				
	MFG APPR.				
INTERPRET GEOMETRIC TOLERANCING PER:	Q.A.				
MATERIAL Lexan	COMMENTS:			SIZE B	DWG. NO. Hybrid	REV A
FINISH					
DO NOT SCALE DRAWING				SCALE: 1:5	WEIGHT:	SHEET 6 OF 16

NEXT ASSY	USED ON
APPLICATION	

WINDOW02

NEXT ASSY	USED ON
APPLICATION	

UNLESS OTHERWISE SPECIFIED:
DIMENSIONS ARE IN INCHES
TOLERANCES:
TWO PLACE DECIMAL ±0.005
THREE PLACE DECIMAL ±0.001

INTERPRET GEOMETRIC TOLERANCING PER:

MATERIAL Quartz

FINISH

DO NOT SCALE DRAWING

	NAME	DATE
DRAWN	SB	11/28/2018
CHECKED		
ENG APPR.		
MFG APPR.		
Q.A.		

COMMENTS:

TITLE: Two Section Hybrid Assembly

SIZE B | DWG. NO. Hybrid | REV A

SCALE: 1:5 | WEIGHT: | SHEET 7 OF 16

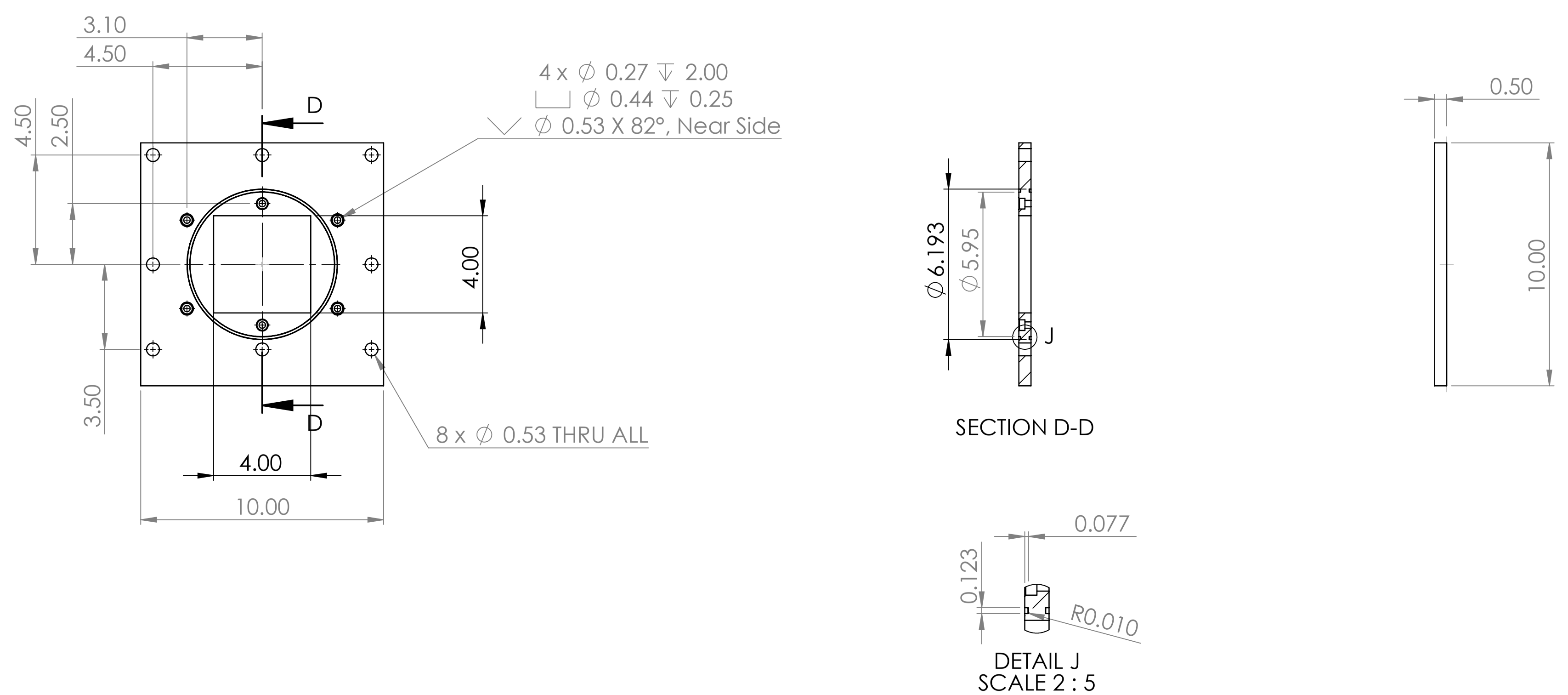

ENDPLATE01

Cut and chamfer all edges

PROPRIETARY AND CONFIDENTIAL

THE INFORMATION CONTAINED IN THIS DRAWING IS THE SOLE PROPERTY OF <INSERT COMPANY NAME HERE>. ANY REPRODUCTION IN PART OR AS A WHOLE WITHOUT THE WRITTEN PERMISSION OF <INSERT COMPANY NAME HERE> IS PROHIBITED.

		UNLESS OTHERWISE SPECIFIED:		NAME	DATE
		DIMENSIONS ARE IN INCHES TOLERANCES: TWO PLACE DECIMAL ±0.005 THREE PLACE DECIMAL ±0.001	DRAWN	SB	11/28/2018
			CHECKED		
			ENG APPR.		
			MFG APPR.		
		INTERPRET GEOMETRIC TOLERANCING PER:	Q.A.		
		MATERIAL Carbon Steel	COMMENTS:		
NEXT ASSY	USED ON	FINISH			
APPLICATION		DO NOT SCALE DRAWING			

TITLE:

Two Section Hybrid Assembly

SIZE	DWG. NO.	REV
B	Hybrid	A

SCALE: 1:5 WEIGHT: SHEET 8 OF 16

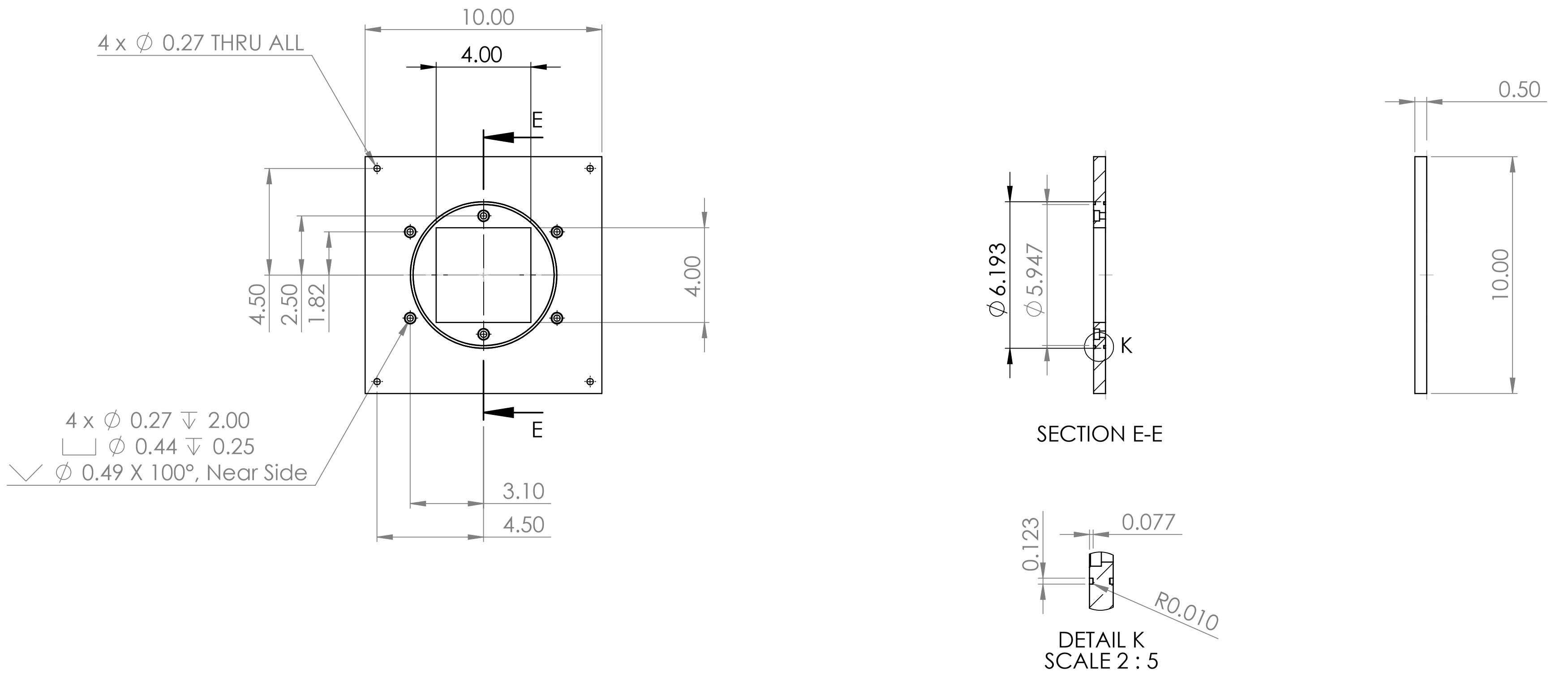

AFTENDPLATE01

Cut and chamfer all edges

NEXT ASSY	USED ON
APPLICATION	

UNLESS OTHERWISE SPECIFIED:
DIMENSIONS ARE IN INCHES
TOLERANCES:
TWO PLACE DECIMAL ±0.005
THREE PLACE DECIMAL ±0.001
INTERPRET GEOMETRIC TOLERANCING PER:
MATERIAL Carbon Steel
FINISH
DO NOT SCALE DRAWING

	NAME	DATE
DRAWN	SB	11/28/2018
CHECKED		
ENG APPR.		
MFG APPR.		
Q.A.		
COMMENTS:		

TITLE: Two Section Hybrid Assembly

SIZE B | DWG. NO. Hybrid | REV A

SCALE: 1:5 | WEIGHT: | SHEET 9 OF 16

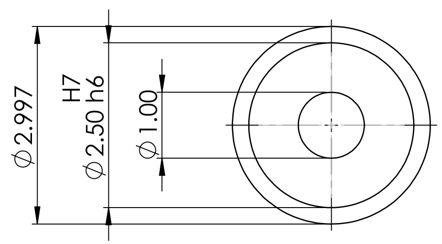

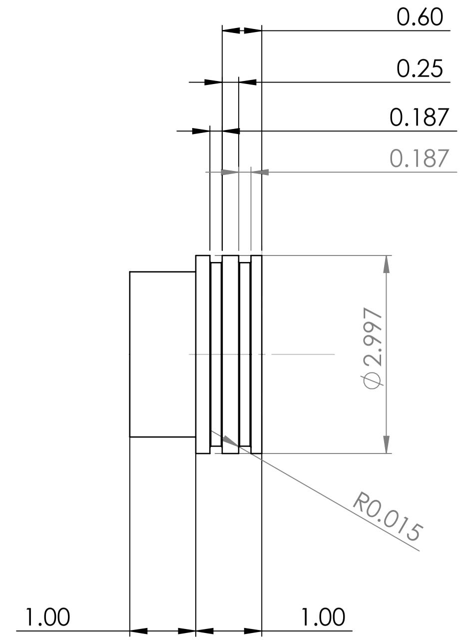

ORIFACE01

Cut and chamfer all edges

UNLESS OTHERWISE SPECIFIED:		NAME / DATE
DIMENSIONS ARE IN INCHES TOLERANCES: TWO PLACE DECIMAL ±0.005 THREE PLACE DECIMAL ±0.001	DRAWN	SB / 11/28/2018
	CHECKED	
	ENG APPR.	
	MFG APPR.	
INTERPRET GEOMETRIC TOLERANCING PER:	Q.A.	
MATERIAL Graphite	COMMENTS:	
FINISH		
DO NOT SCALE DRAWING		

NEXT ASSY	USED ON
APPLICATION	

TITLE: Two Section Hybrid Assembly

SIZE B | DWG. NO. Hybrid | REV A

SCALE: 1:2 | WEIGHT: | SHEET 10 OF 16

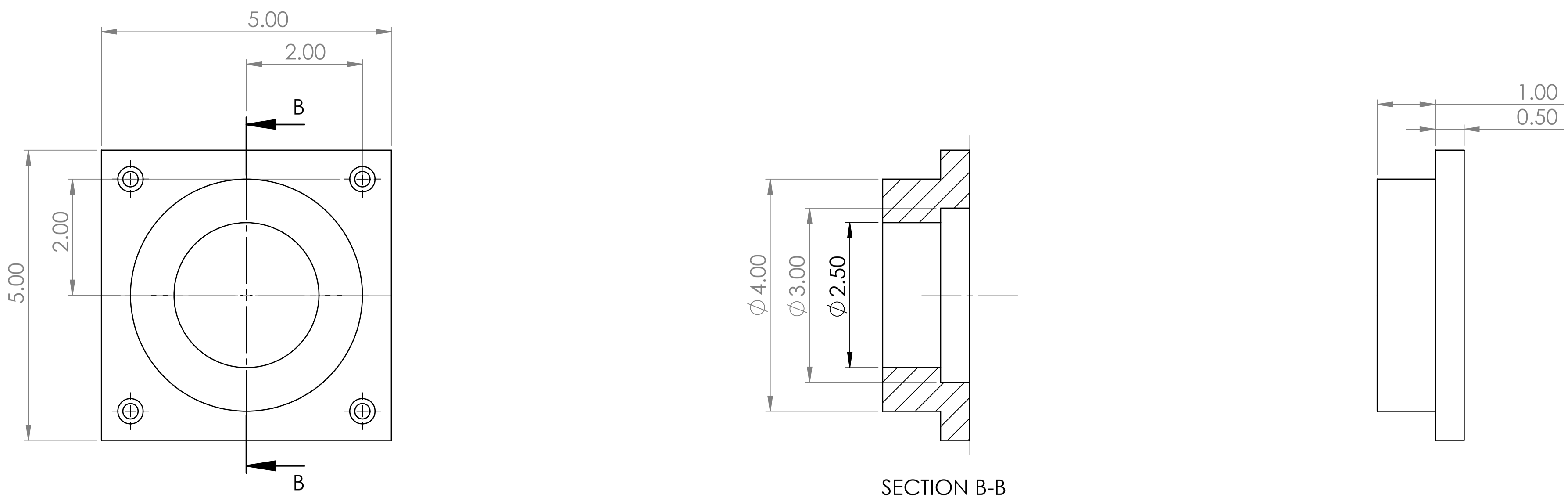

SECTION B-B
SCALE 1 : 2

ORIFACECAP01

Cut and chamfer all edges

NEXT ASSY	USED ON	
APPLICATION		

UNLESS OTHERWISE SPECIFIED:
DIMENSIONS ARE IN INCHES
TOLERANCES:
TWO PLACE DECIMAL ±0.005
THREE PLACE DECIMAL ±0.001

INTERPRET GEOMETRIC TOLERANCING PER:

MATERIAL
Carbon Steel

FINISH

DO NOT SCALE DRAWING

	NAME	DATE
DRAWN	SB	11/28/2018
CHECKED		
ENG APPR.		
MFG APPR.		
Q.A.		

COMMENTS:

TITLE:
Two Section Hybrid Assembly

SIZE B | DWG. NO. Hybrid | REV A

SCALE: 1:2 | WEIGHT: | SHEET 11 OF 16

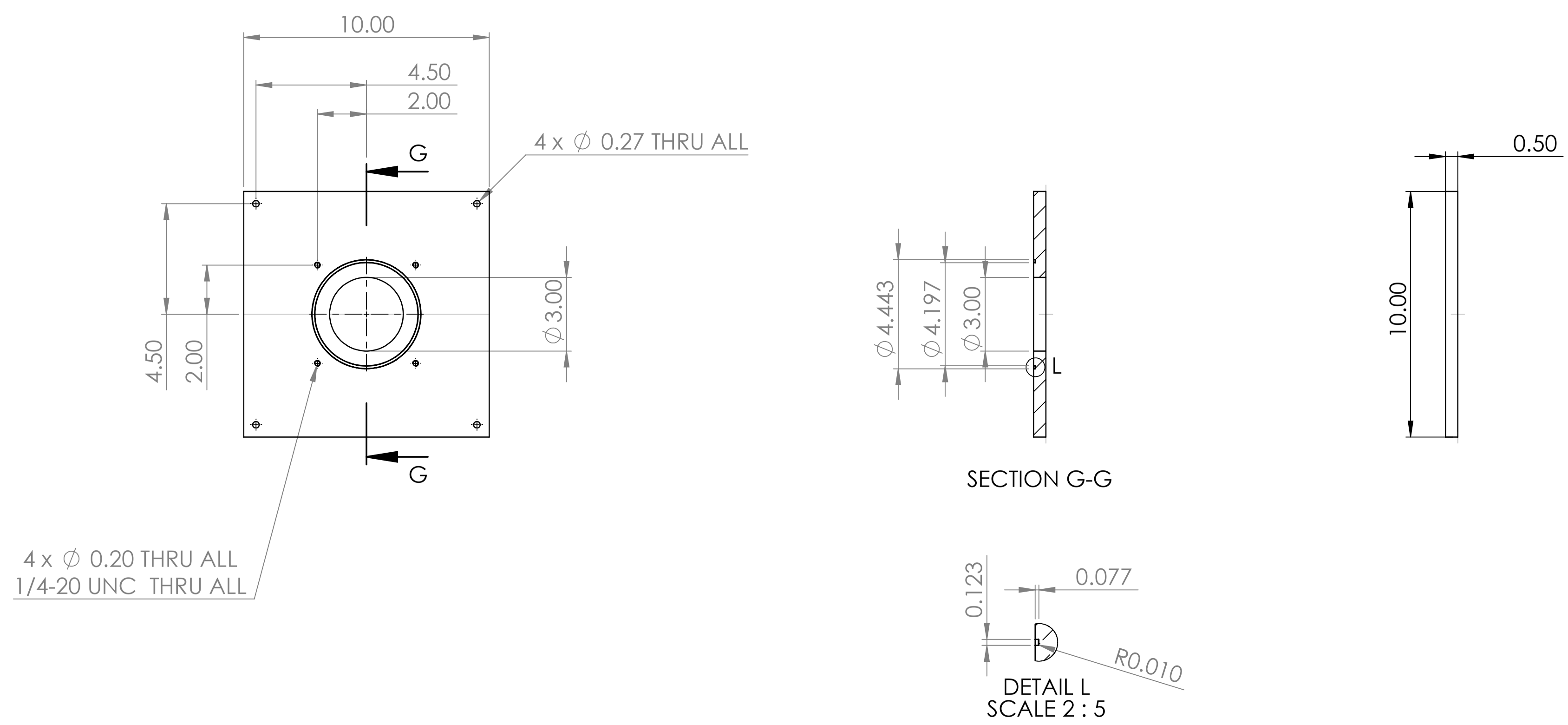

AFTENDPLATE02
Cut and chamfer all edges

NEXT ASSY	USED ON	
APPLICATION		DO NOT SCALE DRAWING

UNLESS OTHERWISE SPECIFIED:
DIMENSIONS ARE IN INCHES
TOLERANCES:
TWO PLACE DECIMAL ±0.005
THREE PLACE DECIMAL ±0.001
INTERPRET GEOMETRIC TOLERANCING PER:
MATERIAL
Carbon Steel
FINISH

	NAME	DATE
DRAWN	SB	11/28/2018
CHECKED		
ENG APPR.		
MFG APPR.		
Q.A.		
COMMENTS:		

TITLE:
Two Section
Hybrid Assembly

SIZE	DWG. NO.	REV
B	Hybrid	A
SCALE: 1:5	WEIGHT:	SHEET 12 OF 16

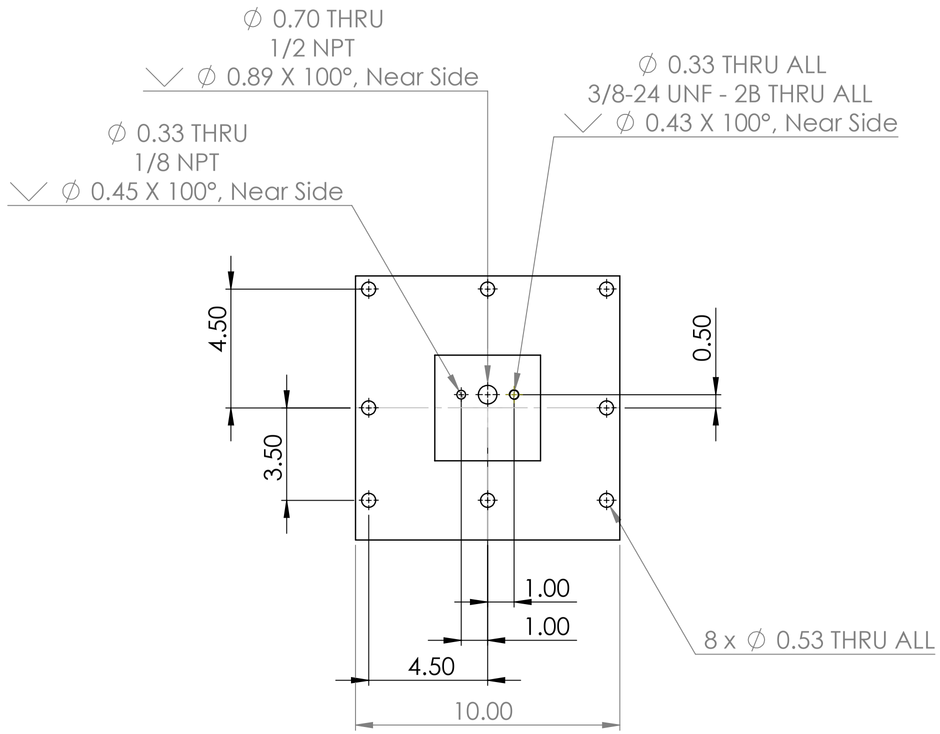

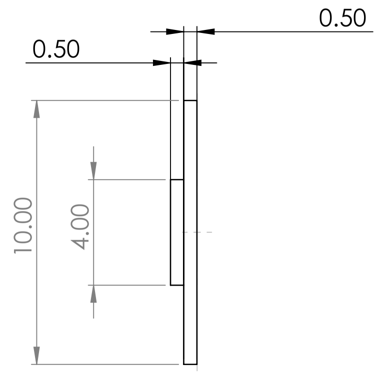

FWDENDPLATE01

Cut and chamfer all edges

		UNLESS OTHERWISE SPECIFIED:		NAME	DATE
		DIMENSIONS ARE IN INCHES TOLERANCES: TWO PLACE DECIMAL ±0.005 THREE PLACE DECIMAL ±0.001	DRAWN	SB	11/28/2018
			CHECKED		
			ENG APPR.		
			MFG APPR.		
		INTERPRET GEOMETRIC TOLERANCING PER:	Q.A.		
		MATERIAL Carbon Steel	COMMENTS:		
NEXT ASSY	USED ON	FINISH			
APPLICATION		DO NOT SCALE DRAWING			

TITLE: Two Section Hybrid Assembly

SIZE	DWG. NO.	REV
B	Hybrid	A
SCALE: 1:5	WEIGHT:	SHEET 13 OF 16

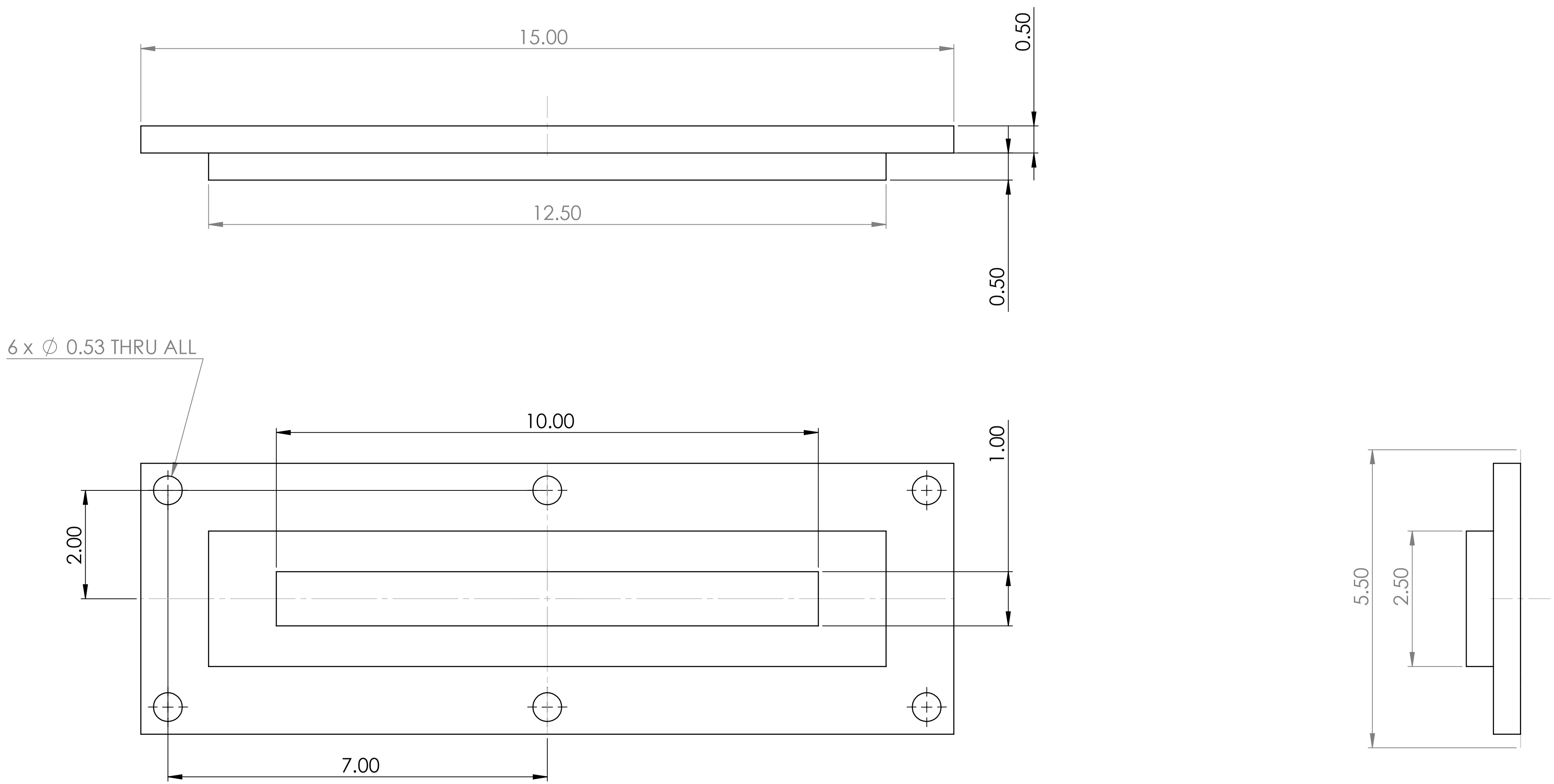

TABLESTOP01

Cut and chamfer all edges

NEXT ASSY	USED ON	
APPLICATION		

UNLESS OTHERWISE SPECIFIED:

DIMENSIONS ARE IN INCHES
TOLERANCES:
FRACTIONAL ±
ANGULAR: MACH ± BEND ±
TWO PLACE DECIMAL ±
THREE PLACE DECIMAL ±

INTERPRET GEOMETRIC TOLERANCING PER:

MATERIAL: Carbon Steel

FINISH

DO NOT SCALE DRAWING

	NAME	DATE
DRAWN	SB	11/28/2018
CHECKED		
ENG APPR.		
MFG APPR.		
Q.A.		

COMMENTS:

TITLE: Two Section Hybrid Assembly

SIZE	DWG. NO.	REV
B	Hybrid	A

SCALE: 1:6 WEIGHT: SHEET 14 OF 16

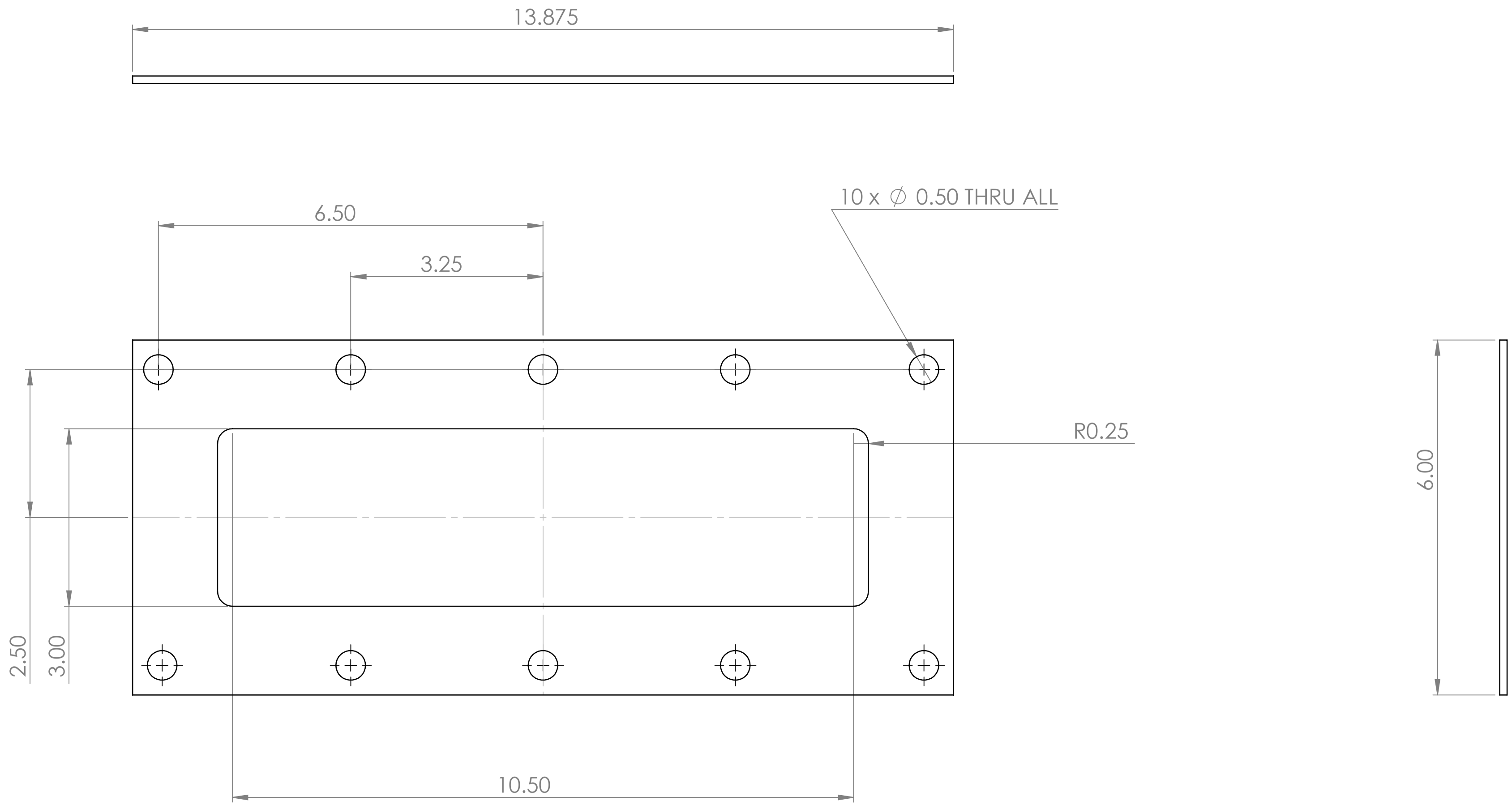

WINDOWPLATE01
Cut and chamfer all edges

PROPRIETARY AND CONFIDENTIAL

NEXT ASSY	USED ON
APPLICATION	

UNLESS OTHERWISE SPECIFIED:
DIMENSIONS ARE IN INCHES
TOLERANCES:
FRACTIONAL ±
ANGULAR: MACH ± BEND ±
TWO PLACE DECIMAL ±
THREE PLACE DECIMAL ±
INTERPRET GEOMETRIC TOLERANCING PER:
MATERIAL Carbon Steel
FINISH
DO NOT SCALE DRAWING

	NAME	DATE
DRAWN	SB	11/28/2018
CHECKED		
ENG APPR.		
MFG APPR.		
Q.A.		
COMMENTS:		

TITLE: Two Section Hybrid Assembly

SIZE B DWG. NO. Hybrid REV A

SCALE: 1:6 WEIGHT: SHEET 15 OF 16

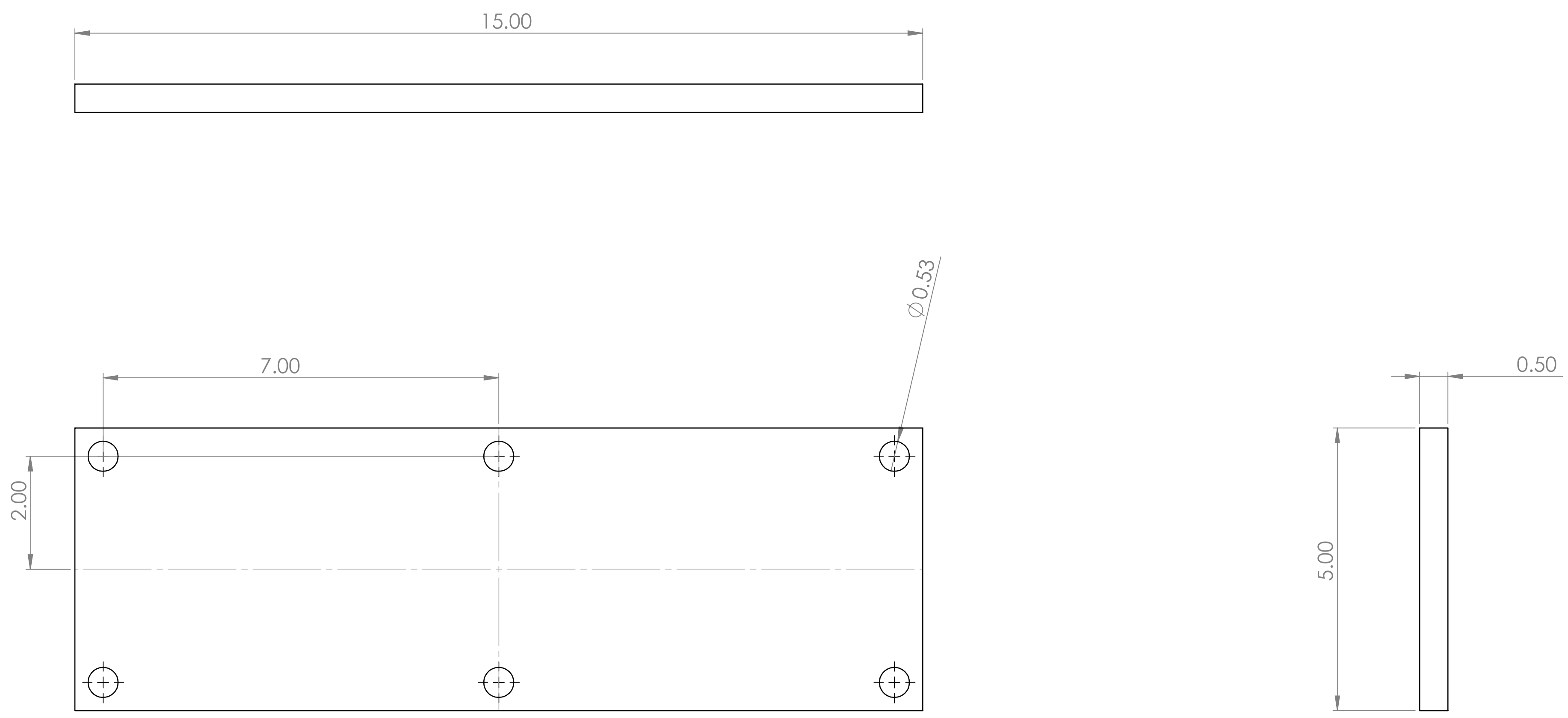

LIFT01

Cut and chamfer all edges

PROPRIETARY AND CONFIDENTIAL

THE INFORMATION CONTAINED IN THIS DRAWING IS THE SOLE PROPERTY OF <INSERT COMPANY NAME HERE>. ANY REPRODUCTION IN PART OR AS A WHOLE WITHOUT THE WRITTEN PERMISSION OF <INSERT COMPANY NAME HERE> IS PROHIBITED.

NEXT ASSY	USED ON	UNLESS OTHERWISE SPECIFIED: DIMENSIONS ARE IN INCHES TOLERANCES: FRACTIONAL ± ANGULAR: MACH ± BEND ± TWO PLACE DECIMAL ± THREE PLACE DECIMAL ±		NAME / DATE
APPLICATION		INTERPRET GEOMETRIC TOLERANCING PER:	DRAWN	SB / 11/28/2018
		MATERIAL: Carbon Steel	CHECKED	
		FINISH	ENG APPR.	
		DO NOT SCALE DRAWING	MFG APPR.	
			Q.A.	
			COMMENTS:	

TITLE: Two Section Hybrid Assembly

SIZE	DWG. NO.	REV
B	Hybrid	A
SCALE: 1:6	WEIGHT:	SHEET 16 OF 16

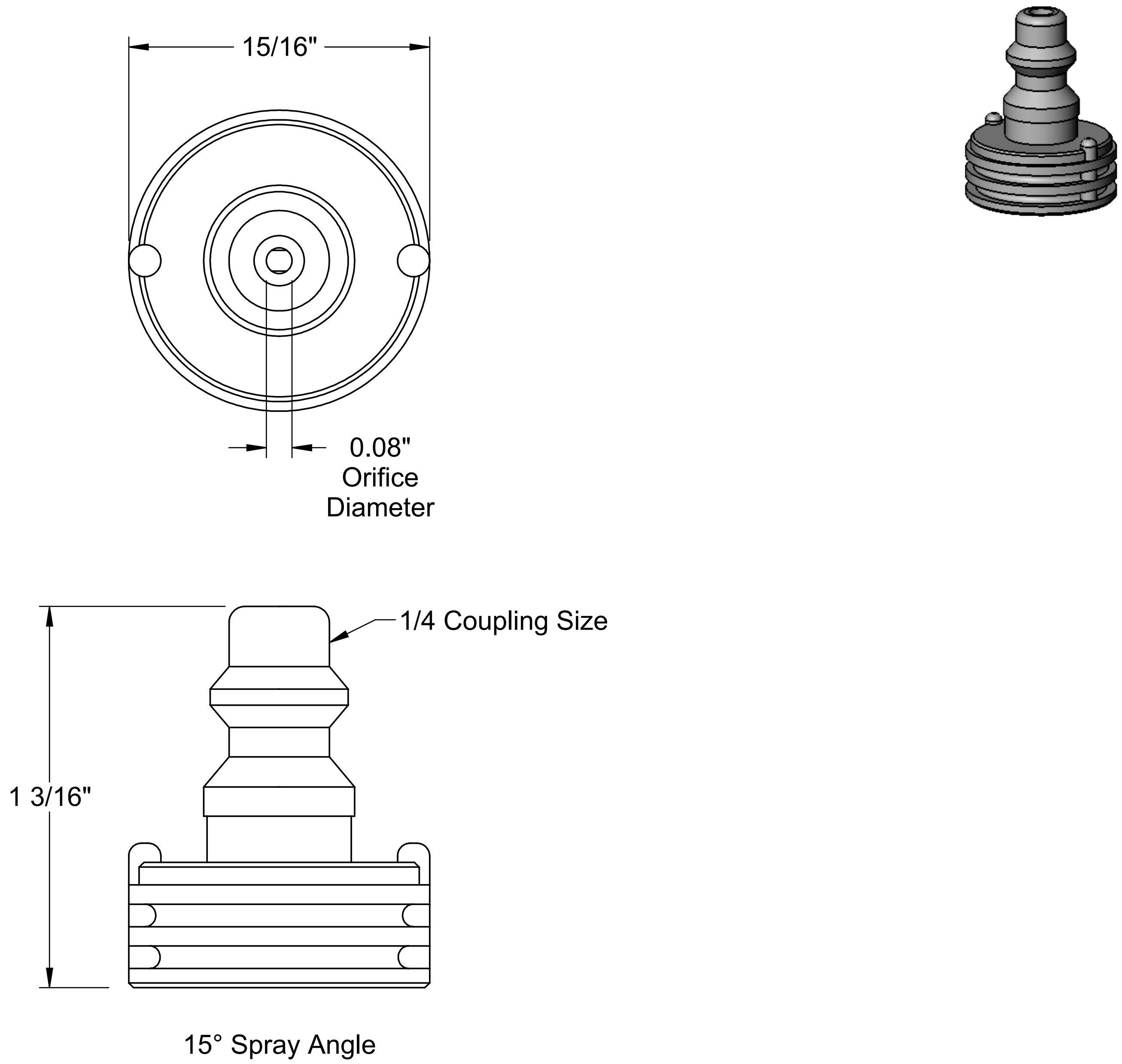

McMASTER-CARR® CAD

PART NUMBER **31905K292**

http://www.mcmaster.com

Quick-Disconnect
High-Pressure Flat Spray Nozzle